

PEOPLE'S DEMOCRATIC REPUBLIC OF ALGERIA
MINISTRY OF HIGHER EDUCATION AND SCIENTIFIC RESEARCH



University of Blida 1
Faculty of Technology
Department of Automation and Electrical Engineering

DOCTORAL THESIS

Field: Electrical Engineering

Option: Electrical Engineering

Entitled

**CONTROL AND OPTIMIZATION OF
MULTIFUNCTIONAL AND MULTILEVEL SOLAR
ACTIVE FILTER**

Presented by:

KHETTAB Soufian

Jury Members

Abdelaziz Ferdjouni	Professor, U. of Blida	President
Messaoud Belazzoug	MCA, U. of Blida	Examiner
Mountassar Maamoun	Professor, U.of USTHB	Examiner
Rafik BRADAI	Professor, U. of Blida	Supervisor
Aissa KHELDOUN	Professor, U. of Boumerdes	Co-Supervisor

ملخص

يوجد العديد من تكوينات الفلاتر الشمسية النشطة ذات المراحل المزدوجة في الأدبيات. وتختلف هذه التكوينات في نوع العاكس، خوارزمية تتبع نقطة القدرة القصوى (MPPT)، عدد المستشعرات، استراتيجية التحقق، ومؤشرات الأداء التي تم تحقيقها، وما إلى ذلك. يمكن تقييم كل تكوين على أنه أفضل من جانب واحد أو أكثر، خصوصاً مؤشرات الأداء مثل التشويه التوافقي الكلي (THD) ومعامل القدرة. ومع ذلك، هناك دائماً مجالاً للتحسين. يقدم هذا البحث بنية جديدة لتحسين أداء الأنظمة الفوتوفولطية (PV) المتصلة بالشبكة من خلال إدخال عدة ابتكارات رئيسية. أولاً، يتم تنفيذ فلتر نشط شمسي أحادي الطور يعتمد على خلية U المعبأة ذات السبعة مستويات (PUC7)، مما يوفر حلاً شاملاً لتخفيف التوافقيات، تعويض القدرة التفاعلية، واستخراج الطاقة بكفاءة من مصدر الـ PV بينما يسهل حقن الطاقة الحقيقية في الشبكة. ثانياً، يتم تعديل خوارزمية حقن القدرة P-Q لاستيعاب استخراج الطاقة الشمسية من المولد الفوتوفولطي إلى الشبكة، مع معالجة الحاجة لحقن التيار التوافقي لتحسين جودة الطاقة. تضمن هذه التعديلات أداءً ديناميكياً من خلال استخراج التيار المرجعي مع المحتوى التوافقي والمعلومات المتعلقة بالطاقة الشمسية، مما يعزز كفاءة النظام العامة. بالإضافة إلى ذلك، يتم تعزيز استراتيجية التحكم التنبئي بالنموذج (MPC) المستخدمة في هذا النظام من خلال دمج طريقة رانج-كوتا ذات الترتيب الرابع (4oRK) على عكس أساليب MPC التقليدية التي تعتمد على التكامل بطريقة أويلر وتُعاني من تدهور الدقة عند استخدام فترات أخذ عينات طويلة، يحقق MPC القائم على 4oRK تحليلاً كبيراً في الخطأ الحسابي، مما يضمن تنبؤات دقيقة للـ trajectories وتصحيحات. تُظهر التحليلات المقارنة أن MPC القائم على 4oRK يحافظ على THD أقل من 5% بشكل مستمر تحت ظروف التحميل غير الخطي وهبوط الجهد، متفوقاً على الطريقة القائمة على أويلر. علاوة على ذلك، يتم تحقيق هذا التحسين دون زيادة في التعقيد الحسابي أو أوقات تنفيذ المهام. أخيراً، يخضع الهيكل المقترح لاختبارات حقيقية في الهواء الطلق، للتحقق من أدائه في جوانب رئيسية متعددة، بما في ذلك تتبع القدرة القصوى، تقليل THD مقارنة بالأعمال السابقة، العمل عند معامل قدرة وحدة، واختبار التشغيل الفعال للوظائف المتعددة. تؤكد محاكاة MATLAB/Simulink واختبارات النموذج الأولي الفعلي صحة MPC القائم على 4oRK، مما يوضح قدرته على تقليل THD، تقليل خسائر التبديل، والحفاظ على أداء تحكم قوي عند ترددات تبديل منخفضة. هذه المساهمات تُظهر بشكل جماعي فعالية النظام المقترح في تحسين جودة حقن الطاقة، تعويض القدرة التفاعلية، والدقة العامة للتحكم تحت الظروف الحقيقية للأنظمة الفوتوفولطية المتصلة بالشبكة، مما يجعله حلاً فعالاً في مجال أنظمة الطاقة المتجددة.

الكلمات المفتاحية:

محول طاقة أحادي الطور PUC7، مرشح طاقة نشط متعدد الوظائف، نظام كهروضوئي ثنائي المرحلة، التحكم التنبئي بالنموذج، التحقق الخارجي.

Abstract

Different configurations of double-stage solar active filters are available in the literature. They differ in either the type of the inverter, the maximum power point tracking (MPPT) algorithm, the number of sensors, the validation strategy, the achieved performance indices, etc. Each configuration can be evaluated as better from one aspect or/and many aspects, particularly the performance indices such as total harmonic distortion (THD) and power factor. However, there is always room for improvement. This research presents a novel architecture to enhance the performance of grid-connected photovoltaic (PV) systems through the introduction of several key novelties. Firstly, a packed U-cell seven-level (PUC7)-based single-phase solar active filter is implemented, offering a comprehensive solution for harmonics mitigation, reactive power compensation, and efficient power extraction from the PV source while facilitating the injection of real power into the grid. Secondly, the P-Q power injection algorithm is modified to accommodate the extraction of solar power from the PV generator to the grid, simultaneously addressing the need for harmonic current injection to improve power quality. This modification ensures dynamic performance by extracting reference current with harmonic content and solar power information, thereby enhancing the system's overall efficiency. Additionally, the Model Predictive Control (MPC) strategy employed in this system is enhanced through the integration of the 4th-order Runge-Kutta (4oRK) method. Unlike conventional MPC approaches that rely on Euler integration and suffer from diminished accuracy at larger sampling intervals, the 4oRK-based MPC achieves a significantly lower computational error, ensuring precise trajectory predictions and corrections. Comparative analysis shows that the 4oRK-based MPC consistently maintains a THD below 5% under nonlinear load and voltage sag conditions, surpassing the Euler-based method. Furthermore, this improvement is realized without increasing computational complexity or task execution times. Lastly, the proposed architecture undergoes real outdoor testing, validating its performance in various key aspects, including maximum power tracking, reduction of THD in comparison with previous work, operation at unity power factor, and testing the effective operation of the multifunction feature. Extensive MATLAB/Simulink simulations and physical prototype experiments further validate the proposed 4oRK-based MPC, showing its ability to minimize

THD, reduce switching losses, and maintain robust control performance at lower switching frequencies. These contributions collectively demonstrate the effectiveness of the proposed system in enhancing power injection quality, reactive power compensation, and overall control precision under real outdoor conditions of PV systems connected to the grid, making it an effective solution in the field of renewable energy systems.

Keywords:

Single-phase PUC7 inverter, Multifunction active power filter, Double-stage photovoltaic system, Model predictive control, outdoor validation.

Résumé

Différentes configurations de filtres actifs solaires à double étage sont disponibles dans la littérature. Elles diffèrent par le type d'onduleur, l'algorithme de suivi du point de puissance maximal (MPPT), le nombre de capteurs, la stratégie de validation, les indices de performance obtenus, etc. Chaque configuration peut être évaluée comme étant meilleure sous un ou plusieurs aspects, en particulier les indices de performance tels que la distorsion harmonique totale (THD) et le facteur de puissance. Cependant, il y a toujours des possibilités d'amélioration. Cet article présente une nouvelle architecture pour améliorer les performances des systèmes photovoltaïques (PV) connectés au réseau grâce à l'introduction de plusieurs innovations clés. Tout d'abord, un filtre actif solaire monophasé à sept niveaux basé sur une cellule U emballée (PUC7) est mis en œuvre, offrant une solution complète pour l'atténuation des harmoniques, la compensation de la puissance réactive et l'extraction efficace de l'énergie de la source PV tout en facilitant l'injection de puissance réelle dans le réseau. Deuxièmement, l'algorithme d'injection de puissance P-Q est modifié pour permettre l'extraction de l'énergie solaire du générateur PV vers le réseau, tout en répondant au besoin d'injection de courant harmonique pour améliorer la qualité de l'énergie. Cette modification assure des performances dynamiques en extrayant le courant de référence avec du contenu harmonique et des informations sur la puissance solaire, améliorant ainsi l'efficacité globale du système. De plus, la stratégie de contrôle prédictif basé sur le modèle (MPC) utilisée dans ce système est améliorée par l'intégration de la méthode de Runge-Kutta d'ordre 4 (4oRK). Contrairement aux approches MPC conventionnelles qui reposent sur l'intégration d'Euler et souffrent d'une précision réduite à des intervalles d'échantillonnage plus grands, le MPC basé sur 4oRK réduit considérablement l'erreur computationnelle, assurant des prédictions et des corrections de trajectoire précises. Une analyse comparative montre que le MPC basé sur 4oRK maintient systématiquement une THD inférieure à 5% dans des conditions de charge non linéaire et de chute de tension, surpassant ainsi la méthode basée sur Euler. De plus, cette amélioration est réalisée sans augmenter la complexité computationnelle ni les temps d'exécution des tâches. Enfin, l'architecture proposée subit des tests réels en extérieur, validant ses performances sous divers aspects clés, notamment le suivi de la puissance maximale, la réduction de la THD par rapport aux travaux précédents, l'opération à facteur

de puissance unitaire et le test du bon fonctionnement de la fonctionnalité multifonctionnelle. Des simulations MATLAB/Simulink et des expériences sur prototype physique valident en outre le MPC basé sur 4oRK, montrant sa capacité à minimiser la THD, réduire les pertes de commutation et maintenir des performances de contrôle robustes à des fréquences de commutation plus faibles. Ces contributions démontrent collectivement l'efficacité du système proposé pour améliorer la qualité de l'injection de puissance, la compensation de la puissance réactive et la précision globale du contrôle dans des conditions réelles extérieures des systèmes PV connectés au réseau, faisant de lui une solution efficace dans le domaine des systèmes d'énergie renouvelable.

Mots clés:

Onduleur monophasé PUC7, Filtre active multifonction, Système photovoltaïque à double étage, Contrôle prédictif du modèle, Validation en extérieur.

Table of Contents

ملخص-----	i
Abstract -----	ii
Résumé-----	iv
Table of Contents-----	vi
List of Figures-----	viii
List of Tables-----	xi
List of Abbreviations-----	xii
Acknowledgements -----	xiv
General introduction -----	1
1.1 OVERVIEW AND MOTIVATIONS -----	1
1.2 CONTRIBUTIONS -----	4
1.3 ORGANIZATION OF THE THESIS -----	4
Chapter 2: Power System and Challenges -----	6
2.1 Introduction -----	6
2.2 Electrical Power Generation -----	6
2.3 Power quality-----	7
2.4 Common forms of issues with power quality-----	8
2.4.1 Voltage Sags and Interruptions -----	8
2.4.2 Voltage Fluctuations -----	9
2.4.3 Imbalance in a Three-Phase Voltage System-----	9
2.4.4 Frequency Variation-----	10
2.5 Harmonic Pollution-----	10
2.5.1 Harmonics of Voltage and Current-----	11
2.5.2 Harmonious Origins in the Power Structure-----	11
2.5.3 Harmonic Effects -----	12
2.5.4 Harmonics Solution -----	13
2.6 Modern techniques for reducing harmonics -----	13
2.6.1 Active Power filter -----	13
2.6.2 Hybrid Harmonic Mitigation Techniques-----	15
2.7 Active power filter Topologies -----	16

2.8 Conclusion -----	22
Chapter 3: System Modeling and Control Design-----	22
3.1 Introduction -----	22
3.2 System configuration -----	22
3.2.1 PV array modelling -----	23
3.2.2 PUC7 inverter -----	25
3.2.3 Boost Converter -----	26
3.3 MPPT controller -----	28
3.4 Modified P-Q theory for power injection -----	29
3.5 MPC procedure -----	30
3.6 Conclusion -----	33
Chapter 4: System assessment: simulation and experimentation -----	34
4.1 Introduction -----	34
4.2 PV IDENTIFICATION AND SIMULATION RESULTS -----	34
4.2.1 PV ARRAY IDENTIFICATION -----	34
4.2.2 SIMULATION RESULTS -----	36
4.3 EXPERIMENTAL RESULTS -----	42
4.4 Conclusion -----	48
Chapter 5: Enhanced MPC Utilizing the Runge-Kutta Method -----	49
5.1 Introduction -----	49
5.2 MPC -----	49
5.2.1 MPC Control Design Using Euler Method -----	50
5.2.2 MPC Control Design Using 4 th order Runge–Kutta Method -----	50
5.3 Fitness Function -----	53
5.4 Simulation results -----	54
5.5 Experimental results -----	62
5.6 Conclusion -----	74
GENERAL CONCLUSION -----	76
BIBLIOGRAPHY -----	78

List of Figures

Figure 2. 1 Voltage Sag and Interruption.	9
Figure 2. 2 Voltage fluctuation	9
Figure 2. 3 Imbalance in a Three-Phase Voltage System	10
Figure 2. 4 Frequency Variation	10
Figure 2. 5 Sinusoidal 50 Hz waveform with 3rd, 5th and 7th Harmonics.	11
Figure 2. 6 Parallel APF.	14
Figure 2. 7 Series APF.....	15
Figure 2. 8 Hybrid connections of active and passive filters.....	16
Figure 2. 9 Diode-Clamped Multilevel Inverter.	18
Figure 2. 10 Capacitor-Clamped (Flying Capacitor).	19
Figure 2. 11 Cascaded H-Bridge.....	21
Figure 2. 12 Single-Phase PUC inverter.....	21
Figure 3. 1 The proposed configuration of the double-stage, single-phase PUC7 inverter..	23
Figure 3. 2 The photovoltaic (PV) source's electrical modeling includes: (a) the PV array and (b) PV module.....	24
Figure 3. 3 DC-DC boost converter with MPPT	27
Figure 3. 4 The P&O method flowchart	28
Figure 3. 5 Modified 'p-q' power injection.	30
Figure 3. 6 Model predictive control (MPC).	31
Figure 4. 1 The I-V curve tracer using capacitor charging and discharging process.....	35
Figure 4. 2 I-V properties of the PV array in use, (a) Experimental curve, (b) Simulated curve.	36
Figure 4.3 P-V properties of the PV array in use, (a) experimental curve, (b) simulated curve.	37
Figure 4. 4 (a) Load current (b) Harmonic spectrum of the load current.	39

Figure 4. 5 (a) Grid current (b) Inverter current and its reference (c) DC-link capacitor voltages (d) Power of the PV, grid, and load (e) Current of the grid, Inverter, and load (f) PV leakage current waveform.....41

Figure 4. 6 The constructed experimental prototype.43

Figure 4. 7 Experimental results: (a) Load and Grid currents, (b) Inverter current and its reference, (c) Inverter output voltage, (d) DC-link capacitor voltages, (e) Power of the PV, grid, and load, (f) Grid current and grid voltage (scale V/15), (g) Power factor, (h) Current of the grid ,inverter ,and load.....47

Figure 5. 1 The functionality of the suggested MPC.....50

Figure 5. 2 (a) Principle of Euler method, (b) Explanation of 4oRK51

Figure 5. 3 Model predictive control (MPC): (a) Using 4oRK Method, (b) Using Euler Method.....53

Figure 5. 4 (a) Load current (b) Harmonic spectrum of the load current.55

Figure 5. 5 Simulation results Using Euler Method with switching frequency 10 kHz: (a) Grid current, (b) Inverter current and its reference, (c) Grid voltage and Grid current (scale I *20), (d) Power factor, (e) DC-link capacitor voltages, (f) Inverter output voltage.....57

Figure 5. 6 Simulation results Using Euler Method with switching frequency 5 kHz: (a) Grid current, (b) Inverter current and its reference, (c) Grid voltage and Grid current (scale I *20).
.....58

Figure 5. 7 Simulation results Using 4oRK Method with switching frequency 10 kHz: (a) Grid current, (b) Inverter current and its reference, (c) Grid voltage and Grid current (scale I *20)59

Figure 5. 8 Simulation results Using 4oRK Method with switching frequency 5 kHz: (a) Grid current, (b) Inverter current and its reference, (c) Grid voltage and Grid current (scale I *20)
.....60

Figure 5. 9 Simulation results Using 4oRK Method with switching frequency 3 kHz: (a) Grid current, (b) Inverter current and its reference, (c) Grid voltage and Grid current (scale I *20)
.....61

Figure 5. 10 The built prototype for the experiment.....62

Figure 5. 11 The experimental results Using Euler Method with switching frequency 10 kHz:: (a) load current; (b) grid current; (c) inverter current and its reference; (d) Grid voltage and

Grid current (scale I *20); (e) power factor; (f) DC-link capacitor voltages; and (g) inverter output voltage.65

Figure 5. 12 Experimental results Using Euler Method with switching frequency 5 kHz: (a) Grid current, (b) Inverter current and its reference, (c) Grid voltage and Grid current (scale I *20).66

Figure 5. 13 Experimental results Using 4oRK Method with switching frequency 10 kHz: (a) Grid current, (b) Inverter current and its reference, (c) Grid voltage and Grid current (scale I *20)67

Figure 5. 14 Experimental results Using 4oRK Method with switching frequency 5 kHz: (a) Grid current, (b) Inverter current and its reference, (c) Grid voltage and Grid current (scale I *20)68

Figure 5. 15 Experimental results Using 4oRK Method with switching frequency 3 kHz: (a) Grid current, (b) Inverter current and its reference, (c) Grid voltage and Grid current (scale I *20)69

Figure 5. 16 Experimental Results Utilizing the Euler Method Across Various Scenarios with 10 KHz: (a) Grid current, Load current (b) Inverter current and its reference, (c) Grid voltage and Grid current (scale I *20), (d) DC-link capacitor voltages.72

Figure 5. 17 Experimental Results Utilizing the 4oRK Method Across Various Scenarios with 3 KHz : (a) Grid current, Load current (b) Inverter current and its reference, (c) Grid voltage and Grid current (scale I *20), (d) DC-link capacitor voltages.....73

Figure 5. 18 Power of the grid74

Figure 5. 19 Task Execution Time: (a) Euler Method, (b) 4oRK Method.74

List of Tables

Table 2. 1 Comparative Analysis of the PUC 7 Inverter and Conventional Seven-Level Inverter Topologies.....	22
Table 3. 1 PUC7 inverter state switching.	25
Table 4. 1 PV array identification's results	36
Table 4. 2 PV system components specifications.....	38
Table 4. 3 Comparison with previous work.....	48
Table 5. 1 data of the system components	54
Table 5. 2 THD comparison of the simulation results.....	62
Table 5. 3 THD comparison of the experimental results.....	70

List of Abbreviations

VSI	Voltage source inverters
PV	Photovoltaic
DC	Direct current
PCC	Point of common coupling
PQ	Power quality
MLI	Multilevel inverter
PUCs	Packed 'U' cells
HIL	Hardware-in-the-loop
MPC	Model Predictive Control
MPPT	Maximum power point tracking
P&O	Perturb and Observe Algorithm
THD	Total harmonic distortion
4 th RK	4 th order Runge-Kutta
K_1, K_2, K_3 and K_4	Gains for 4 th order Runge-Kutta
APF	Active Power Filter
PFs	Passive filters
SMPS	Switch-mode power supply
L _f	Line inductor
PCC	Point of common coupling
$I_{f_ref_cal}$	The predicted values of the inverter current
$I_{inv_ref}(k)$	Inverter current's reference
$V_{dc2_ref}(k)$	Reference of the DC-link capacitor voltages
I_f	Inverter current
I_L	Load current
V_s	Grid voltage
V_{dc1}, V_{dc2}	The capacitor voltages
g	Cost function
T_s	Sampling time

$V(k)$	Voltage vector
$V_{an}(k)$	Voltage vector generated by the inverter
IGBTs	Insulated Gate Bipolar Transistors
PWM	Pulse Width Modulated
HF	Hybrid filter
FCMLI	Flying capacitor multilevel inverters
DCMLI	Diode-clamped multilevel inverters
CHB	Cascaded H-Bridge
MMC	Modular multilevel converters
NPC	Neutral-point-clamped
I_{ph}	The photocurrent
V_{PV}	Photovoltaic voltage
$I_{PV_measured}$	Measured PV current
R_s	Series resistance
I_D	Current flowing via a diode
α	Ideality factor of the diode
V_{th}	Thermal voltage
I_{sc}	Short-circuit current
V_{oc}	Open-circuit voltage
V_{dc}	Voltage across the DC-link capacitor
I_{inv}	Inverter's current
V_{grid}	Grid voltage
V_{out}	output voltage
D	Duty ratio
P_{Loss}	Power Losses
V_{grid} (RMS)	Grid voltage
F_s	Grid frequency
V_{mp}	Maximum power voltage
I_{mp}	Maximum power current

Acknowledgements

Alhamdulillah, all praises to Allah for the strengths and His blessing in completing this thesis.

I extend my profound gratitude to my esteemed supervisors, **Prof. Bradai Rafik** and **Prof. Kheldoun Aissa**, whose unwavering support, incisive guidance, and scholarly mentorship have been pivotal in shaping the course of this research. Their unparalleled expertise and steadfast commitment to academic excellence have served as a continual source of inspiration throughout my doctoral journey. It has been an extraordinary privilege to work under their tutelage, and I am deeply appreciative of the invaluable insights and contributions they have provided, which have been instrumental in bringing this thesis to fruition.

We would like to extend our heartfelt thanks to the members of the board of examiners for their time, effort, and valuable contributions in proofreading and evaluating our thesis. Our deepest gratitude goes to **Prof. Abdelaziz Ferdjouni**, from the University of Blida, for giving us the honor of chairing the examination committee. Your support and insights have been greatly appreciated. We also extend our sincere thanks to **Mr. Messaoud Belazzoug**, MCA at the University of Blida, and **Prof. Mountassar Maamoun**, from the University of USTHB, for serving as examiners. Your constructive feedback and thoughtful remarks have helped strengthen the quality of this work. We are truly grateful for your participation and dedication.

I am deeply grateful to my family my beloved parents, whose unconditional love, endless prayers, and unwavering encouragement have been the bedrock of my success. Their sacrifices and belief in my abilities have motivated me to strive for excellence. I also extend heartfelt thanks to my brothers and sisters, who have been a constant source of strength, support, and joy, cheering me on every step of the way. To my fiancée, I deeply value your unwavering patience and the encouragement you have so graciously offered throughout this journey. Your steadfast faith in my abilities has been a guiding light, instilling strength and motivation even during the most challenging moments. I also wish to express my gratitude to my friends and colleagues, whose camaraderie, thoughtful discussions, and encouragement have enriched my personal and professional growth. Your support has made this challenging journey more fulfilling and meaningful.

Finally, I am grateful to all who have directly or indirectly contributed to this work. Your support, guidance, and encouragement have been invaluable, and I am forever grateful for the impact you have had on my life and research.

May Allah bless you all abundantly.

General introduction

1.1 OVERVIEW AND MOTIVATIONS

Recently, there has been a substantial worldwide increase in the use of renewable energies [1, 2]. This extensive adoption is motivated by the necessity to reduce the overdependence on traditional energy sources, which are known to contribute to environmental pollution. Utility companies are requesting more solar energy systems to be installed than ever before, driven by advancements in renewable energy sources [3-5]. As a result, there has been a growing focus on PV systems connected to the grid and the power conversion topologies they use.

Voltage source inverters (VSIs) are essential to improving the quality of the injected power in the grid-tied process [6-8], achieving this by removing current harmonics and adjusting the grid's reactive power at the point of common coupling (PCC) [9, 10]. Reactive power is required by local linear AC loads or nonlinear loads, while harmonics are generated by the connection of power electronics-interfaced loads and generators. Reactive power consumption in electric power systems alters its operation from both economic and technical point of view while the presence of harmonics is strongly undesirable. They contribute in overheating the key equipment of power systems: transformers and generators. Classical passive filters are no more appropriate solutions because of their limitations such as bulkiness, possible resonance, and load dependent effectiveness. To this, active filters appear to be the appropriate solution as they can ensure both reactive power compensation and harmonic mitigation. Furthermore, compared to passive filters, they provide fine response in spite of changing loads and harmonic variations. However, they are expensive and not affordable for every nonlinear load. Nowadays, researchers are attracted by the tremendous growth in PV energy installation which are connected to the grid utility through inverters. Therefore, the economic solution is to take advantage of any grid-tied PV system and use it for other purposes such as active filtering and reactive power compensation. Several studies have proposed such topology being based on the two-level VSIs to act as multifunction active filter [11-14]. These topologies have shown a good performance for eliminating current

harmonics and compensating for reactive power. However, two-level VSIs have two main drawbacks which are 1) high harmonic content of its output voltage in and 2) high switching losses.

Moreover, using a multilevel inverter as an interface between the PV array and the PCC in the grid can enhance power quality (PQ) by generating multi-level voltages that approximate the desired shape. The multilevel inverter outperforms the traditional two-level inverter in producing AC voltages and currents with reduced harmonic distortion. Many recent papers have focused on multilevel inverter (MLI) topologies, including the Flying Capacitors Inverter [15], neutral-point-clamped inverter [16], cascaded H-Bridge inverter [17], and packed ‘*U*’ cells (PUCs) inverter [18]. PUC is the most commonly used topology in single-phase applications due to its superior economy compared to other topologies [19].

PUC7 stands out as the superior choice compared to both PUC5 and classical inverters due to its higher power conversion efficiency, improved power density and size, enhanced reliability and durability. These advantages make PUC7 the preferred option for various applications, ranging from renewable energy systems to electric vehicles and industrial automation. PUC7 inverter has been suggested for this application due to its low component count and ability to generate seven output voltage levels [20]. Several control strategies have been proposed for grid-tied PUC inverters, such are traditional PI controllers using modulation techniques [21, 22]. However, there are some drawbacks to this approach, including hard implementation, complexity of the PWM modulator, and challenges in balancing capacitor voltages. Multi-objective MPC techniques have recently been created for PUC inverters [23]. Predictive control relies on a system model to anticipate the future behavior of controlled variables, guiding optimal actuation based on predefined criteria.

- Hysteresis-based predictive control: This method modifies actuation in response to anticipated behavior in an effort to keep variables within predetermined hysteresis boundaries.
- Trajectory-Based Control: This approach involves directing the system to closely follow a predetermined route in order to force variables to follow it.
- Deadbeat Management, by taking decisive action to decrease error and aim for instantaneous convergence, this approach aims to reach zero error in the next sampling moment.

- MPC is a method of improving actuation by taking future predictions into account. This minimizes the given cost function.

These methods provide many methodologies to accomplish control goals, each adapted to particular system specifications and performance standards. The reasons we chose MPC for our control application were its adaptability, capacity to follow trajectories, optimal control performance, and capacity to manage intricate restrictions.

The MPC technique is an easy-to-use and efficient way to manage MLIs. It has received a great deal of research in power converter control [24,25]. By employing this technique, fewer PI controllers are needed, and a modulation step is not required. Furthermore, DC-link capacitor voltage balancing is a simple addition to the control target that results in a considerably cleaner converter output. The MPC method is based on estimating how controlled variables will behave in the future for each switching scenario and comparing the results to references using a cost function to get the best possible state. In addition, the MPC offers several intriguing features including precise tracking, quick dynamic response, and the capacity to include restrictions and nonlinearities in controller design [26].

Many configurations of double stage solar active filter are proposed in literature. Each one has its features and differs from the others with respect to the type of the inverter, the MPPT algorithm, the number of sensors, the control strategy, the validation method, or the achieved results, etc. Each configuration can be evaluated as better than the others from one aspect or/and many aspects particularly the performance indices such as THD and power factor. In [27] and [28], authors employed an H-bridge inverter with an LCL filter for PV power integration into the grid. However, these configurations did not consider the active filtering function and validated their proposals using PV emulators. However, authors in [29] employed an H-bridge inverter with an L-filter as the active power filter, yet encountered higher THD levels, and notably, a classical inverter was utilized. Authors in [30] opted for a modified PUC5 inverter with an L filter for active power injection. However, they validated their proposal using hardware-in-the-loop (HIL) simulations.

This research presents the development and the outdoor implementation of a single-phase grid-tied PV system using a PUC7 multilevel inverter. To control the single-phase active filter while injecting the solar power into the grid, a modified MPC technique has been employed. This strategy aims to offset the impact of a contaminated load with low power

factor, improve reactive power control, eliminate harmonic currents content at the PCC, and inject real power generated by PV array with low THD. Furthermore, during periods when PV power is unavailable, such as at night, the proposed architecture continues to provide services such as reactive power compensation and harmonic mitigation, enhancing the quality of power drawn from the grid. In order to offer high power factor correction, limit switching frequency, reduce the complexity of calculation, and guarantee DC-link capacitor voltage balancing, the suggested MPC method is used. Detailed simulations in the MATLAB/Simulink environment are used to verify the performance of this setup, and an experimental validation utilizing a real-time CU-SLRT Std (DS1104 Equivalent interface and features) is conducted without the use of temperature and irradiance sensors.

1.2 CONTRIBUTIONS

This work's main contributions are summed up as follows:

- A new architecture of multifunction solar active power using double-stage, single-phase PUC7 inverter is proposed.
- A newly developed MPC algorithm is used for PUC7 inverter to ensure the power injection and voltage balance of the source and the capacitor.
- A real-time CU-SLRT Standard (DS1104 Equivalent interface+ features) is used to implement and validate the suggested control method while an I-V tracer is designed to support the validation process.
- The efficiency of the multifunctional solar active filter architecture that has been suggested is validated under real outdoor conditions. Neither PV emulator nor weather sensors (temperature and irradiance) are used for the implementation.

1.3 ORGANIZATION OF THE THESIS

The remainder of this thesis is organized as follows:

Chapter 2 provides a brief overview of about power generation that nowadays necessitates the conversion into renewable resources. In addition to the concept of power related problems

which are briefly classified in this chapter. Harmonics in the main concern of this project, with quick description of the harmonic's mitigation methods. Chapter 3 provides a detailed exploration of the system components, along with their corresponding mathematical models. The models are systematically organized into subsections, beginning with the presentation of the PV array model, followed by an analysis of the PUC7 inverter, and concluding with the DC/DC boost converter. The control system is designed such that the DC-link may be regulated by using the modified p-q theory for power injection in conjunction with the MPPT algorithm. Furthermore, an analysis is conducted of the suggested MPC approach for the PUC7 inverter, specifically focusing on grid-tied operations and applications using APF. Chapter 4 presents the validation tests, beginning with the identification and simulation results of the PV system. To verify the superior performance of the proposed system architecture, this chapter details experimental findings obtained through implementation using a real-time CU-SLRT standard (similar to the DS1104 interface). Chapter 5 presents the Enhanced MPC Utilizing the Runge-Kutta Method and the experimental results. The last chapter culminates the thesis with the main conclusions drawn from the conducted work and recommendations for future work.

Chapter 2: Power System and Challenges

2.1 Introduction

Widespread use of renewable energy sources, especially solar PV systems, depends on affordable technology developments that reduce global emissions while precisely improving electricity quality. Power quality (PQ) issues in utility distribution networks are not new, but in light of the growing reliance on technology based on power electronics, their significance has increased recently.

Harmonic distortion in distribution systems is mostly caused by increasingly commonplace devices including DC motor drives, electronic ballasts, electronic power supplies, battery chargers, and adjustable-speed motor drives. Particularly in grid-connected systems, where it may deteriorate both current and voltage quality and eventually affect system performance, this harmonic distortion creates a range of PQ problems.

Passive filters (PFs) and active power filters (APFs) have become useful tools for reducing these difficulties. Although passive filters provide a simple, conventional method of reducing harmonic distortion, their use frequently results in larger, heavier, and more expensive systems, especially in high-power applications. On the other hand, active power filters provide a number of benefits over passive filters, making them a more effective and adaptable choice for handling PQ problems associated to harmonics.

2.2 Electrical Power Generation

Recent years have seen a notable rise in the demand for energy worldwide, which has been strongly correlated with improvements in socioeconomic development and living standards. Forecasts suggest that the world's electrical energy consumption will keep rising dramatically [31]. As a result, strategic planning is now essential in the energy industry to satisfy the rising demand for power production. However, there are a number of difficulties associated with this growing demand. The traditional method of producing electricity, which mostly relies on large-scale facilities that burn fossil fuels like coal, gas, and oil, has raised

serious environmental and social issues. The limited supply of fossil fuels and their detrimental effects on the environment, such as greenhouse gas emissions and other pollutants, have forced a change in emphasis toward more sustainable energy sources.

Governments and academics throughout the world are investigating and putting into practice cutting-edge technologies and approaches in response to these difficulties, with the goal of satisfying the growing demand for power while maintaining environmental integrity. Nowadays, most people agree that renewable energy sources like solar, wind, hydro electric, and biomass are good substitutes. These sources help modernize electrical power networks in addition to making energy supplies more robust and varied. Additionally, they are essential in halting environmental deterioration and advancing global economic sustainability [32, 33].

2.3 Power quality

PQ is now a top priority for all power users, regardless of use volume. "Any disturbance in voltage, current, or frequency that results in the malfunction or improper operation of customer equipment" is the definition of PQ difficulties. The quality of the electrical power supply has been greatly influenced by the widespread use of gadgets based on power electronics. Many contemporary applications depend on these gadgets, which include arc welding machines, dimmers, current regulators, frequency converters, switch-mode power supply (SMPS), and energy-efficient lighting systems. However, when these power electronics-based loads run, harmonics are introduced into the electrical system. These harmonics can cause distortion and other problems in the distribution network, which can lower the overall quality of the electricity. The problem is made more difficult by the growing incorporation of renewable energy sources, such wind and solar power, into the mix of electricity generation. Although these renewable energy sources are essential for the development of sustainable energy, the distribution network is more vulnerable to PQ issues due to their intermittent nature and the instability they bring to the grid. As a result, upholding strict standards of power quality is becoming more and more important to both end consumers and electric utilities. In order to satisfy customer expectations, utilities are putting a variety of techniques and technologies into practice. They understand that certain users, especially those with sensitive equipment, need greater levels of power quality than what is

often offered by standard electric networks. Power quality management is constantly improving as a result of these issues, ensuring the stability and dependability of contemporary electrical systems.

2.4 Common forms of issues with power quality

Issues with power quality, or PQ, have grown in importance recently. Electric loads have changed significantly as a result of the increased usage of power electronics and electronic gadgets. These loads are both the primary source of power quality issues and the ones most affected by them. These loads cause a variety of disruptions in the voltage waveform because of their non-linear nature. It is essential to categorize power quality disturbances in order to use management solutions that are specifically suited to the particular variation in issue. This classification also helps to ensure that the right methods and analysis are applied in an efficient manner.

The most typical categories of Power Quality problems are as follows:

2.4.1 Voltage Sags and Interruptions

A voltage sag refers to a sudden decrease in voltage to a level between 10% and 90% of the nominal voltage, persisting for a duration ranging from 10 milliseconds to several seconds. These sags are frequently triggered by natural events such as lightning, as well as faults within the installation or the power grid, encompassing both public networks and user-owned systems. Additionally, voltage sags can occur during switching operations that involve significant current surges, such as when motors are started or transformers are energized.

Conversely, a voltage interruption is defined by a sudden drop in voltage to a level below 90% of the nominal value or a complete loss of voltage. The duration of these interruptions typically spans from 10 milliseconds to one minute for short interruptions and exceeds one minute for prolonged interruptions. Most electrical devices can withstand a total power outage lasting less than 10 milliseconds without malfunction. Figure 2.1 illustrates examples of both a voltage sag and a voltage interruption.

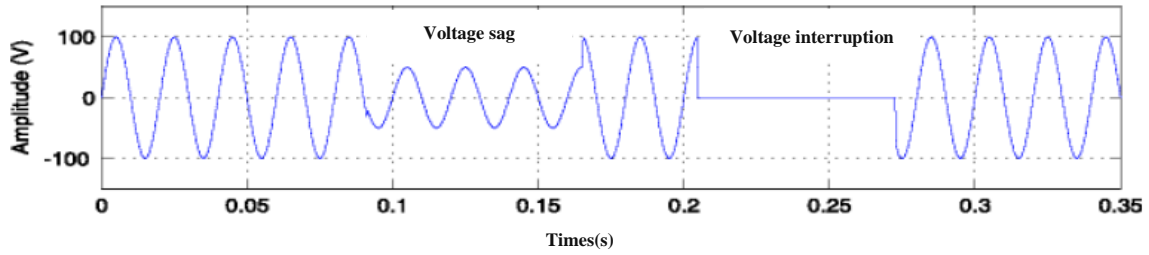


Figure 2. 1 Voltage Sag and Interruption.

2.4.2 Voltage Fluctuations

Periodic variations in the voltage waveform envelope, known as voltage fluctuations, are defined as abrupt amplitude shifts within a $\pm 10\%$ range that take place over a few hundredths of a second [34]. The main source of these oscillations is the large inrush currents that are transmitted across network cables. These kinds of currents frequently come from equipment like welding machines and arc furnaces that have constantly fluctuating power requirements. Current intensity changes as a result of these oscillations, and these changes are especially apparent in lighting systems. Flicker is a visually noticeable disruption that may be caused by even a small voltage change of 1%. Figure 2.2 shows an illustration of a voltage fluctuation.

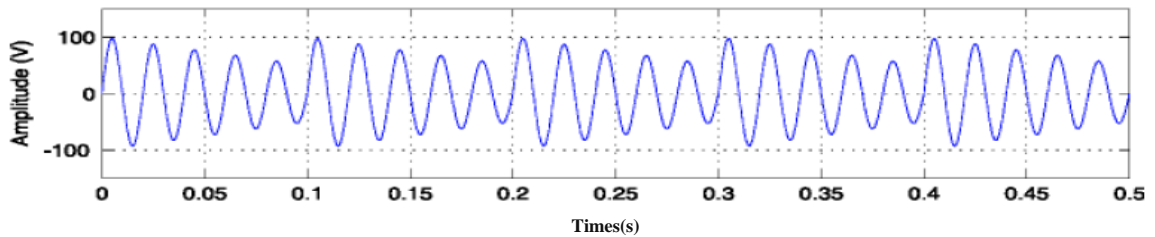


Figure 2. 2 Voltage fluctuation

2.4.3 Imbalance in a Three-Phase Voltage System

An imbalance in a three-phase voltage system occurs when the three voltages differ in amplitude and/or are not phase-shifted by 120° relative to each other, as illustrated in Figure 2.3. When a balanced three-phase electrical network supplies an unbalanced three-

phase load, voltage imbalances arise due to the flow of unbalanced currents through the network's impedances.

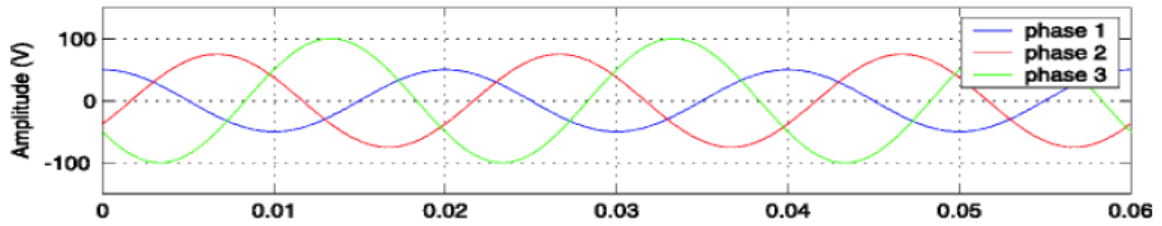


Figure 2. 3 Imbalance in a Three-Phase Voltage System

2.4.4 Frequency Variation

A significant variation in network frequency can occur in networks that are either not interconnected, as depicted in Figure 2.4. In distribution or transmission networks, such frequency variations are exceedingly rare and only manifest under exceptional circumstances, such as severe network faults. Under normal operating conditions, the average value of the fundamental frequency should be maintained within the range of 50 Hz \pm 1%. [34]

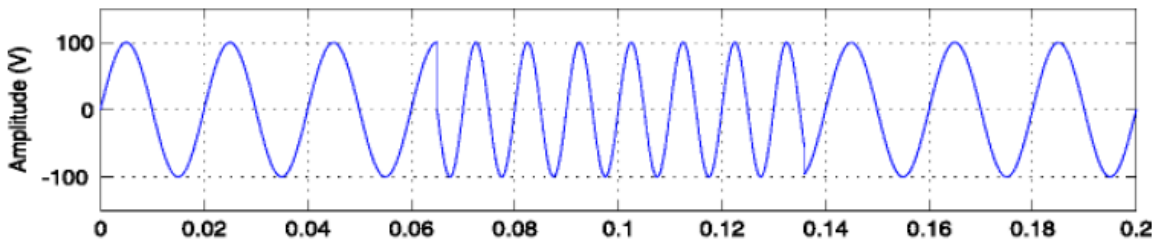


Figure 2. 4 Frequency Variation

2.5 Harmonic Pollution

Harmonics refer to sinusoidal voltage or current components that are periodic and have frequencies that are integer multiples of the fundamental frequency. In a given system, if the fundamental frequency is (f_0), the frequency of the (n-th) harmonic is (nf_0). Harmonics are often used to describe the distortion of a sinusoidal signal, which is associated with

currents or voltages of varying amplitudes and frequencies. This distortion can lead to a deterioration in power factor performance.

2.5.1 Harmonics of Voltage and Current

Though separate, the effects of harmonics in voltage and current are related. Non-linear loads at the consumer end introduce harmonic currents into the power system, which is why they are frequently categorized as harmonic current sources. As a result, the system's linear impedances and harmonic currents combine to produce harmonic voltages. Voltage harmonics are produced by the voltage decreases across system resistances brought about by the passage of harmonic currents. As a result, the linear impedances of the power system and current harmonics both affect voltage harmonics.

A voltage waveform with a peak value of 220 V, which corresponds to the secondary distribution level, is shown in Figure 2.5. Additionally, it shows the harmonic mechanisms, which have frequencies that are three, five, and seven times the fundamental frequency, and amplitudes that range from one-third to one-fifth and one-fifth to one-seventh of 220 V. assuming that the harmonic currents passing through the system resistances are the cause of the voltage harmonics.

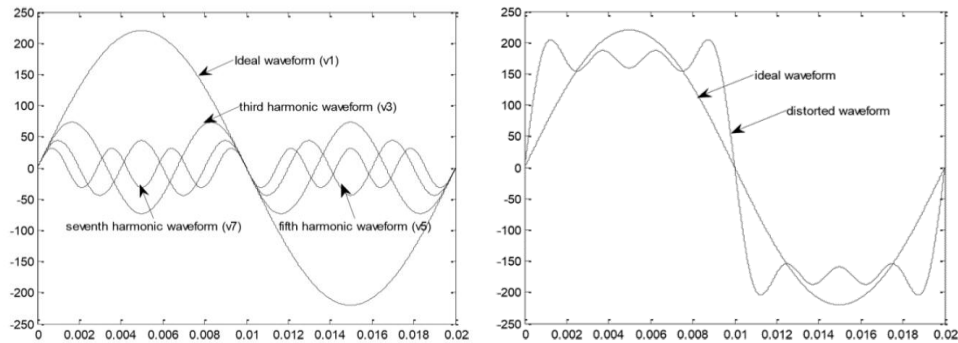


Figure 2. 5 Sinusoidal 50 Hz waveform with 3rd, 5th and 7th Harmonics.

2.5.2 Harmonious Origins in the Power Structure

Modern electrical engineering places a premium on harmonic sources in power systems, especially as power networks get more intricate and integrated with a variety of non-linear loads. Power electronics, variable frequency drives, and other non-linear devices are some of the origins of these harmonics, which are basically voltage or current waveforms that diverge from the fundamental frequency. These harmonic components generate

distortions that can lower power quality, result in inefficiencies, and cause sensitive equipment to overheat or malfunction by superimposing on the fundamental waveform. Furthermore, the prevalence of power electronic converters and the expansion of renewable energy sources have made harmonics more prevalent in power systems, requiring the employment of sophisticated analytical techniques and mitigation measures. Comprehending the origins, transmission, and consequences of harmonics is essential for the development and functioning of sturdy, effective, and dependable power systems, especially when it comes to upholding grid stability and guaranteeing the durability of electrical infrastructure [35].

2.5.3 Harmonic Effects

Harmonics pose significant risks to the power system and its connected equipment. The primary impacts of voltage and current harmonics include:

- ✓ Amplification of Harmonic Levels: Series and parallel resonances can amplify harmonic levels.
- ✓ Power Factor Degradation: Harmonics can deteriorate the power factor.
- ✓ Overheating of Conductors: Both phase and neutral conductors can overheat.
- ✓ Reduced Generator Efficiency: Harmonics progressively diminish generator efficiency.
- ✓ Transformer Losses: Harmonics cause eddy current and hysteresis losses in transformers.
- ✓ Overheating of System Components: Generators, motors, and transformers are prone to overheating.
- ✓ Additional Current in Power Capacitors: Harmonics induce extra current flow through power capacitors.
- ✓ Decreased Lifespan of Incandescent Lamps: Harmonics shorten the useful life of incandescent lamps.
- ✓ Increased Skin and Proximity Effects: Harmonics exacerbate skin and proximity effects.
- ✓ Telecommunication Interference: Harmonics can interfere with telecommunication systems.
- ✓ Relay Protection System Issues: Harmonics adversely affect relay protection systems.

Given these detrimental effects, it is crucial to mitigate harmonics through the appropriate design of active or passive filters.

2.5.4 Harmonics Solution

Maintaining power quality and making sure that electrical infrastructure is durable and dependable require addressing harmonics in power systems. Harmonic mitigation involves both preventative and remedial strategies, which are essential for reducing the harmful impacts of harmonics. Active or passive harmonic filters are designed and implemented as part of preventive strategies. By attenuating undesirable components, passive filters which are made up of resistors, capacitors, and inductors are set to certain harmonic frequencies. Conversely, active filters use compensatory currents to dynamically offset harmonic distortions.

Ensuring power quality is a global concern, and several international standards have been established to regulate harmonic levels and mitigate their adverse effects on electrical systems. The IEEE 519 standard provides guidelines for limiting harmonic distortion in electrical power systems, specifying maximum allowable voltage and current harmonics at different system voltage levels. The IEC 61000 series of standards, particularly IEC 61000-3-2 and IEC 61000-3-12, set limits for harmonic emissions in low-voltage and medium-voltage networks [74]. Compliance with these standards is crucial for maintaining the reliability of electrical grids and preventing excessive harmonic distortion that could lead to overheating, reduced equipment lifespan, and operational inefficiencies. These regulations drive the development and adoption of advanced filtering techniques to ensure stable and high-quality power delivery.

2.6 Modern techniques for reducing harmonics

2.6.1 Active Power filter

In order to properly cancel out the initial harmonic disturbance, an Active Power Filter (APF) works by introducing a current or voltage distortion that is identical in size but opposite in phase to the distortion already present inside the network. Fast-switching Insulated Gate Bipolar Transistors (IGBTs) are used in these filters to produce an output current with a particular waveform. On the source (grid) side, this current creates a clean sinusoidal waveform by canceling out the harmonics produced by the load when it is delivered into the

AC lines. Based on how their circuitry is set up, APFs can be further divided into parallel and series APFs. Depending on the particular application and the kind of harmonic disturbances in the power system, each configuration has unique benefits.

➤ *Parallel APF*

APF is the most widely adopted type of APF due to its superior form and function compared to its series counterpart. As its name suggests, this filter is connected in parallel with the main power circuit as shown in Figure 2.6, strategically positioned between the voltage source and the non-linear load. The primary role of the parallel APF is to inject a compensating current into the network, effectively neutralizing the harmonic currents generated by the load. This process ensures that the waveform on the source side remains a pure sine wave, free from distortion. One of the key advantages of the parallel APF is its ability to specifically target and cancel out the harmonic components of the load current, without needing to handle the entire load current of the circuit. This selective compensation not only enhances the power quality but also contributes to the efficiency and longevity of the electrical system. Additionally, the parallel APF is designed to adapt to evolving load conditions, making it an indispensable tool for managing current disturbances such as harmonics, imbalances, and reactive power in modern power systems. [36–41].

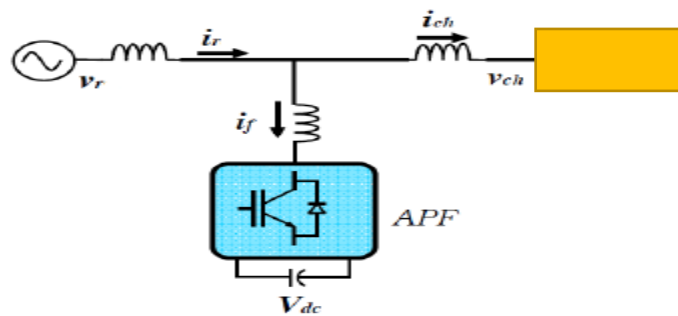


Figure 2. 6 Parallel APF.

➤ *Series APF*

The Series APF is a critical component in power systems, designed to improve voltage quality by mitigating harmonic distortions. Connected in series with the electrical network, the series APF operates as a voltage source that generates harmonic voltages. These harmonics, when combined with the network voltage, result in a clean sinusoidal waveform that is delivered to the load. The primary objective of the series APF, as illustrated in Figure 2.7, is to reduce voltage harmonic distortions and enhance the overall quality of the voltage supplied to sensitive equipment. This is accomplished by producing a sinusoidal Pulse Width Modulated (PWM) voltage waveform across the connection transformer. This waveform is then added to the supply voltage, compensating for distortions caused by the supply impedance, and ensuring that a pure sinusoidal voltage is delivered to the load.

However, a notable consideration for series APFs is that they must carry the full load current, which increases their current ratings and I^2R losses compared to parallel filters. This is particularly significant on the secondary side of the coupling transformer, where the full load current is managed, demanding careful design and implementation to maintain efficiency and reliability. [40]

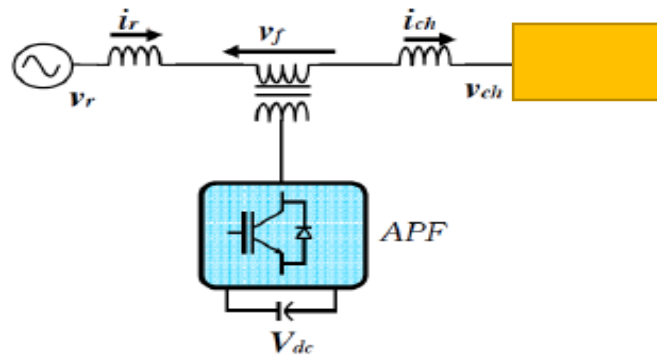


Figure 2. 7 Series APF.

2.6.2 Hybrid Harmonic Mitigation Techniques

Hybrid arrangements of Series and Parallel Active Power Filters (APFs) are being used more frequently to lower harmonic distortion levels in power networks, as Figure 2.8

illustrates. This is especially true when Passive Filters (PF) with fixed compensation characteristics are not able to adequately filter current harmonics. By removing harmonic currents using a switching-mode power converter, APFs overcome the drawbacks of PFs. Unfortunately, APFs are not widely used in power systems because to their large power ratings and high construction costs in industrial applications. Hybrid filter (HF) topologies have been designed to effectively regulate reactive power and harmonic currents in order to tackle these difficulties. When a low-cost PF is integrated into the HF, the active converter's power rating is lowered considerably in comparison to an independent APF, making this a more economical alternative that nevertheless achieves good harmonic reduction [42–47].

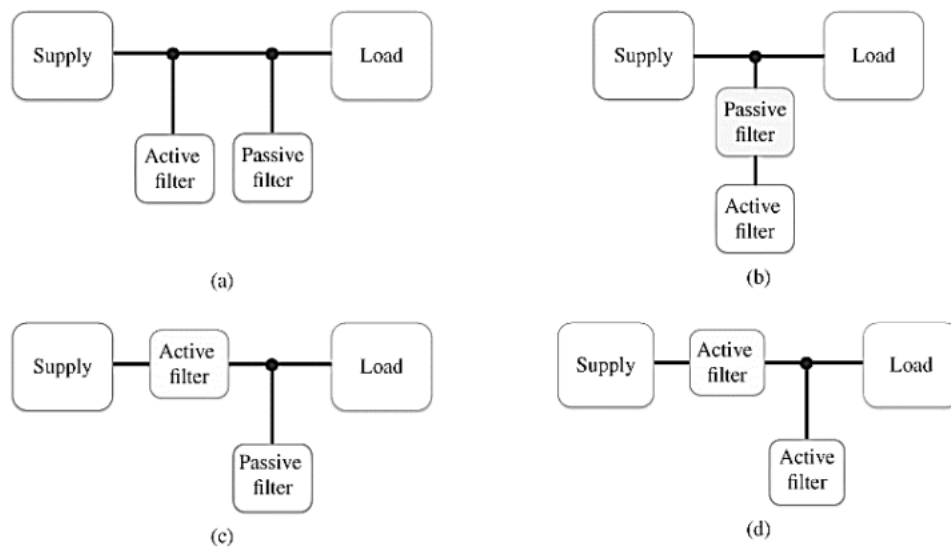


Figure 2. 8 Hybrid connections of active and passive filters.

2.7 Active power filter Topologies

Nonlinear loads at high voltages have become much more common in industrial settings. These nonlinear loads cause harmonic distortions, which lower power quality. Applying traditional active filters to high-voltage, high-power systems presents difficulties. Nevertheless, the incorporation of multilayer inverters into active filters provides an effective way to reduce harmonics in these kinds of systems, doing away with the requirement for big, costly transformers.

Because multilevel inverters (MLIs) can provide high-quality voltage waveforms with lower harmonic distortion and switching losses, they are crucial in power conversion applications. Numerous topologies have been created, such as flying capacitor multilevel

inverters (FCMLI), which rely on capacitors to reach various voltage levels, and diode-clamped multilevel inverters (DCMLI), which employ diodes for voltage clamping. While packed U-cell (PUC) inverters, such PUC5 and PUC7, provide compact designs with fewer components, cascaded H-Bridge (CHB) inverters offer a modular structure with distinct DC sources for each H-bridge. Medium- and high-voltage applications can benefit from the excellent scalability of modular multilevel converters (MMC).

While hybrid inverters mix characteristics from many topologies for flexible designs, asymmetrical cascaded inverters use uneven DC sources to produce more levels with fewer cells. Furthermore, for cost-effective solutions, reduced component MLIs concentrate on reducing switches, capacitors, and diodes. With selection criteria based on voltage level, efficiency, cost, and control complexity, these configurations serve a variety of applications, such as industrial drives, renewable energy systems, and HVDC transmission. Because PUC is more economical than other topologies, it is the topology that is most frequently employed in single-phase applications.

2.7.1 Diode-Clamped Multilevel Inverter

The first practical generation of MLI is the neutral-point-clamped (NPC) PWM architecture (Figure 2.9); clamping diodes are used to clamp this multilevel inverter. It aids in lowering the voltage tension in electrical equipment. First presented by Nabae et al. in 1981, the three-level NPC was regarded as the first-generation MLC [48, 49]. However, if utilized as high-power converters, this architecture has technical issues. It requires high-speed clamping diodes that can withstand reverse recovery stress. The design complexity is a major problem because of the diodes' series connection. The maximum output voltage is equal to half of the input DC voltage. Increasing the amount of components, including switches and diodes, will easily solve this issue [50–52]. Like other approaches, this topology has pros and disadvantages. One advantage is that it uses back-to-back inverters and has a simple control method. The switch voltage is just half of the DC-link voltage, which is another advantage. Another advantage is that when the number of levels increases along with the distortion, the amount of material decreases. Aside from the capacitor's modest and preloaded capacity, efficiency is also quite high at the fundamental frequency. Notwithstanding these advantages, the diode clamped multilevel inverter has many

drawbacks, including the requirement for more clamping diodes as the number of levels rises and when control and monitoring are improper, a significant amount of DC will be released [53].

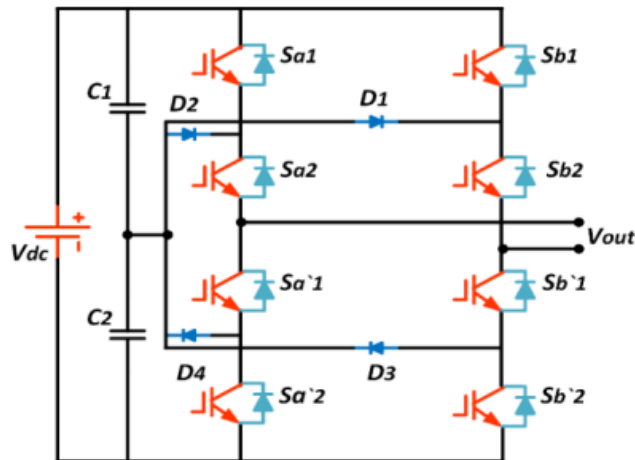


Figure 2. 9 Diode-Clamped Multilevel Inverter.

2.7.2 Capacitor-Clamped (Flying Capacitor)

Similar to the diode-clamped inverter in [54, 55], this multilevel inverter type [56, 57] clamps the unit's voltage using capacitors rather than diodes [56]. Another modification of the multilayer inverter architecture was the flying capacitor (FLC) converter, which was first introduced by [57, 58] in the 1990s. The clamped switching cell of the capacitors was serially connected during its production, enabling the passage of restricted voltages to the electrical devices via the capacitors. Capacitors, rather than diodes, are what separate the DC supply voltages, which is how it varies from the diode-clamped MLI. Nevertheless, the voltage across each switch and capacitor is represented by V_{DC} . $(2m-2)$ switches and $(m-1)$ capacitors are required for an inverter with a m level flying cap [53]. A ladder-structured capacitor is present on the DC side of this design, and the voltage flowing through each adjacent capacitive branch varies. The output voltage phase size, which is equal to V_{DC} , is determined by taking this voltage differential into account. The main advantage of the flying capacitor inverter over the diode-clamped multilevel converter is that it has internal voltage level redundancies. In other words, two or more separate valid switches must be combined

in order to provide a comparable output voltage. Additionally, the flying capacitor topology exhibits phase redundancy, whereas the diode-clamped inverters only show line redundancy. Because it serves as the foundation for the application of capacitive branch voltage balancing control approaches, this aspect is crucial. The number of duplicate states is determined by the output voltage level; in this type of MLC, the capacitor voltage balance needs to be maintained. This can be accomplished by employing the proper control sequences, which will allow the internal capacitors to gradually recharge and discharge uniformly. However, the following are some hazards [59, 60]:

- Capacitors generally struggle to maintain stable voltage levels, and precharging all of them to the same voltage level is a complex and challenging task.
- Switching has a low efficiency. A diode-clamped MLI uses a number of capacitors, which are typically more costly and large than the clamping diodes. Figure 2.10 below depicts a flying capacitor multilevel topology.

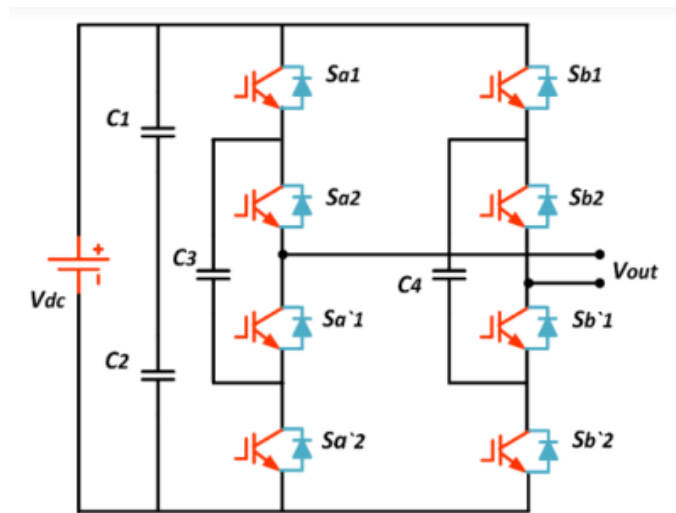


Figure 2. 10 Capacitor-Clamped (Flying Capacitor).

2.7.3 Cascaded H-Bridge

In the middle of the 1970s, Baker and Bannister [61] patented the first converter topology that could generate multilevel voltages by using a certain DC voltage source. In order to overcome the limitations of FLC and NPC topologies, including the need for extra clamping

diodes and capacitors, a cascaded H-bridge converter was proposed by [62]. Compared to diode-clamped and flying capacitor inverters, the cascaded H-bridge MLI uses fewer components per switching stage. The word "H-bridge" refers to the collection of switches and condensers in a cascade H-bridge MLC that consists of separate DC voltage sources [63]. This configuration makes use of multiple DC sources in the H-bridge inverter. Because multiple power conversion cells are connected, each converter produces output at varying levels, as seen in Figure 2.11. Two switches and condensers make form the H-bridge. Each H-bridge produces a sinusoidal voltage output while achieving a different input DC value. The inverter uses a series of attached H-bridge cells, each of which generates three distinct DC voltage levels: zero, negative, and positive. The average voltage output of each H-bridge cell is calculated by adding up all of the voltages that are generated. The number of output voltage levels will be $(2m+1)$ if there are m cells. The structure of a five-level H-bridge inverter is shown in Figure 2.11. Lai and Peng's (1997) study, which was subsequently patented in 1997, concentrated on the quirks of the FLC and NPC topologies.

Since then, a number of applications have shown a great deal of interest in cascaded H-bridge MLCs (CHBMLCs) because of their appealing features, which include:

- Easy packing and storage.
- Reducing stress by generating voltage in common mode.
- Tiny input current distortions.

It can operate at both basic switching frequencies.

- The output waveform's THD is extremely low in the absence of a filter circuit.

Nevertheless, the inverter has shortcomings, including:

- Different DC sources or capacitors are required for each module.
- A more sophisticated controller is necessary due to the increased number of capacitors.

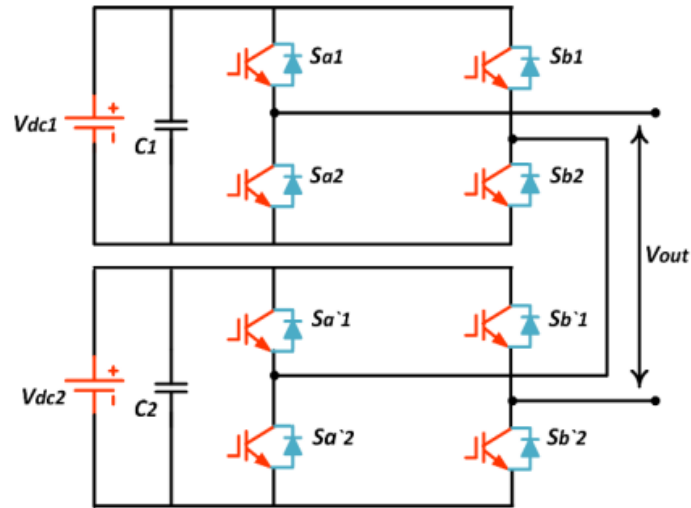


Figure 2. 11 Cascaded H-Bridge.

2.7.4 PUC INVERTER

Youssef Ounejjar and colleagues were the pioneers in introducing the Packed U-Cell (PUC) inverter topology [64]. As illustrated in Fig. 2.12, this topology consists of six active switches, a single isolated DC supply, and a DC capacitor serving as a secondary DC source (or dependent DC source). This configuration is the focus of our research, and subsequent sections will delve into the modeling and control strategies for this topology.

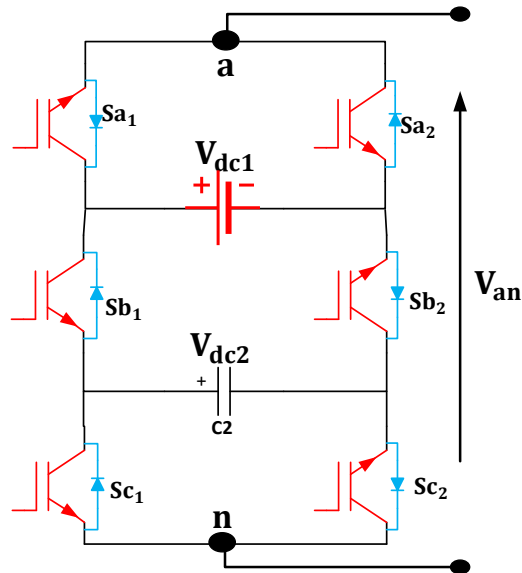


Figure 2. 12 Single-Phase PUC inverter.

Table 2. 1 Comparative Analysis of the PUC 7 Inverter and Conventional Seven-Level Inverter Topologies

Feature	Diode-Clamped (NPC)	Flying Capacitor (FLC)	Cascaded H-Bridge (CHB)	Hybrid Cascaded H-Bridge	Packed U-Cell (PUC)
Capacitors	6	6	3	2	2
Clamping Diodes	10	0	0	0	0
Switches	12	12	12	8	6
Control Complexity	High	High	Moderate	Moderate	Low
Efficiency	Moderate	Moderate	High	High	High
Voltage Balancing	Challenging	Requires additional control	Moderate	Simplified	Simplified
Application Suitability	Medium-to-high voltage	Medium voltage	High voltage	High voltage	Suitable for single-phase applications
Cost-effectiveness	Moderate	Expensive	High	Moderate	Economical

2.8 Conclusion

Power quality, as defined at the conclusion of this chapter, refers to the reliability and stability of the energy being utilized. Electrical disturbances, particularly harmonics that originate within the system, can lead to damage or malfunction of critical equipment, resulting in costly repairs or replacements and reduced productivity. A thorough understanding of power quality issues and the available mitigation strategies is essential for selecting a cost-effective system.

Chapter 3: System Modeling and Control Design

3.1 Introduction

This chapter presents the detailed modeling and control strategies for a double-stage, single-phase PUC7 inverter system, which integrates photovoltaic (PV) power into the electrical grid. The focus is on optimizing power generation, ensuring grid compatibility, and addressing the challenges posed by nonlinear loads, such as harmonic distortion and reactive power compensation. Key components, including the PV array, PUC7 inverter, and boost converter, are modeled, with an emphasis on their operation under real-world conditions. Additionally, advanced control techniques such as Maximum Power Point Tracking (MPPT) using the Perturb and Observe (P&O) algorithm, Modified P-Q Theory for power injection, and Model Predictive Control (MPC) are introduced to enhance system efficiency and stability. This chapter sets the foundation for the design and operation of an efficient, grid-connected PV system that ensures high power quality and optimal energy utilization.

3.2 System configuration

The proposed configuration of the double-stage, single-phase PUC7 inverter, along with the proposed MPC controller and its corresponding control scheme, are illustrated in Fig 3.1. The system that is being studied consists of an AC source, a nonlinear load that is connected in series, and the PUC7 inverter that is connected in parallel to the grid via a line inductor (L_f) at the PCC. The PV system is connected to the PUC7 inverter's single DC-link capacitor by means of a boost converter, which has the ability to raise the voltage of the PV array to a high DC-link voltage. The main objectives of this specific configuration are the efficient integration of generated PV power into the electrical grid while ensuring high-quality grid current. Furthermore, this setup aims to address reactive power compensation and alleviate harmonic components induced by nonlinear loads at the PCC.

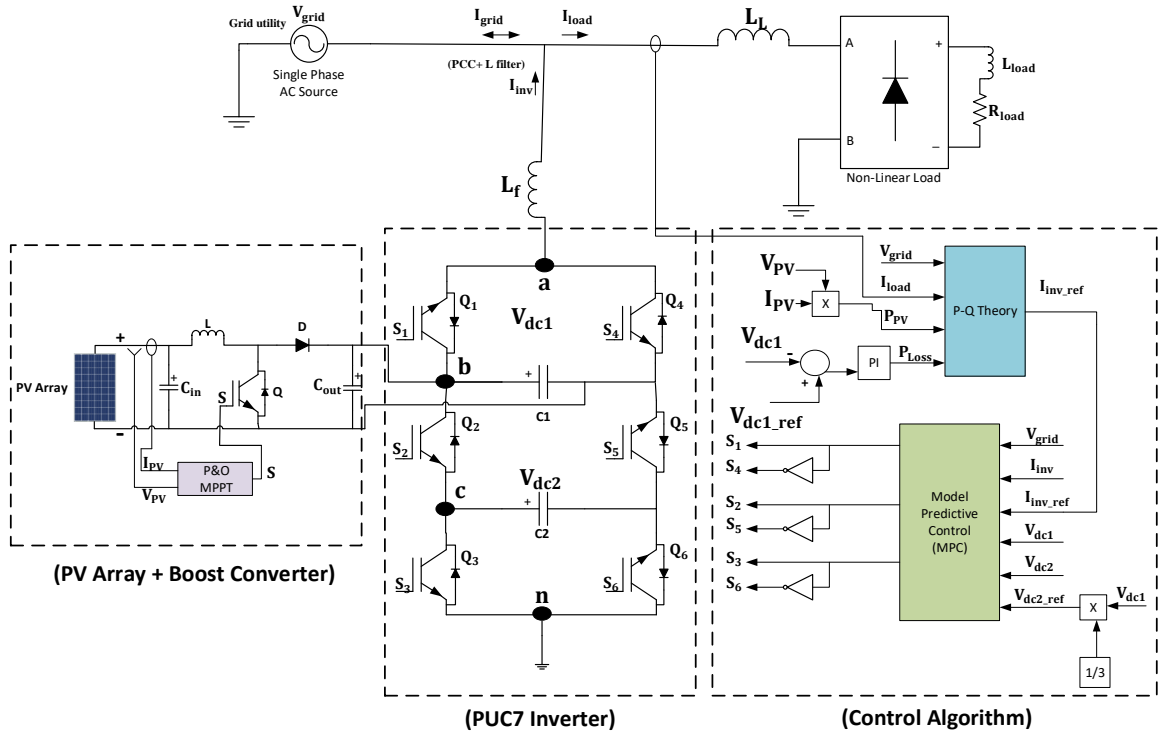


Figure 3. 1 The proposed configuration of the double-stage, single-phase PUC7 inverter.

3.2.1 PV array modelling

Through the photovoltaic effect, solar radiation is directly converted into DC electric power using a photovoltaic cell. Following its operation, the electric circuit that is capable to simulate the behavior of PV cell conversion consists of a DC current source connected in parallel with a diode as depicted by dashed line in Fig 3.2(a). Upon adding series and shunt resistance, the previous model is improved to account for the PV cell losses and leakage current in the PV junction. This model (Fig 3.2(a)) is widely adopted to model the behavior of a real PV module [13, 65]. Real life applications of PV involve the connection of more than one module in series or in parallel. This PV array consists of N_{par} parallel strings with N_{ser} series-connected modules.

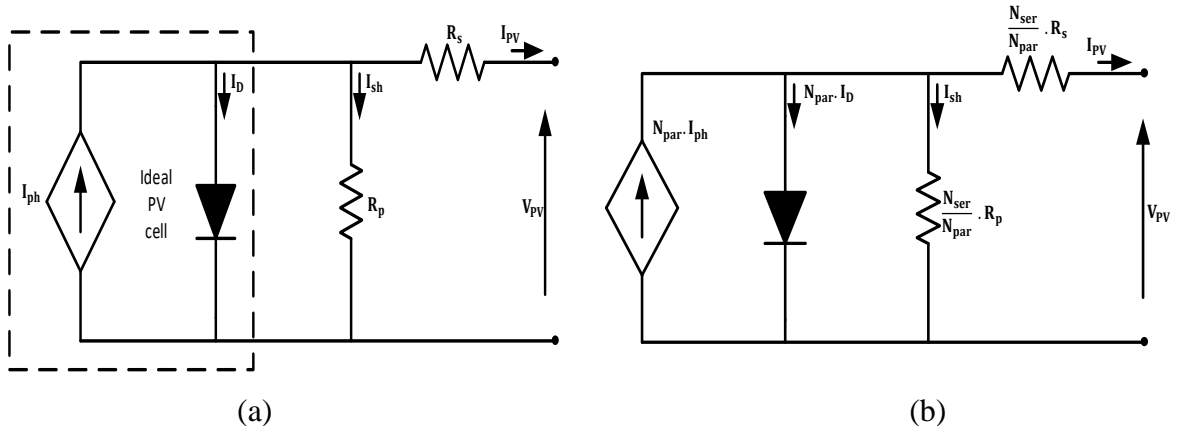


Figure 3. 2 The photovoltaic (PV) source's electrical modeling includes: (a) the PV array and (b) PV module.

The output voltage is related to the PV array's output current by equation (3.1):

$$I_{PV} = N_{par} \cdot I_{ph} - N_{par} I_D - \frac{V_{PV} + I_{PV} \frac{N_{ser}}{N_{par}} R_s}{\frac{N_{ser}}{N_{par}} R_p} \quad (3.1)$$

The photocurrent, denoted as I_{ph} , is a variable that is influenced by both irradiance and temperature, as stated in equation (3.2).

$$I_{ph} = \frac{G}{G_{ref}} \left(I_{ph_ref} + \alpha_{T_ISC} (T - T_{ref}) \right) \quad (3.2)$$

The current flowing via a diode, denoted as I_D , is determined by the well-known Shockley equation (3.3):

$$I_D = I_S \left(\exp \left[\frac{V_{PV} + I_{PV} \frac{N_{ser}}{N_{par}} R_s}{\alpha \cdot V_{th} \cdot N_{ser}} \right] - 1 \right) \quad (3.3)$$

where α is the ideality factor of the diode and I_S is the reverse saturation current that is given as equation (3.4)

$$I_S = \frac{I_{SC,ref} + \alpha_{T_ISC} (T - T_{ref})}{\exp \left[\frac{V_{oc,ref} + \alpha_{T_Voc} (T - T_{ref})}{\alpha \cdot V_{th} \cdot N_{ser}} \right]} \quad (3.4)$$

In the following, V_{th} is the thermal voltage of N_s series connected cells constituting one PV module. This voltage mainly depends on the PV cell temperature:

$$V_{th} = \frac{N_s K}{q} \cdot T \quad (3.5)$$

One must distinguish N_s , the number of a module's series-connected cells, from N_{ser} , the number of series-connected modules in a photovoltaic array.

3.2.2 PUC7 inverter

The configuration of the PUC converter is recent and it is based on the association of packed U cells where two switches and a capacitor constitute the cell [64]. Authors in [64] introduced the PUC inverter, which consists of six active switches, an isolated DC supply, and a DC capacitor that acts as a dependent DC source, as shown in Fig 3.1.

The PUC7 has the same number of components as other designs, but it has lower power losses and costs due to reduced switch count. Table 3.1 exhibits the output voltage levels, with switches S1, S2, and S3 functioning in conjunction with switches S4, S5, and S6, respectively. It is important to note that each pair of switches, namely (S1, S4), (S2, S5), and (S3, S6), cannot be activated simultaneously.

Table 3. 1 PUC7 inverter state switching.

State Switching (x)	s ₁	s ₂	s ₃	s ₄	s ₅	s ₆	V _{an}
State 1	1	0	0	0	1	1	V _{dc1}
State 2	1	0	1	0	1	0	V _{dc1} -V _{dc2}
State 3	1	1	0	0	0	1	V _{dc2}
State 4	1	1	1	0	0	0	0
State 5	0	0	0	1	1	1	0
State 6	0	0	1	1	1	0	-V _{dc2}
State 7	0	1	0	1	0	1	V _{dc2} -V _{dc1}
State 8	0	1	1	1	0	0	-V _{dc1}

The PUC inverter can produce seven levels of output voltage by using two capacitors. One-third of the DC bus voltage (V_{dc1}) should be the capacitor's voltage (V_{dc2}), so that the output voltage levels are $0, \pm V_{dc2}, \pm 2V_{dc2},$ and $\pm 3V_{dc2}$. However, the primary constraint of the PUC7 inverter is that it cannot provide an output voltage greater than the DC bus voltage. The benefit of employing the PUC inverter lies in its capability to mitigate load voltage harmonics by segmenting the DC bus voltage into multiple levels. This, in turn, diminishes

the requirement for bulky filters at the inverter's output. The mathematical representation of the single-phase active power filter system utilizing the PUC7 inverter is depicted in the following equations:

$$\frac{di_{inv}(t)}{dt} = -\frac{R_f}{L_f} I_{inv} + \frac{1}{L_f} (V_{an} - V_{grid}) \quad (3.6)$$

$$\frac{dV_{dc}(t)}{dt} = \frac{1}{C} I_{inv} \quad (3.7)$$

Where V_{dc} is the voltage across the DC-link capacitor, I_{inv} and V_{grid} are the inverter's current and grid voltage, respectively.

The PUC7 inverter generates a voltage (V_{an}) that is based on the states of the switches s_1 , s_2 and s_3 . To simplify the estimation of (V_{an}), two variables, **S1** and **S2**, are defined based on the following equations:

$$\mathbf{S1} = s_1 - s_2 \quad (3.8)$$

$$\mathbf{S2} = s_2 - s_3 \quad (3.9)$$

Applying Kirchhoff's Law (KVL) to the PUC7 circuit shown in Fig.3.1 allows to derive the equation of the inverter's generated voltage, that is:

$$\begin{aligned} V_{an} &= V_{ab} + V_{bc} + V_{cn} \\ V_{an} &= (s_1 - 1) \cdot V_{dc1} + (1 - s_2) \cdot (V_{dc1} - V_{dc2}) + (1 - s_3) \cdot V_{dc2} \\ V_{an} &= (s_1 - s_2) \cdot V_{dc1} + (s_2 - s_3) \cdot V_{dc2} \end{aligned} \quad (3.10)$$

Upon substituting (3.8) and (3.9) in (3.10), one can find the simplified equation of V_{an}

$$V_{an} = \mathbf{S1} \cdot V_{dc1} + \mathbf{S2} \cdot V_{dc2} \quad (3.11)$$

Moreover, the voltage across the capacitors may be described as follows in terms of their charging current:

$$\begin{aligned} V_{dc1} &= -\mathbf{S1} \cdot \frac{1}{C_1} \int i_{inv} dt \\ V_{dc2} &= -\mathbf{S2} \cdot \frac{1}{C_2} \int i_{inv} dt \end{aligned} \quad (3.12)$$

3.2.3 Boost Converter

A boost converter is a type of DC/DC switch-mode power supply designed to elevate the input voltage from a direct current (DC) source, such as a photovoltaic (PV) array. Its purpose is to generate a stable, higher output voltage. The boost converter comprises essential components, including an inductor, a semiconductor switch (usually a MOSFET), a diode, and a capacitor.

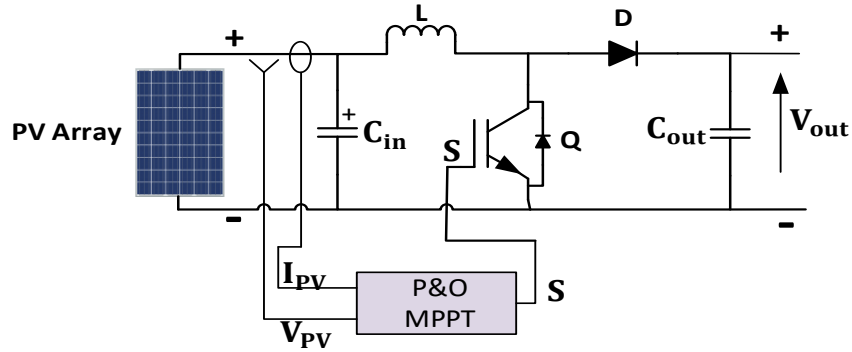


Figure 3. 3 DC-DC boost converter with MPPT

A boost converter is controlled using the MPPT method, specifically the P&O algorithm. The goal is to achieve the MPP by dynamically adjusting the output voltage of the PV panel. Figure 3.3 illustrates a PV DC-DC boost converter with integrated MPPT functionality.

The relationship between the converter’s output voltage (V_{out}) and its input voltage (V_{pv}) is expressed by Equation (3.13)

$$V_{out} = \frac{V_{pv}}{1-D} \quad (3.13)$$

Here, (D) represents the duty ratio of the MOSFET switch. The duty ratio is modulated through a PWM signal, which is then applied to the MOSFET gate. By adjusting the duty cycle, the boost converter optimizes its output voltage based on the available solar energy.

3.3 MPPT controller

A method called maximum power point tracking (MPPT) can optimize a photovoltaic system's power generation under a variety of environmental circumstances. The MPP of the PV array is a unique point at which maximum power is obtained and this operating point corresponds to a given PV voltage and current obtained at a given environment and load conditions. One of the most commonly used MPPT algorithms is Perturb and Observe (P&O). It operates by altering the voltage or current of the PV array gradually and assessing the ensuing power.

The MPPT controller continues to adjust the voltage or current (by modifying the chopper's duty cycle) in the same direction if the power keeps increasing. When the power drops, the controller adjusts the control signal in the opposite direction. This process is repeated as many as needed to meet the condition stating that the variation of the power with respect to the change of the voltage or current is null. This point is known as the MPP of the 'P-V' characteristic. These steps are summarized in the flowchart of P&O technique that is depicted in Fig 3.4. As it can be noticed from the flowchart, the P&O algorithm is simple, easy to implement and therefore widely applicable [66, 67].

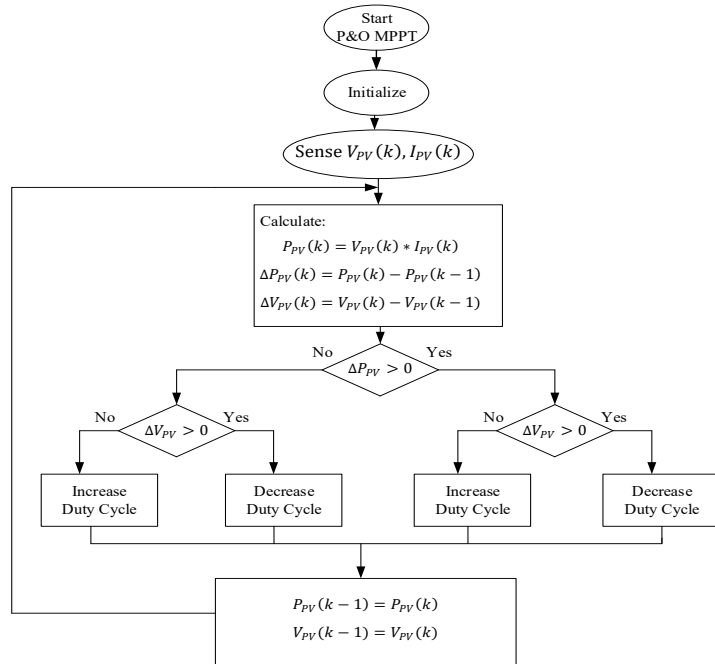


Figure 3. 4 The P&O method flowchart

3.4 Modified P-Q theory for power injection

The theory of instantaneous reactive power, commonly referred to as the 'p-q' theory, stands out as one of the most effective approaches for obtaining instantaneous reference signals crucial for active power filtering. Originally designed for three-phase systems, encompassing both three- and four-wire configurations [68], the advantages of the multi-phase 'p-q' theory can now be expanded to single-phase systems through a recently proposed extension. Moreover, in scenarios involving unbalanced supply voltage and/or load conditions, the single-phase 'p-q' theory demonstrates the capability to generate a sinusoidal source current and efficiently manage multi-phase systems, surpassing the performance of the three-phase theory [69].

The core concept of the single-phase 'p-q' theory involves shifting the initial system voltage and current by $\pi/2$ in either direction, creating a pseudo two-phase system. This approach facilitates the expression of the entire system in α - β coordinates, where α -axis values correspond to the initial source voltage and load current, and β -axis quantities result from the displacement of the source voltage and load current by $\pi/2$. The representation of single-phase source voltage involves a $\pi/2$ forward shift in α - β coordinates.

$$\begin{bmatrix} V_\alpha(\omega t) \\ V_\beta(\omega t) \end{bmatrix} = \begin{bmatrix} V_{grid}(\omega t) \\ V_{grid}(\omega t + \frac{\pi}{2}) \end{bmatrix} \quad (3.14)$$

In a similar way, the load current representation in a coordinate system with a $\pi/2$ forward shift.

$$\begin{bmatrix} I_\alpha(\omega t) \\ I_\beta(\omega t) \end{bmatrix} = \begin{bmatrix} I_{load}(\omega t) \\ I_{load}(\omega t + \frac{\pi}{2}) \end{bmatrix} \quad (3.15)$$

The power components 'p' and 'q' can be represented together since they are related to the same α - β voltages and currents.

$$\begin{bmatrix} p(\omega t) \\ q(\omega t) \end{bmatrix} = \begin{bmatrix} V_\alpha(\omega t) & V_\beta(\omega t) \\ -V_\beta(\omega t) & V_\alpha(\omega t) \end{bmatrix} \cdot \begin{bmatrix} I_\alpha(\omega t) \\ I_\beta(\omega t) \end{bmatrix} \quad (3.16)$$

The expressions for the $p(\omega t)$ and $q(\omega t)$ are:

$$p(\omega t) = \bar{p}(\omega t) + \tilde{p}(\omega t) \quad (3.17)$$

$$q(\omega t) = \bar{q}(\omega t) + \tilde{q}(\omega t) \quad (3.18)$$

The instantaneous fundamental active and reactive power is represented by the DC components $\bar{p}(\omega t)$ and $\bar{q}(\omega t)$, while the harmonic power is represented by the AC components $\tilde{p}(\omega t)$ and $\tilde{q}(\omega t)$. In the following, the AC component ($\tilde{p}(\omega t)$) of active power and the overall reactive power ($q(\omega t)$) are employed for computing the harmonic reference current.

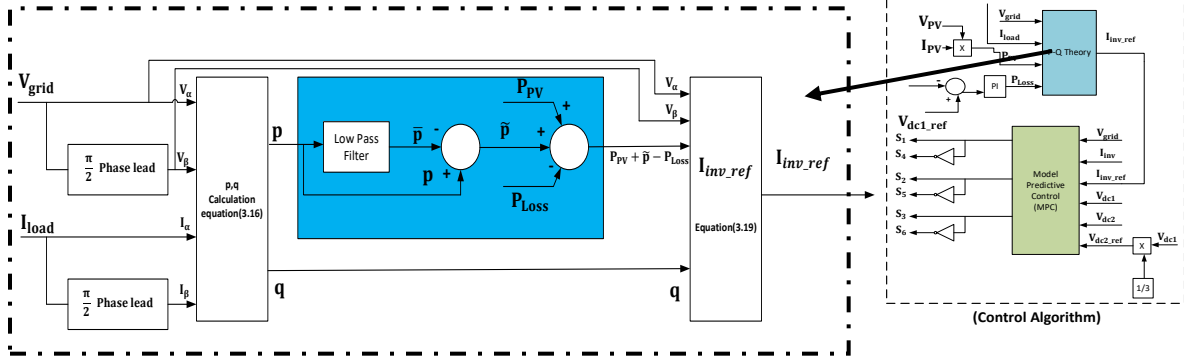


Figure 3. 5 Modified ‘p-q’ power injection.

To counterbalance voltage source inverter switching losses and maintain the desired DC-link voltage, the shunt active power filter draws a minimal amount of real power (P_{Loss}) either from the single-phase AC source or an external power source. In addition to reducing harmonics, it will provide active power from the PV array connected via a boost converter to the inverter. To inject this power into the grid, we thus updated the PQ theory and included the PV power with the AC component ($\tilde{p}(\omega t)$) of active power. Therefore, as seen in Fig 3.5, we need a particular feedback signal to force the control circuit to include power and harmonics in its output. The reference compensating current can be obtained by this equation:

$$I_{inv_ref} = \frac{((V_{\alpha} * (P_{PV} + \tilde{p} - P_{Loss})) - V_{\beta} * q)}{V_{\alpha}^2 + V_{\beta}^2} \quad (3.19)$$

3.5 MPC procedure

MPC is a control technique that is more sophisticated and efficient than traditional PID control. It forecasts the future behavior of the controlled variable using a mathematical model of the system under study. MPC is a powerful and successful technique for controlling power converters in general. The suggested MPC allows the PUC7 inverter to operate in both the active power filter and grid-connected PV system modes. The flowchart in Fig 3.6 illustrates the functionality of the suggested MPC.

For each of the eight switching states, the inverter current (I_{inv}) measured values, grid voltage (V_{grid}), and capacitor voltages (V_{dc1} , V_{dc2}) are used to calculate the anticipated values of the inverter current (I_{ref_cal}) and the capacitor voltage (V_{dc2_cal}). Next, the best switching state that matches its minimal value is chosen using a cost function (g).

The switching pulses are created based on the suitable switching state picked up by the MPC from the switching table, and they provide the PUC7 inverter with the ideal switching state selected for the next sampling period. The variables that the suggested MPC must regulate are the capacitor voltage (V_{dc2}) and the future inverter current (I_{inv}). The cost function (g) incorporates these control goals in the following function:

$$g = \lambda_1 (I_{ref_cal}(k+1) - I_{inv_ref}(k))^2 + \lambda_2 (V_{dc2_cal}(k+1) - V_{dc2_ref}(k))^2 \quad (3.20)$$

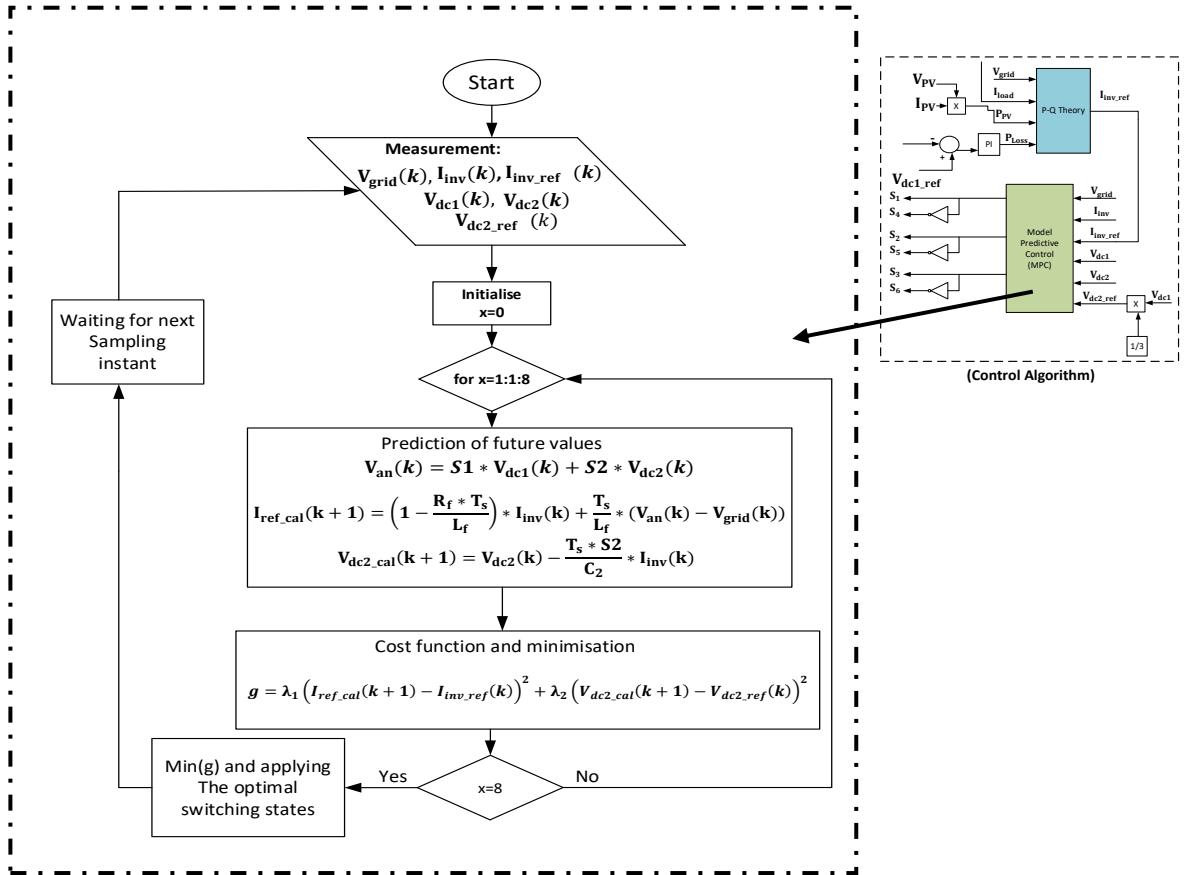


Figure 3. 6 Model predictive control (MPC).

Where the weighting factors are denoted by λ_1 and λ_2 . A branch and bound approach may be used to reduce the number of simulations needed to determine the appropriate value for the weighting factor. In our research, we adopt a uniform weighting factor, where both λ_1 and λ_2 are set to 1, instead of employing an optimization process to determine the appropriate weighting factor. By adopting such a strategy, no tuning of parameters is required during the implementation of the controller.

The inverter current's reference and future values are provided by the variables $I_{inv_ref}(k)$ and $I_{ref_cal}(k + 1)$, respectively. Likewise, the reference and future values of the DC-link capacitor voltages are indicated by the variables $V_{dc2_ref}(k)$ and $V_{dc2_cal}(k + 1)$, respectively. These variables are essential for evaluating and regulating the inverter.

The derivative of the inverter current $\frac{dI_{inv}(t)}{dt}$, is replaced by a forward Euler approximation.

In other words, the derivative of the current is reduced to the following formula:

$$\frac{dI_{inv}(t)}{dt} = \frac{I_{inv}(k+1) - I_{inv}(k)}{T_s} \quad (3.21)$$

Substituting Eq. (3.21) in Eq. (3.6) allows obtaining the equation to forecast the load current at time $(k+1) T_s$ in the future for each of the eight voltage vector values $V_{an}(k)$ produced by the inverter.

This expression is given as:

$$I_{ref_cal}(k + 1) = \left(1 - \frac{R_f * T_s}{L_f}\right) * I_{inv}(k) + \frac{T_s}{L_f} * (V_{an}(k) - V_{grid}(k)) \quad (3.22)$$

The derivative of the capacitor voltages may be calculated using the same estimate of the derivative as in the previous equation:

$$\frac{dV_{dc}(t)}{dt} = \frac{V_{dc}(k+1) - V_{dc}(k)}{T_s} \quad (3.23)$$

Combining Eq. (3.7) and Eq. (3.23), the capacitor voltage's discrete-time equation can be derived as follows:

$$V_{dc2_cal}(k + 1) = V_{dc2}(k) - \frac{T_s * S_2}{C_2} * I_{inv}(k) \quad (3.24)$$

3.6 Conclusion

In conclusion, Chapter 3 provides a comprehensive exploration of the innovative double-stage, single-phase PUC7 inverter system, focusing on both its modeling and control strategies. The detailed modeling of the PV array, PUC7 inverter, and boost converter offers a clear understanding of their individual roles in optimizing power generation and grid integration. By addressing critical issues such as reactive power compensation, harmonic distortion, and voltage stabilization, this chapter lays the groundwork for achieving high-efficiency, reliable PV systems in real-world applications. The MPPT controller, driven by the P&O algorithm, ensures dynamic voltage adjustment for optimal power output, while the modified P-Q theory facilitates effective power injection and harmonic compensation in single-phase systems. Furthermore, the implementation of Model Predictive Control (MPC) enhances the inverter's operational efficiency, providing advanced predictive capabilities for better performance and stability. Together, these advanced modeling techniques and control strategies form the backbone of a robust, high-performance PV power conversion system, paving the way for successful implementation and optimization in grid-connected applications.

In the next chapter, we will validate the effectiveness of these designs through both simulation and experimental testing, demonstrating their practical applicability and performance in real-world scenarios.

Chapter 4: System assessment: simulation and experimentation

4.1 Introduction

This chapter focuses on validating the performance of the proposed multifunction solar active filter in a grid-connected PV system under real outdoor conditions. Section 4.2 introduces the identification process of the PV array parameters, which are essential for simulating and implementing the PV system. An experimental setup is used to trace the I-V curve of the PV array, followed by parameter extraction through an optimization process employing a modified African Vulture Algorithm. These parameters are then utilized in both simulation and experimental validation to ensure accurate representation of the PV system's behavior. Section 4.3 presents the experimental results obtained using a laboratory prototype, which includes the proposed PUC7 inverter, boost converter, and modified control algorithms (MPPT, MPC, and the modified p-q controller). The efficacy of the control system is evaluated across three distinct scenarios, assessing its capabilities in harmonic mitigation, maximum power point tracking, power balancing, and grid power injection. This chapter highlights the robustness of the proposed system in achieving low THD, efficient power distribution, and multifunctionality under varying load and environmental conditions.

4.2 PV IDENTIFICATION AND SIMULATION RESULTS

4.2.1 PV ARRAY IDENTIFICATION

Conducting simulation scenarios of PV system, whether it is islanded or grid connected, requires the data of each component involved in the system depicted in Fig 2.1. The preceding section has outlined the modeling of each of these components. Some components are designed such, as the chopper, the inverter, and the filter, while others are computed, such as the parameters of the proposed controllers. However, the parameters of the PV array model, typically supplied by the manufacturer, are based on standard test conditions (STC) data. These parameters include open circuit voltage, short circuit current, maximum power, maximum power point voltage, and maximum power point current at STC. For simulation purposes, one needs the internal parameters of the PV array as well as those of the other PV system components. In the present study, an experimental setup is proposed to identify these

parameters. Fig 5.1 shows the main components of the proposed setup. The PV array is connected to a RC circuit with two switches. The identification process is carried out on two steps, 1) measurement of I-V curve then 2) extraction of the PV array model's parameters. To obtain the I-V curve, the capacitor is charged by turning on switch Q_1 to the maximum voltage of the PV that is the open circuit voltage then discharged over the resistance to enable conducting next measurement.

While the current drops from short-circuit current (I_{sc}) to zero throughout the charging process, the capacitor's voltage rises from 0 to the PV array's open-circuit voltage (V_{oc}). To get the PV current and voltage data, two sensors are used. The resulting I-V may then be plotted, as seen in Fig 4.2 (a). The second step, aiming at extracting the PV parameters from the measured I-V curve, is carried out by solving equation (4.1):

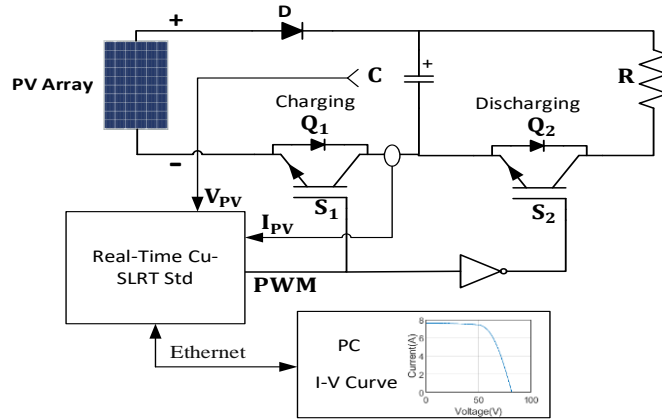


Figure 4. 1 The I-V curve tracer using capacitor charging and discharging process.

$$RMSE = \sqrt{\frac{1}{n} \sum_{i=1}^N (I_{PV_measured} - I_{PV})^2} \quad (4.1)$$

where:

- $I_{PV_measured}$ is the measured PV current.
- I_{PV} is the computed PV current.
- N is the total number of measurements (samples).

It is evident from Eq. (3.1) that in order to calculate the PV current, one must be aware of the model parameters. To do this, solving Eq.(4.1) is converted to an optimisation process where a metaheuristic algorithm is employed, as detailed in [65] . In fact, a modified African Vulture algorithm is selected for its good performance then applied to minimize Eq. (4.1).

The acquired parameters of the PV array are displayed in Table 1. It has to be mentioned that besides identification of the PV array parameters, the I-V curve will be used to check the effectiveness of the proposed control system in both simulation and experimental validation.

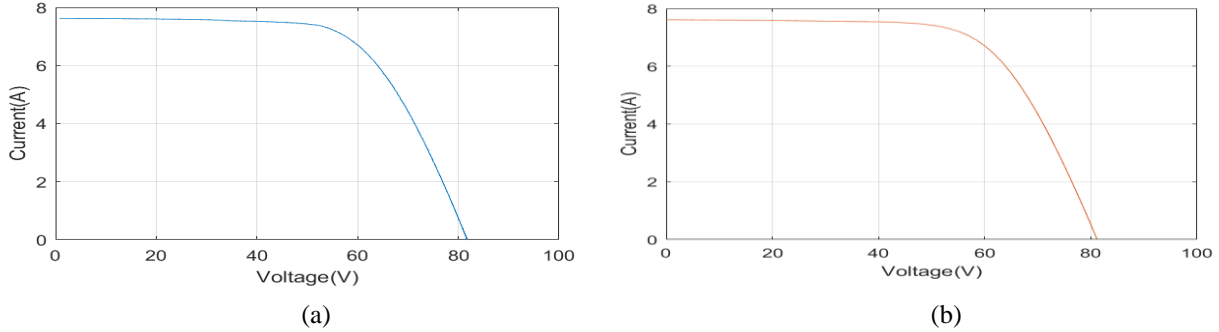


Figure 4. 2 I-V properties of the PV array in use, (a) Experimental curve, (b) Simulated curve.

Table 4. 1 PV array identification’s results

Parameter	$I_{PV}(A)$	$I_s(A)$	a	$R_s(\Omega)$	$R_p(\Omega)$
Value	7.6418	$6.1593 \cdot 10^{-8}$	1.1221	0.4273	146.389

Upon substituting the parameters shown in Table 4.1 in the model of the PV array, Eqs. (3.1, 3.3 and 3.5), and solving them for the PV current, the I-V curve of the PV array is obtained as shown in Fig 4.2 (b). Notice that the values of the voltage being used while solving Eqs. (3.1, 3.3 and 3.5) are those obtained from the experimental part.

4.2.2 SIMULATION RESULTS

To evaluate the performance of the suggested design, a MATLAB/Simulink software, comprising every part of the PV system mentioned in section 1, has been created. The simulation runs at a sampling frequency of 30 kHz, while the controller (MPC) operates at a sampling frequency of 20 kHz. Table 4.2 depicts the data of these components. Before performing both the experimentation and simulation test in order to assess the suggested PV

system's efficacy, both experimental and simulated I-V have been identified and used to derive the experimental and simulated P-V curves, respectively, by multiplying the PV voltage by the PV current.

Fig 4.3 illustrates the measured and the computed P-V curves using extracted PV model parameters. They are obtained under the weather conditions when the PV array was identified. It has to be mentioned that, as stated in the objectives of this work, the proposed multifunction solar active filter is evaluated under real outdoor conditions without using both irradiance and temperature sensors. A contrast between the experimental and the simulated P-V curves reveals that the real maximum power point, that is 403.538 W corresponding to the PV array voltage 58.891V, is almost the same with that obtained by simulated the PV array using the extracted model parameters ($P_{max}=403.823$, $V_{mp}=58.4352$ V).

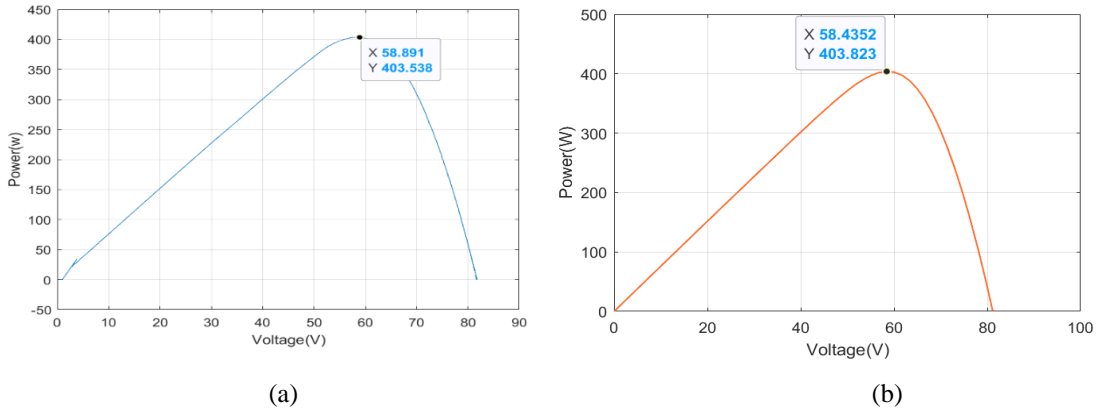


Figure 4.3 P-V properties of the PV array in use, (a) experimental curve, (b) simulated curve.

The parameters of the proposed PV system architecture were identified under varying irradiance and temperature conditions. These parameters were then utilized in the simulation to replicate the experimental results, ensuring consistency and accuracy across different operating scenarios. Therefore, the whole simulation time is broken down to three scenarios in order to evaluate the suggested control system's efficacy.

- The first scenario starts from 0sec to 12sec and during which the PV array remains disconnected. The objective of this scenario is to check the filtering function of the proposed architecture.
- The second scenario begins from 12 sec to end at $t=22$ sec. During this period, the inverter is linked to the PV array and therefore two distinct functions can be

assessed; the direction of power from or to the grid utility, as well as the maximum power point tracking.

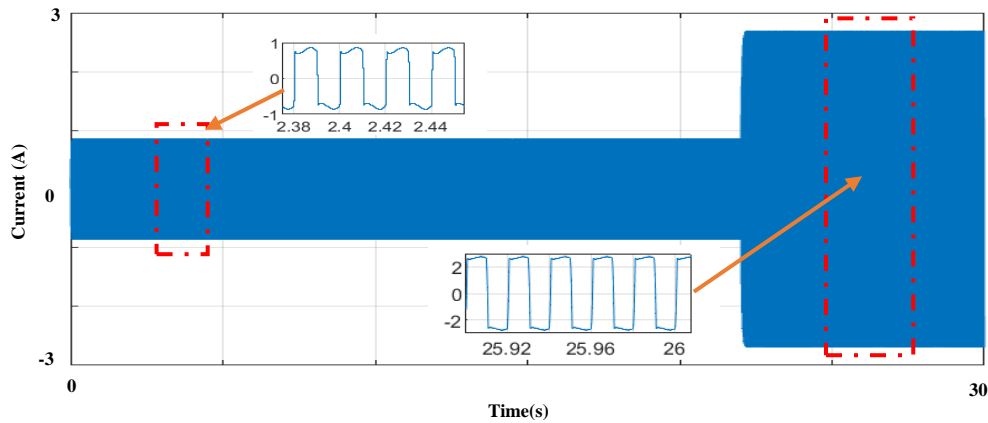
- Last scenario, starts at 22 sec and ends at $t=30$ sec. The nonlinear load is varied in a way to increase its impedance and therefore the power to the grid is altered. During this period, the focus will be on the power balance's assessment.

Table 4. 2 PV system components specifications

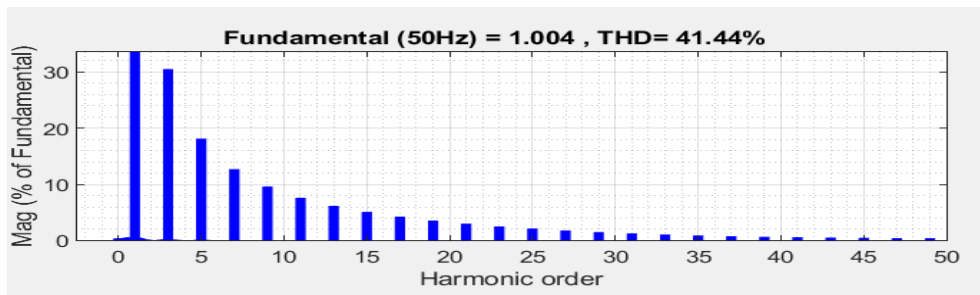
Grid	Grid voltage, V_{grid} (RMS)	63 V
	Grid frequency, F_s	50 Hz
Nonlinear load	AC-side rectifier inductor, L_L	3 mH
	DC side load: resistor, R_{load}	70 Ω
	DC side load; inductor, L_{load}	0.7 H
Filter	Filter inductance, L_f	15 mH
	DC capacitor, $C_1 = C_2$	1500 μ F
PUC7 inverter	DC voltage reference	120 V
	Input capacitor, C_{in}	47 μ F
Boost converter	Output capacitor, C_{out}	390 μ F
	Inductance, L	5 mH
	Maximum power (P_{max})	600 W
PV array (STC)	Open circuit voltage (V_{oc})	90.5 V
	Short circuit current (I_{sc})	8.49 A
	Maximum power voltage (V_{mp})	74.6 V
	Maximum power current (I_{mp})	8.04 A

Figs 4.4 (a) and (b) illustrate the current drawing by the nonlinear load and its harmonic spectrum analysis respectively. The current looks constant during the first two scenarios. However, this current is drawn from grid during the first scenario while from the PV during the second scenario. The control could ensure smooth switching between the two sources. Fig 4.4 (b) shows the harmonic content of the load current that is evaluated by its THD of 41.44%. This level is far away from the one required by the standard of grid connection. The current's increase in the third scenario is due to the decrease of the resistance in the DC side from 70 Ω to 23 Ω . Fig 4.5 (b) depicts the variation of the inverter current and the reference current. The latter is generated by the modified 'p-q' power injection controller, while the MPC ensures the injection of this current into the PCC to mitigate these harmonics. It is clear that, during the two first periods, in spite of the switching between grid utility and the PV, the current being injected is the one that corresponds to minimum THD and the requirement

of the load in terms of power. As for the THD result, the grid current becomes sinusoidal and the THD remains less than 5% in all scenarios, according to the IEEE 519-2022 without making any changes to the nonlinear load that keeps absorbing the distorted current. The worst THD is obtained during the power injection and it is evaluated as 2.63%. The voltage of the DC-link V_{dc} is kept at the reference value (120 V) as shown in fig 4.5 (c). Furthermore, perfect voltage balance between the two capacitors V_{dc1} and V_{dc2} is achieved where the voltage across the second capacitor kept constant and equal to one third of the first cell capacitor voltage (40 V). This voltage constraint is required for the PUC7 inverter to deliver seven (7) level single phase voltage. Fig 4.5 (d) displays the PV's power, of the grid utility, and that of the load.

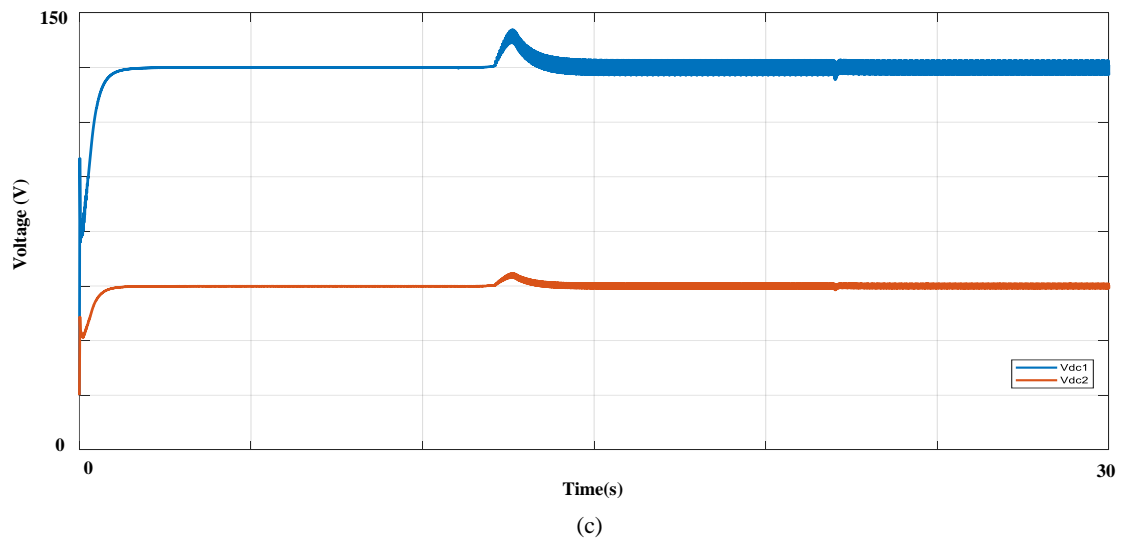
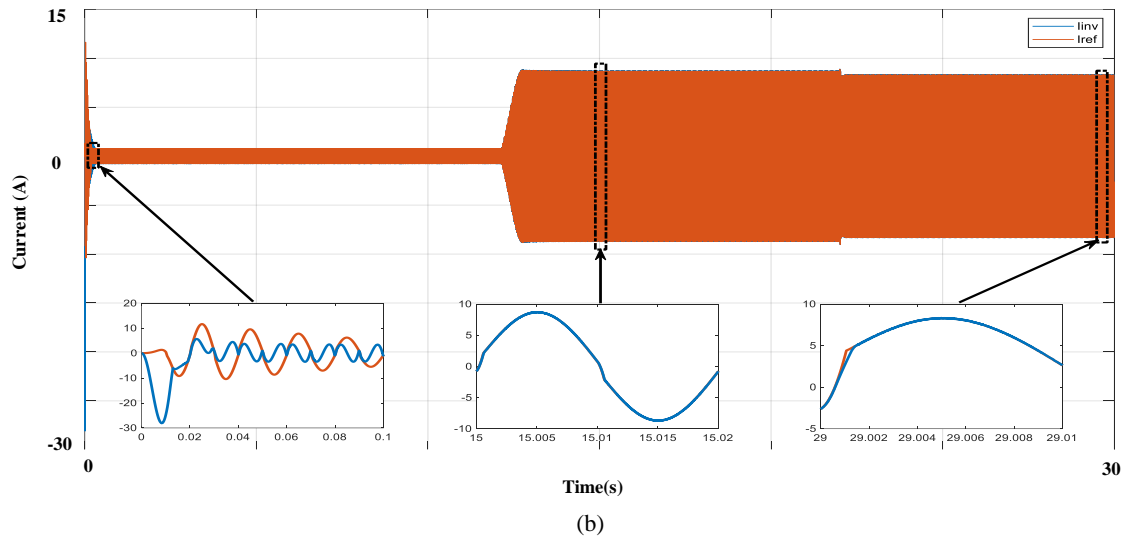
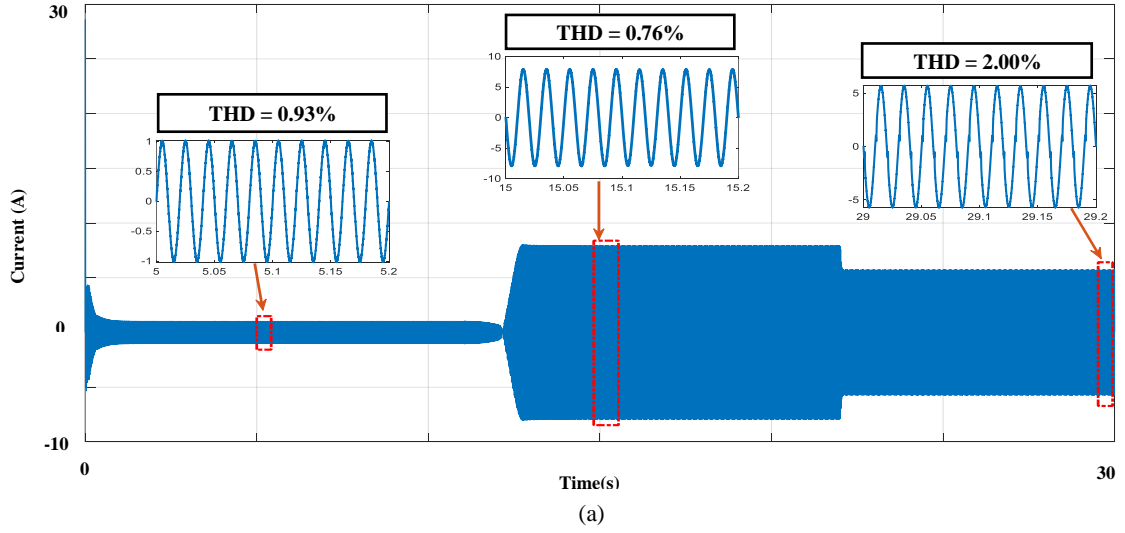


(a)



(b)

Figure 4. 4 (a) Load current (b) Harmonic spectrum of the load current.



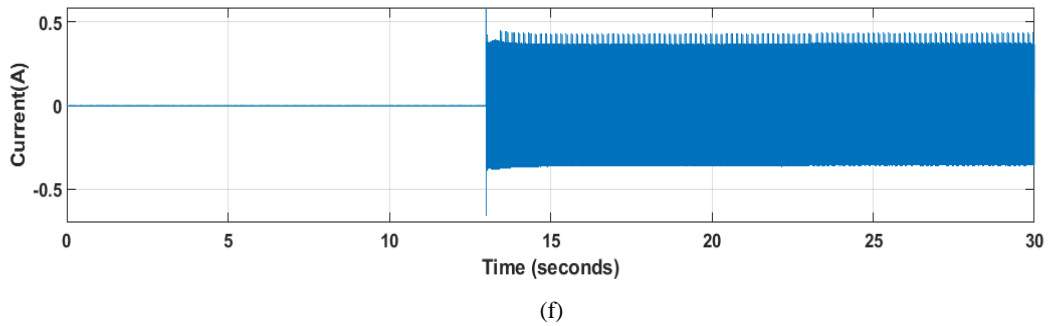
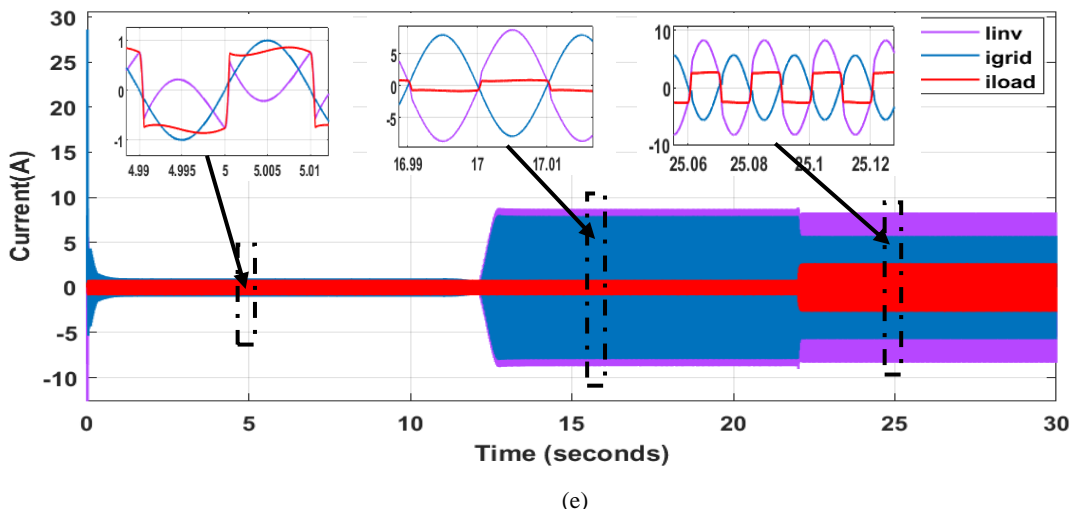
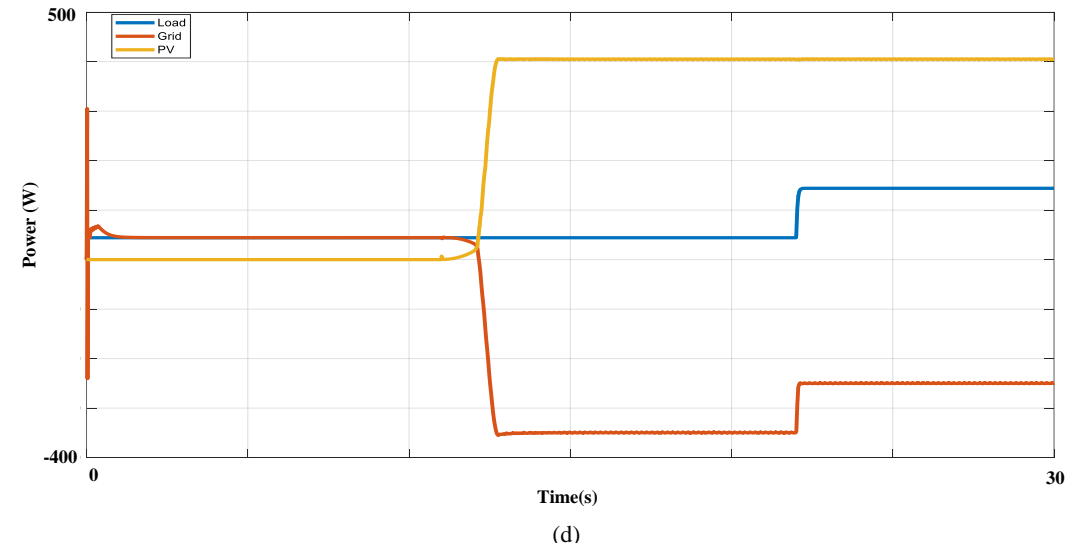


Figure 4. 5 (a) Grid current (b) Inverter current and its reference (c) DC-link capacitor voltages (d) Power of the PV, grid, and load (e) Current of the grid, Inverter, and load (f) PV leakage current waveform.

During the first scenario, there is no power coming from that PV and therefore the grid supplies the load. After the connection of the PV array, the control moved the power source from the grid to the photovoltaic array, sending any extra solar energy back to the grid (grid power is negative).

It is evident that the highest possible level of power harvesting is attained as the power drawn during the last two scenarios is matching with maximum power in the experimental PV shown in Fig 4.3 (a). Furthermore, during the last scenario, the increase in load has resulted in the decrease in the power being sent to the grid utility while power from the PV remains the same as long as there is no change in the weather conditions. In summary, this proposed control system has ensured the distribution of power between the grid, the PV source and the nonlinear load by giving priority to the PV and maintain the THD to its minimum level. As a result, as shown in Fig 4.5 (f), the suggested PUC7 inverter system shows very little leakage current. The aforementioned discovery highlights the appropriateness of the multilevel inverter (MLI) PUC7 architecture for single-phase PV applications involving low and medium power conversion systems.

4.3 EXPERIMENTAL RESULTS

A laboratory prototype for the proposed multifunction solar active filter has been built using six 600V, 12A, IGBT active switch of type G4PC30UD. A real-time CU-SLRT Std (DS1104 like interface) is used for the implementation of the different designed controllers (MPPT algorithm, Modified P-Q controller, and the MPC). The real-time CU-SLRT board offers the same features as those provided by the DS1104 while the computation capabilities are better and more functions are integrated as it includes 6-core 2.6 GHz processor, FPGA-based I/O, 16 analog inputs, 8 analog outputs, 16 digital I/O ports, and 16 PWM outputs.

Additionally, it has two encoders and communication interfaces such as Ethernet and RS232 connectors. Fig 4.6 displays the prototype for the experiment. As the prototype illustrates, the PV array that is composed of 4 PV modules is mounted outdoor the laboratory room. A boost converter connects it to the PUC7 inverter. The real-time CU-SLRT generates pulses to the FPGA card to integrate a $3\ \mu\text{s}$ dead time allowing to avoid a short circuit in the PUC7. Finally, the signals are received by the gate drive card to control the six IGBTs of the PUC7 inverter. The most significant advantage of this research is the implementation of grid

connected system using an outdoor PV array and without the need of the irradiance and temperature sensors.

Despite the importance of these latter as the validation of the PV array's performance strongly depends on the knowledge of their outputs, however, in this study, the experimental prototype shown in Fig 4.1 allows to trace the I-V curve of the PV array at a given moment and subsequently from the maximum power on the P-V curve is identified (V_{mp} , P_{mp}). At this time, the experiment shown in Fig 4.6 is conducted and then the results can be compared with those identified to confirm the suggested control system's efficacy.

The same system parameters are employed in simulations as they are in practical testing which are shown in Table 4.2. Furthermore, the sampling frequency of the real-time CU-SLRT is 20 kHz while the controller (MPC) operates at the same frequency. During the experiment, the three scenarios are implemented to facilitate the comparison and highlight the effectiveness of each function of the control system.

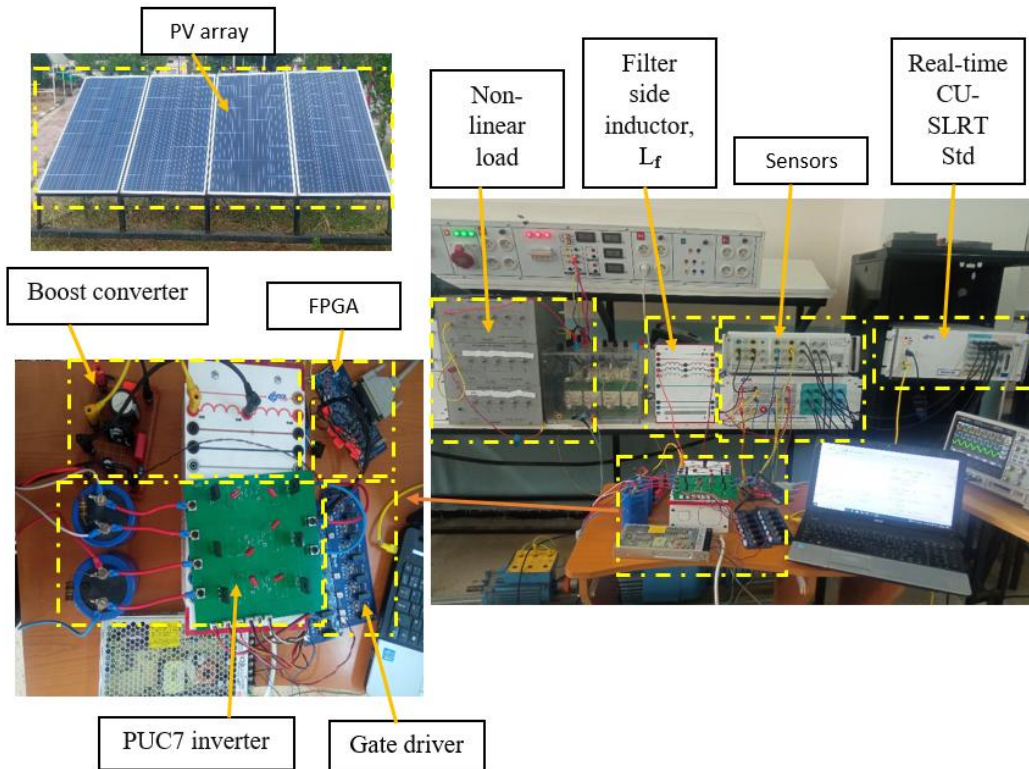


Figure 4. 6 The constructed experimental prototype.

Figure 4.7 presents the empirical findings from our comprehensive experiments, encompassing a diverse set of parameters. These include load and grid currents, inverter

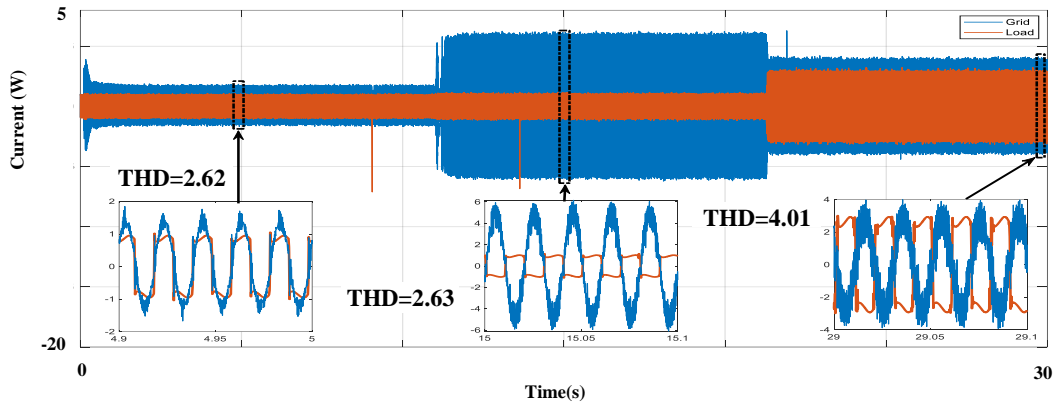
output voltage, inverter current, its reference, DC-link capacitor voltages, and power profiles associated with the PV system, grid, and load. Additionally, we delve into grid current and voltage dynamics. In the first scenario ($t \leq 12$ sec), we examine the inverter-generated current (depicted in Figure 4.7 (b)) to validate the effectiveness of the modified ‘p-q’ injection method in mitigating harmonics. Notably, the grid current (as shown in Figure 4.7 (a)) maintains a sinusoidal behavior, with a THD of 2.62%. During the second scenario ($t > 12$ sec), after connecting the PV array, we observe that the power drawn closely aligns with the maximum power point (P_{mp}), as indicated in Figure 4.3 (a). Precise computations reveal an identified Pmp of 403.53W, while the implemented Perturb and Observe (P&O) algorithm yields $P_{mp} = 390$ W. Consequently, our MPPT efficiency stands at an impressive 96.65%, comparable to efficiencies reported in prior research [70-73].

Given that the load necessitates approximately 60W, surplus power remains within the inverter. Our control system intelligently routes this excess power back into the grid utility, as depicted in Figure 4.7 (e). Throughout all scenarios, the inverter’s output voltage remains remarkably consistent, maintaining the same number of voltage levels (as illustrated in Figure 4.7 (c)). Furthermore, we demonstrate the efficacy of our proposed MPC by ensuring that the voltage across the second cell capacitor remains constant and equals one-third of the first cell’s capacitor voltage (as evidenced by Figure 4.7 (d)). Lastly, in the third scenario, we vary the resistance of the nonlinear load from 70 Ω to 23 Ω , resulting in an increased power demand. The effectiveness of our proposed MPC strategy becomes evident through the sustained voltage across the second cell capacitor, consistently maintaining a value equivalent to one-third of the first cell’s capacitor voltage (as depicted in Figure 4.7(d)). During this scenario, as the nonlinear load’s resistance varies from 70 Ω to 23 Ω , this requires supplying additional power, Figure 4.7(e) illustrates an increase in load power to 160W, accompanied by a corresponding decrease in injected power to 230W, thus preserving power balance between grid, PV array and load.

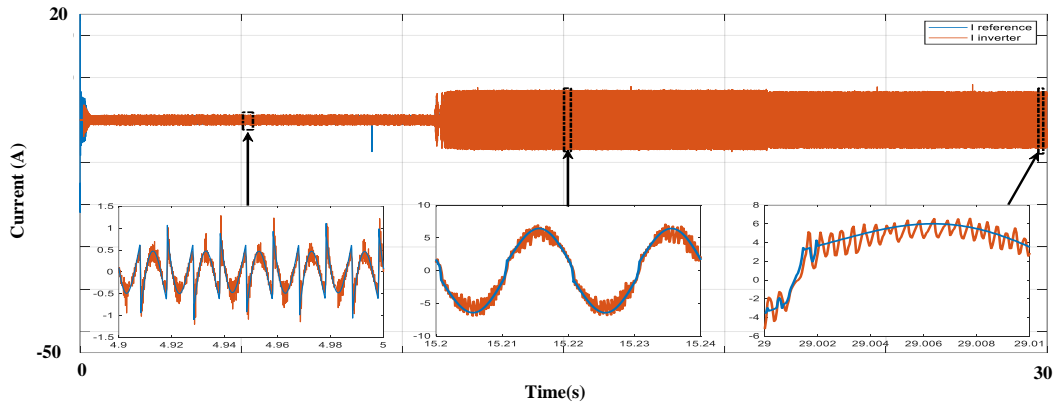
As a result, our control system adeptly facilitates power injection into the grid while simultaneously meeting local load requirements and ensuring that THD remains below the IEEE standard threshold. Regarding reactive power compensation, unity power factor is consistently maintained across all scenarios. During the first scenario, Figure 4.7(g) demonstrates a positive unity power factor (with a shift angle of zero), signifying in-phase

alignment between grid current and voltage as the grid supplies power to the load (as depicted in Figure 4.7(f)). On the other hand, during both the second and third scenarios, where power flows from the PV system to both the grid and the load, Figure 4.7(g) illustrates a negative unity power factor (with a shift angle of 180°), indicating power transfer from the grid to the load.

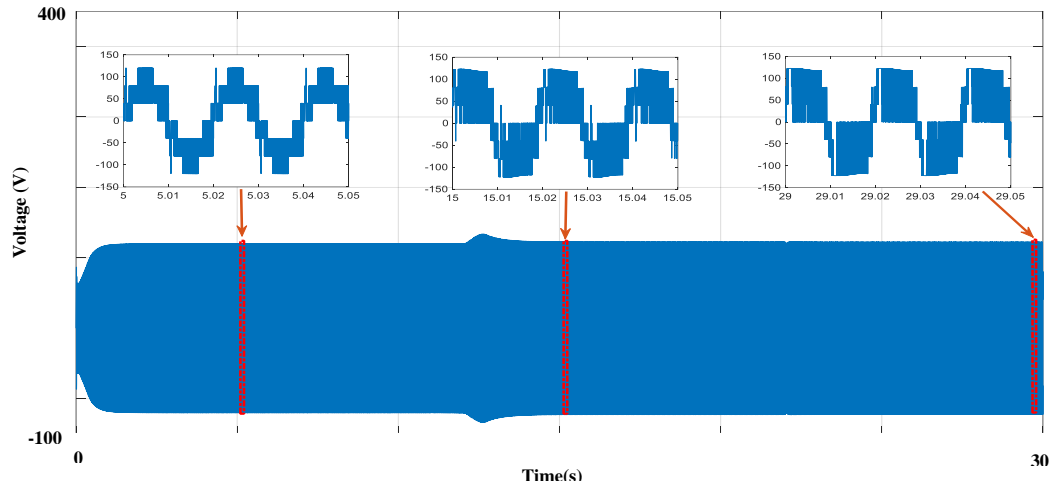
Furthermore, the good matching between the experimental results and the simulated ones witnesses the accuracy of the proposed control system as well as the identification process.



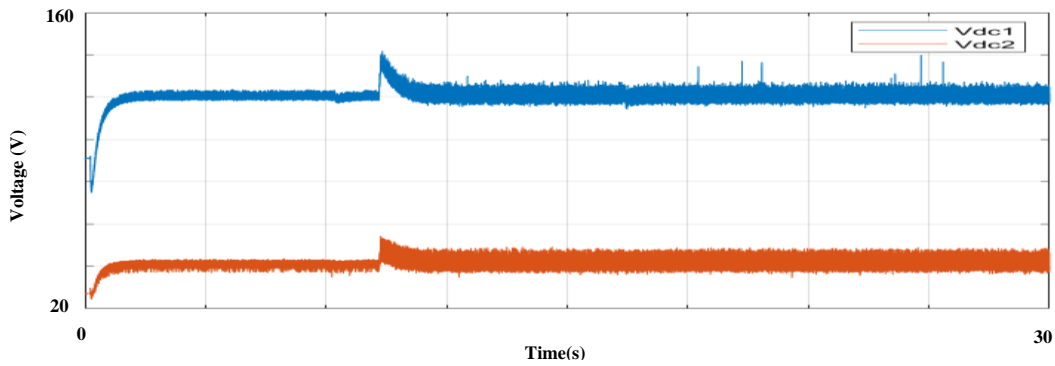
(a)



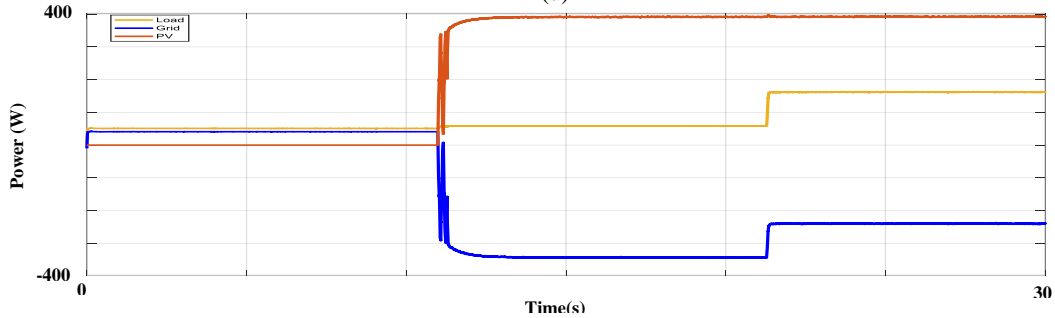
(b)



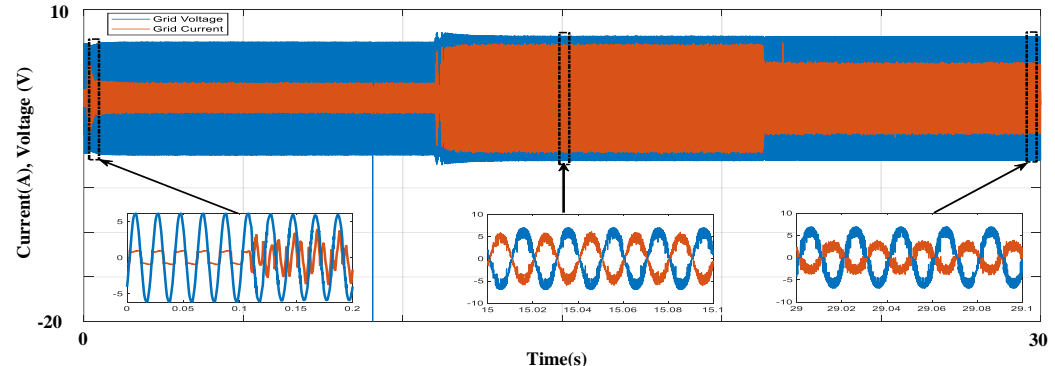
(c)



(d)



(e)



(f)

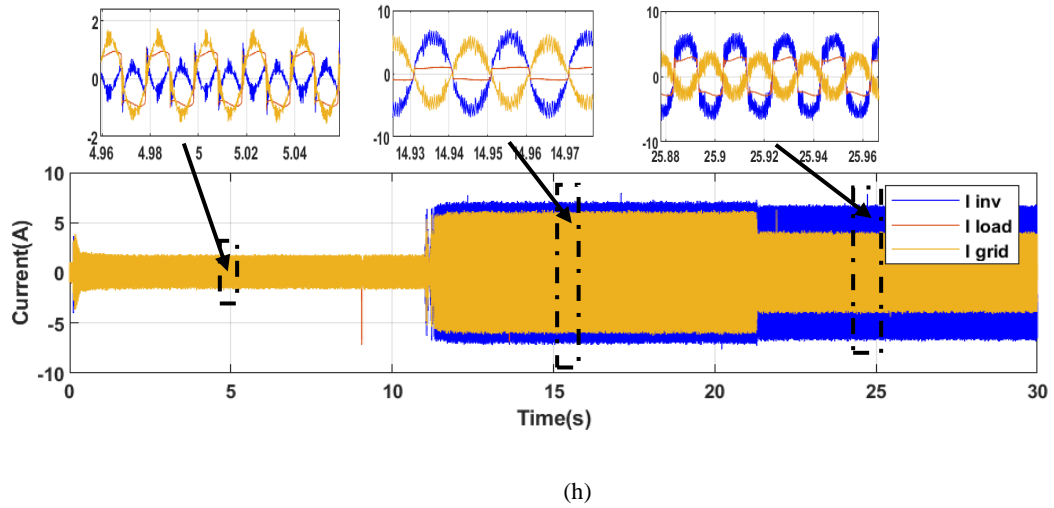
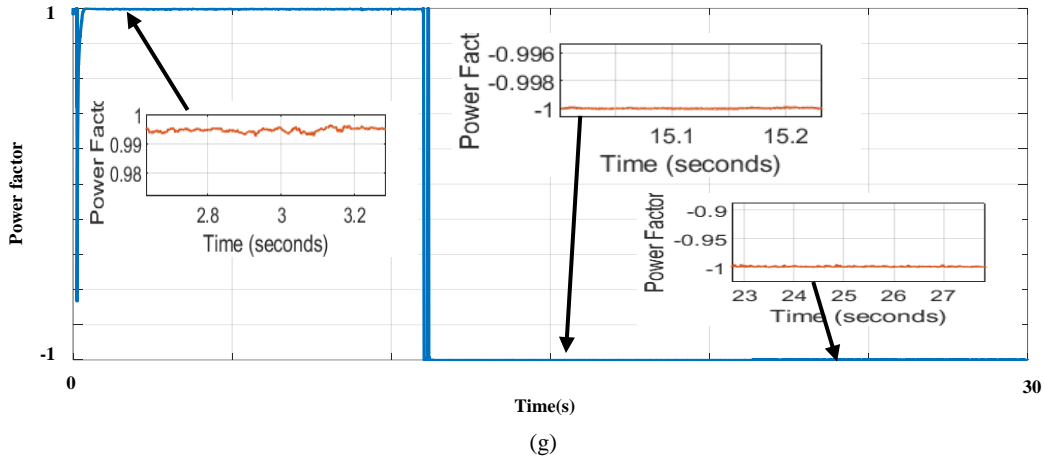


Figure 4. 7 Experimental results: (a) Load and Grid currents, (b) Inverter current and its reference, (c) Inverter output voltage, (d) DC-link capacitor voltages, (e) Power of the PV, grid, and load, (f) Grid current and grid voltage (scale V/15), (g) Power factor, (h) Current of the grid ,inverter ,and load.

In Table 4.3, the comparison between various approaches reveals distinct attributes of each configuration, particularly concerning THD and the simultaneous implementation of the inverter's multifunctionality. The comparison is based on the type of the inverter, the implementation of all functions of the inverter, the value of the THD, and the type of the filter. The comparison reveals that our approach integrates a multifunctional active power filter for grid power injection, which has been validated using real outdoor conditions.

The absence of irradiance and temperature sensors further distinguishes our approach from both simulation and implementation points of view. With a THD of 2.63% in the grid current, the proposed configuration showcases the best performance, highlighting its viability for real-world applications. Thus, our proposed configuration stands out for its outdoor validation, multifunctional capabilities, and superior THD performance compared to classical inverters and even PUC5 inverters.

Table 4. 3 Comparison with previous work

Papers	[70]	[71]	[72]	[73]	Proposed configuration
Experimental validation	No	No	Yes	No	Yes
Type of validation	PV simulator	Solar emulator	Real PV indoor validation	HIL	Real PV outdoor validation
APF function	Not included	Included	Included	Included	Included
MPPT	IC	P&O	P&O	VO	P&O
THD of grid current	3.67%	3%	5%	3.11%	2.63%
Filter	LCL	LCL	L	L	L
DC bus controller	PI controller	LQR controller	PI controller	MPC	MPC
Inverter type	H-Bridge Inverter	H-Bridge Inverter	H-Bridge Inverter	MPUC5	PUC7
Test of multifunction simultaneously	No	No	No	Yes	Yes

4.4 Conclusion

The validation tests conducted in this chapter confirm the effectiveness and reliability of the proposed multifunction solar active filter in grid-connected PV systems. By employing a comprehensive PV array identification process, the extracted parameters enabled accurate modeling and simulation of the system. The experimental results, obtained under real outdoor conditions, closely align with the simulated outcomes, demonstrating the precision of the proposed control system. The PUC7 inverter, combined with advanced control strategies such as MPC and P&O-based MPPT, ensures optimal power distribution between the grid, PV array, and nonlinear load while maintaining the THD of grid current below the IEEE 519-2022 standard. Additionally, the system achieves unity power factor and effective harmonic mitigation without requiring irradiance and temperature sensors, further

enhancing its practicality and adaptability for real-world applications. Comparisons with previous work highlight the superior performance and multifunctional capabilities of the proposed architecture, establishing it as a viable solution for low and medium-power grid-connected PV systems. The next chapter will focus on refining the MPC framework by incorporating the Runge-Kutta method, thereby addressing the limitations inherent in the Euler method and further enhancing system performance.

Chapter 5: Enhanced MPC Utilizing the Runge-Kutta Method

5.1 Introduction

Model Predictive Control (MPC) is widely used in control systems for its ability to handle constraints and optimize performance. However, conventional MPC methods often employ Euler integration for trajectory computation, which introduces computational errors that escalate with the sampling time, leading to diminished tracking performance and higher switching frequencies, particularly at larger intervals. To address these challenges, we propose a novel approach that integrates the 4th-order Runge-Kutta (4oRK) method into MPC. The 4oRK method offers improved accuracy over Euler integration by significantly reducing computational errors through its higher-order approximation. A comparative analysis of the two methods, conducted under varying load profiles and voltage sag conditions, revealed that while the Euler-based approach produces grid currents with a Total Harmonic Distortion (THD) exceeding 5%, the 4oRK-based method consistently achieves a THD below 5%, ensuring superior harmonic suppression. Moreover, the 4oRK method effectively reduces power losses without increasing computational complexity, as demonstrated by comparable task execution times. This improvement is achieved through a two-stage computation process prediction and correction that enhances MPC's performance at larger sampling intervals while reducing control adjustment frequency.

5.2 MPC

MPC is an advanced and efficient strategy for regulating power converters. It relies on the mathematical model of the system under study to predict the future behavior of the controlled variables. To do this, a cost function is defined and evaluated to select the optimal control action. In essence, MPC is a powerful tool that can help improve the performance and efficiency of power converters by anticipating their behavior and taking appropriate action in advance. The flowchart in Figure 5.1 illustrates the functionality of the suggested MPC.

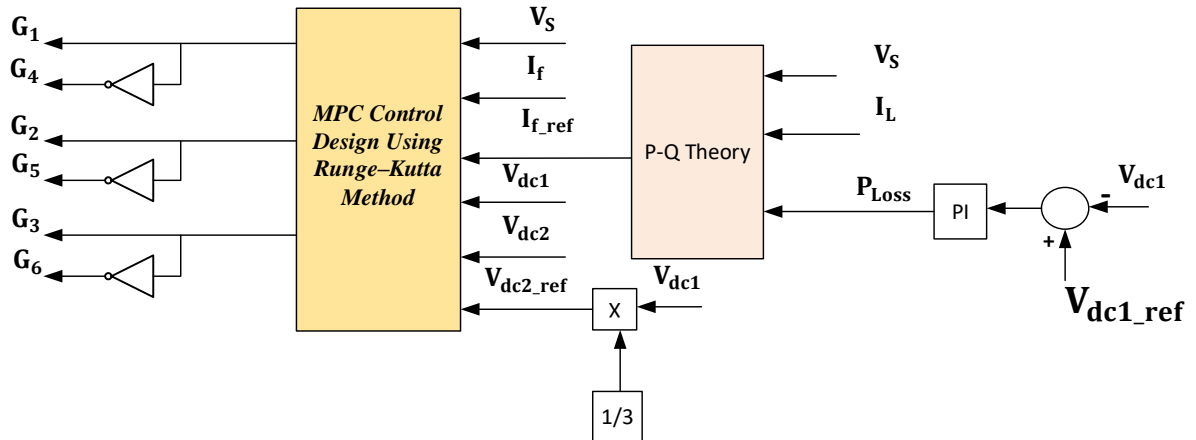


Figure 5. 1 The functionality of the suggested MPC.

5.2.1 MPC Control Design Using Euler Method

To predict the future value of load current, a discrete-time equation can be obtained by using the forward Euler approximation to create a discrete-time system representation. The discrete-time model can be achieved by using the simple derivative approximation. As a result, predictions of the future output current at the moment of $(k + 1)$ for different values of voltage vector $V(k)$ can be acquired,

$$\frac{dI_f(t)}{dt} = \frac{I_f(k+1) - I_f(k)}{T_s} \quad (5.1)$$

Where T_s is the sampling time.

Equation 3.6 is replaced with an expression that predicts the future load current at time $(k + 1)$ for each of the eight values of voltage vector $V_{an}(k)$ generated by the inverter.

This expression is given as:

$$I_{f_ref_cal}(k + 1) = \left(1 - \frac{R_f * T_s}{L_f}\right) * I_f(k) + \frac{T_s}{L_f} * (V_{an}(k) - V_s(k)) \quad (5.2)$$

5.2.2 MPC Control Design Using 4th order Runge-Kutta Method

The 4oRK is a numerical method used to solve differential equation problems. In this method, the slope of the tangent line at each point is approximated by using a fourth-order function. The 4oRK method is used to substitute the state-space representation of a system in discrete time.

The 4oRK is a refined technique for solving ODEs, providing high accuracy. Starting at an initial point, $y=f(x_i)$, it approximates $f(x_i+h)$ by computing four intermediate slopes (k -

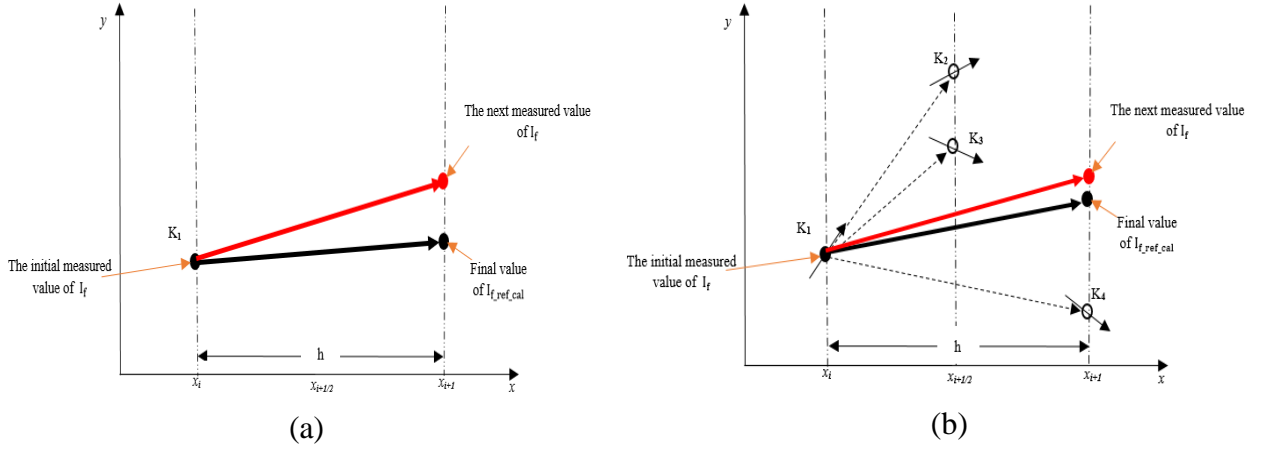


Figure 5. 2 (a) Principle of Euler method, (b) Explanation of 4oRK

1. **k1**: Initial approximation using Euler's method.
2. **k2**: Calculated using k_1 , evaluated at the midpoint.
3. **k3**: Derived from k_2 , re-evaluated at the midpoint.
4. **k4**: Based on k_3 , evaluated at the endpoint.

The next value is calculated using a weighted average of these four slopes, which provides a more accurate approximation.

$$I_{f_ref_cal}(k+1) = I_f(k) + \frac{T_s}{6} * (K_1 + 2 * K_2 + 2 * K_3 + K_4) \quad (5.3)$$

Where K_1 is given by

$$K_1 = \left(-\frac{R_f}{L_f}\right) * I_f(k) + \frac{1}{L_f} * (V_{an}(k) - V_S(k)) \quad (5.4)$$

The second term in (5.3) is computed after the update of $I_{f_ref_cal}$ as shown in (5.5)

$$\begin{cases} I_{f_ref_cal_1}(k+1) = I_f(k) + T_s * K_1 \\ K_2 = I_{f_ref_cal_1}(k) + T_s * K_1/2 \end{cases} \quad (5.5)$$

In the same manner, the third term of 4oRK is given by (5.6)

$$\begin{cases} I_{f_ref_cal_2}(k+1) = I_f(k) + T_s * K_2 \\ K_3 = I_{f_ref_cal_2}(k) + T_s * K_2/2 \end{cases} \quad (5.6)$$

And finally, the fourth term of (5.3) is computed as given by (5.7)

$$\begin{cases} I_{f_ref_cal_3}(k + 1) = I_f(k) + T_s * K_3 \\ K_4 = I_{f_ref_cal_3}(k) + T_s * K_3/2 \end{cases} \quad (5.7)$$

➤ **Comparison with Euler Method**

The Euler method calculates the next value of the state variable using the slope at the current point, which can lead to significant numerical errors at larger step sizes. These errors are particularly pronounced in systems with high dynamics, such as power electronic systems. The 4oRK method, on the other hand, introduces intermediate computations (k-values) that refine the prediction, enabling better current tracking and reduced harmonic distortion. This makes it particularly suitable for applications like active power filters, where precision and stability are paramount.

5.3 Fitness Function

The optimization of the fitness function is a crucial step in predicting the output currents $I_{f_ref_cal}(k+1)$ as illustrated in Figure 5.3. The voltage space vector is selected based on the minimized cost function.

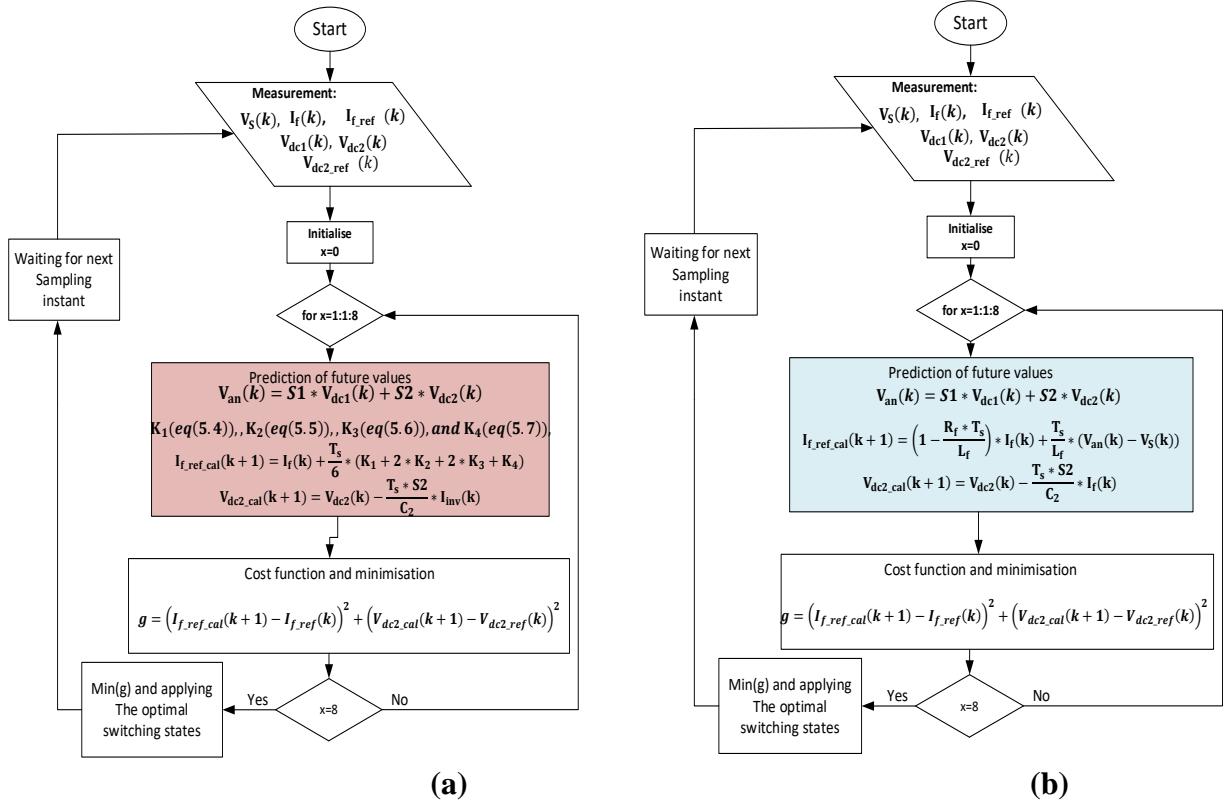


Figure 5. 3 Model predictive control (MPC): (a) Using 4oRK Method, (b) Using Euler Method

The predicted values of the inverter current ($I_{f_ref_cal}$) and the capacitor voltage (V_{dc2_cal}) are derived from the measured values of the inverter current (I_f), grid voltage (V_s), and the capacitor voltages (V_{dc1}, V_{dc2}) for each of the eight switching states (table 3.1). Next, a cost function (g) is employed to select the optimal switching state that corresponds to its minimum value. The PUC7 inverter receives the optimal switching state selected for the next sampling time through the switching pulses, which are generated based on the appropriate switching state chosen by the MPC from the switching table (Table 3.1). The future inverter current (I_f) and capacitor voltage (V_{dc2}) are the variables that the proposed MPC has to control. These control objectives are incorporated in the cost function (g) as follows:

$$g = \left(I_{f_ref_cal}(k + 1) - I_{f_ref}(k) \right)^2 + \left(V_{dc2_cal}(k + 1) - V_{dc2_ref}(k) \right)^2 \quad (5.8)$$

The reference and future values of the inverter current are given by the variables $I_{f_ref}(k)$ and $I_{f_ref_cal}(k + 1)$, respectively. Likewise, the reference and future values of the DC-link capacitor voltages are indicated by the variables $V_{dc2_ref}(k)$ and $V_{dc2_cal}(k + 1)$, respectively. These variables are essential for evaluating and regulating the inverter system.

5.4 Simulation results

In order to assess the effectiveness of the proposed method, we have created a Matlab/Simulink program that integrates all the system components described in Section 1. Detailed information about these components is provided in Table 5.1.

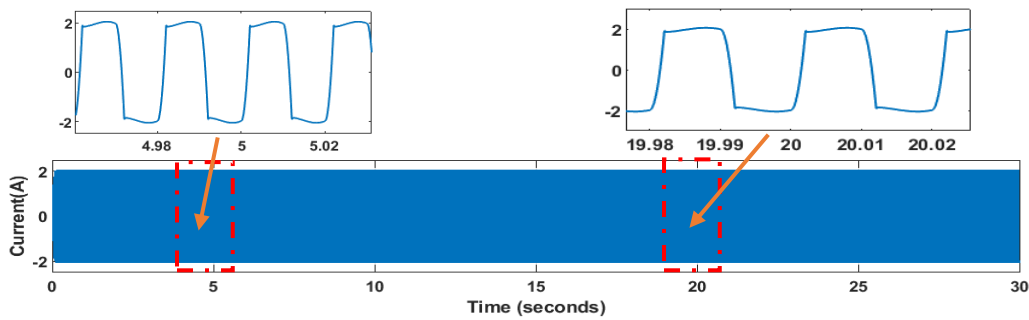
Table 5. 1 data of the system components

Grid	Grid voltage, V_s (RMS)	63 V
	Grid frequency, f_s	50 Hz
Non-linear load	Rectifier AC side inductor, L_L	3 mH
	Load DC side: resistor, R	25 Ω
	Load DC side; inductor, L	0.7 H
Filter	Filter inductance, L_f	10 mH
PUC7 inverter	DC capacitor, $C1=C2$	1500 μ F
	DC voltage reference	120 V

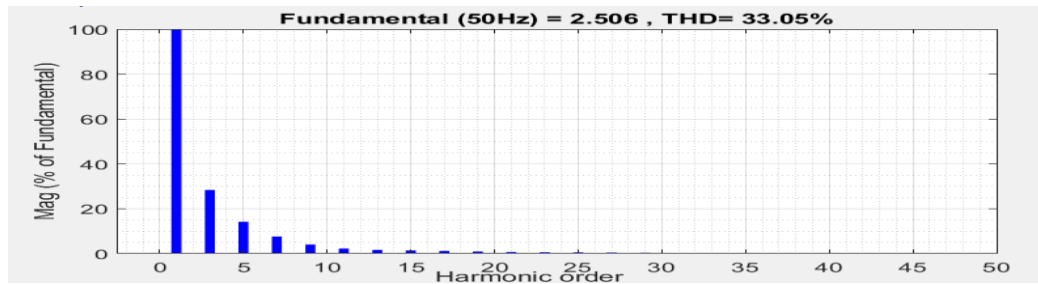
The current waveform produced by the nonlinear load and the associated harmonic spectrum analysis are shown in Fig.5.4 (a), (b), respectively. The harmonic content of the load current, as determined by its THD of 33.05%, is displayed in Fig.5.4 (b). The simulation results produced with a 10 kHz switching frequency using the Euler Method are shown in Figure 5.5. Among the subplots are (a) Grid current, (b) Inverter current and its reference, (c) Grid voltage and Grid current, (d) Power factor, (e) DC-link capacitor voltages, (f) Inverter output voltage. As a result, as seen in Fig. 5.5(a) and Fig. 5.4(c), respectively, the grid current becomes sinusoidal while the nonlinear load continues to consume a distorted current. The simulation results produced with a 5 kHz switching frequency using the Euler Method are

shown in Figure 5.6. Interestingly, we find that the Total Harmonic Distortion (THD) is higher than what we found with switching frequencies of 10 kHz. This suggests that the Euler approach performs worse when used to low frequencies.

The simulation results obtained with a switching frequency of 10 kHz using the Runge–Kutta Method are shown in Figure 5.7. Significantly, this technique performs better than the Euler method, as seen by the Total Harmonic Distortion (THD) of 1.4%. Moreover, we find that the THD is still better than that obtained by the Euler technique when we decrease the switching frequency, as shown in Fig.5.8 (at 5 kHz) and Fig.5.9 (at 3 kHz).



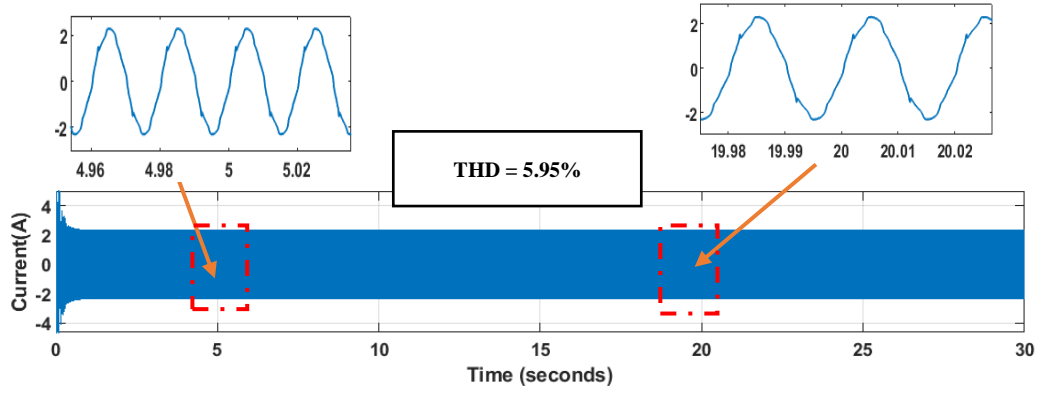
(a)



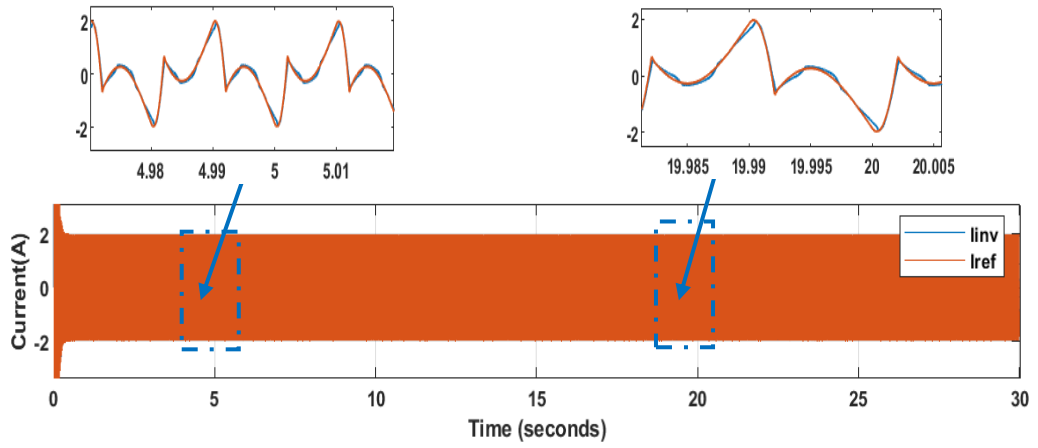
(b)

Figure 5. 4 (a) Load current (b) Harmonic spectrum of the load current.

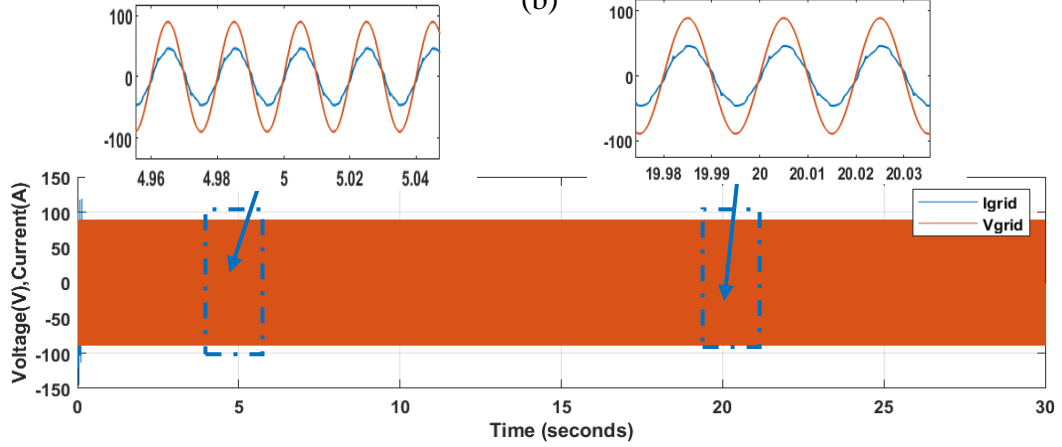
As a result, we can state with confidence that the 4oRK Method works especially well at low switching frequencies. Table 5.2 presents a comparison of the simulation findings for Total Harmonic Distortion (THD). We conclude that, especially at low switching frequencies, the 4oRK technique performs better than the Euler method.



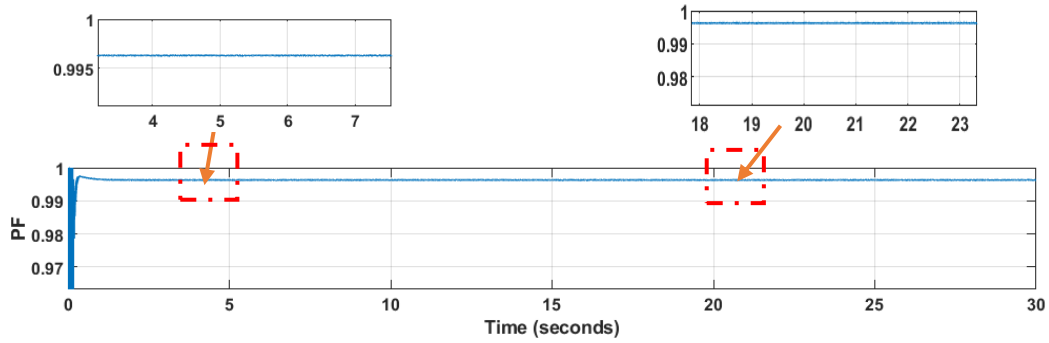
(a)



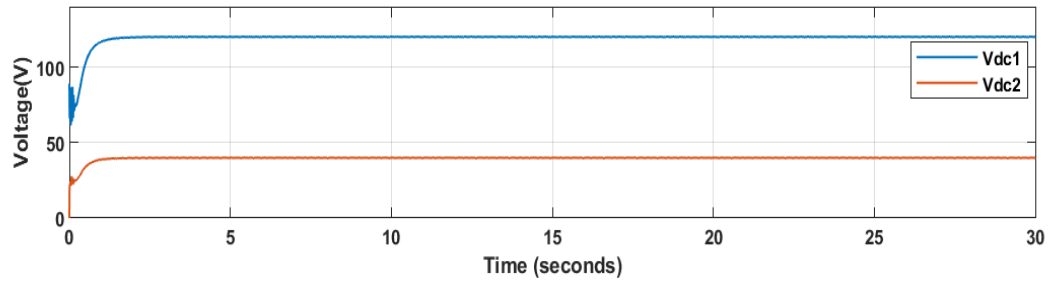
(b)



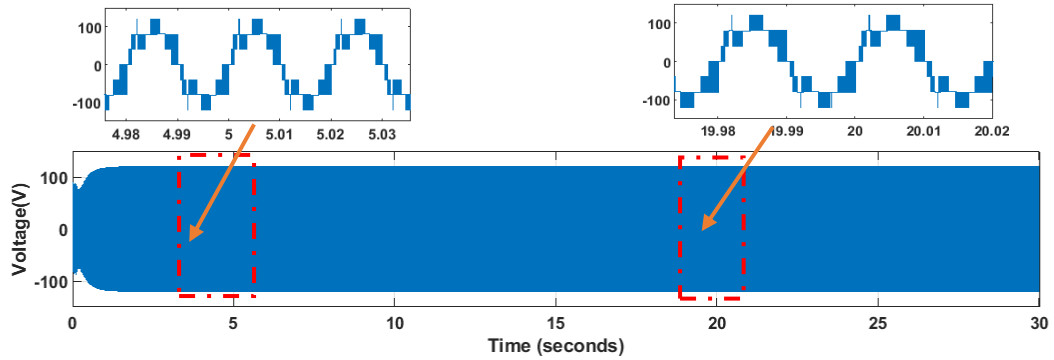
(c)



(d)



(e)



(f)

Figure 5. 5 Simulation results Using Euler Method with switching frequency 10 kHz: (a) Grid current, (b) Inverter current and its reference, (c) Grid voltage and Grid current (scale $I * 20$), (d) Power factor, (e) DC-link capacitor voltages, (f) Inverter output voltage.

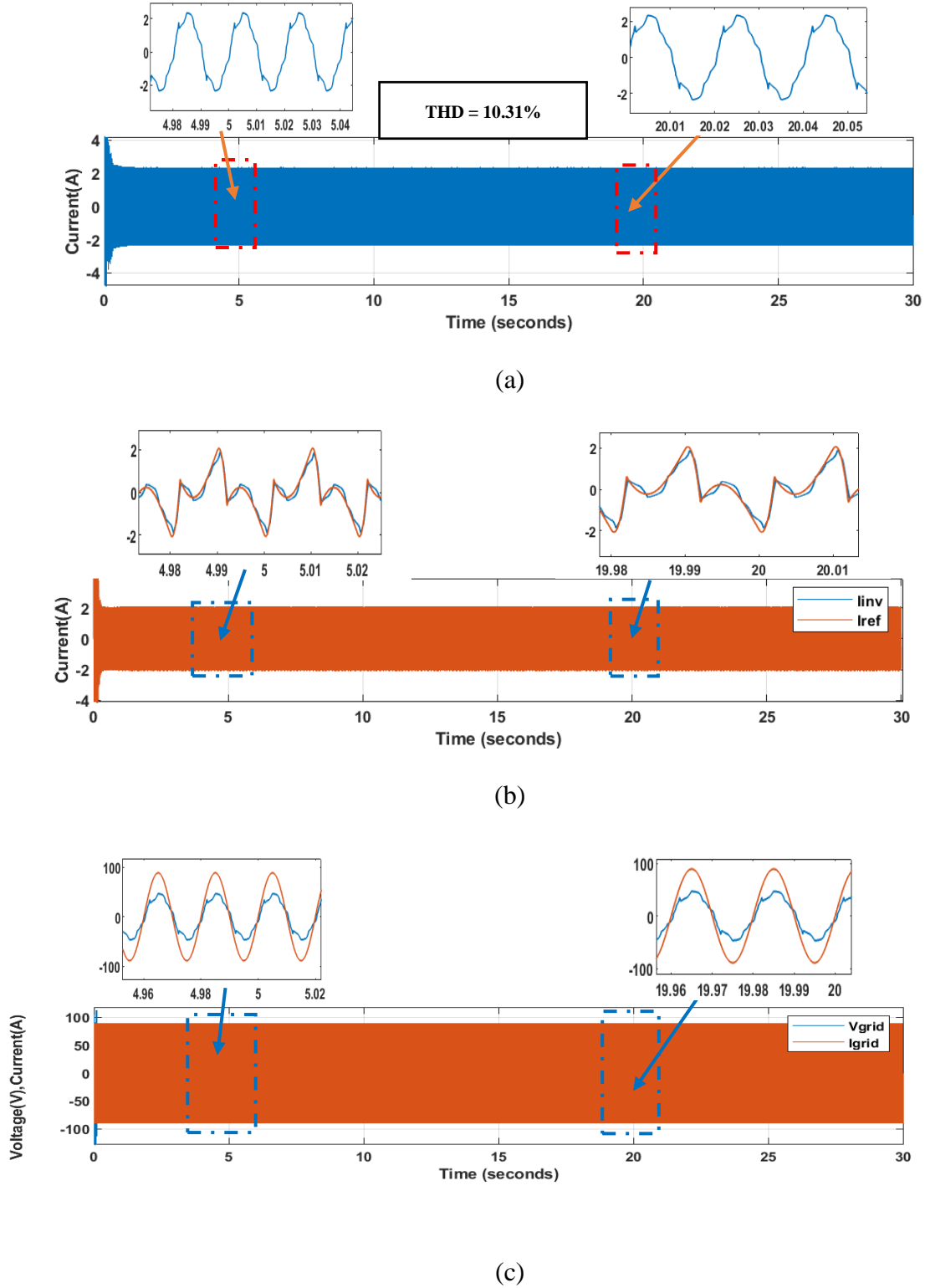
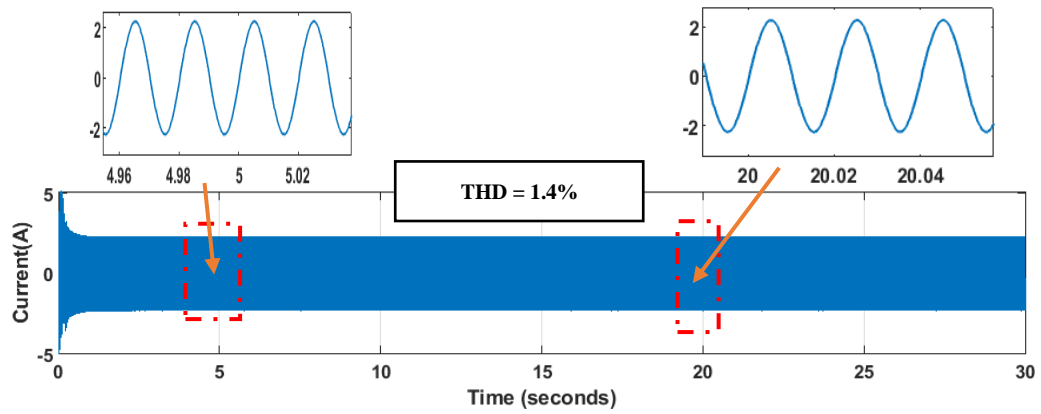
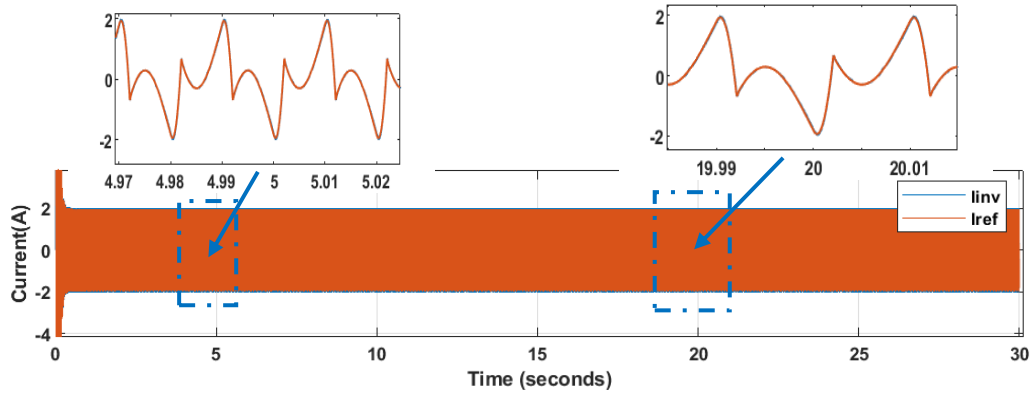


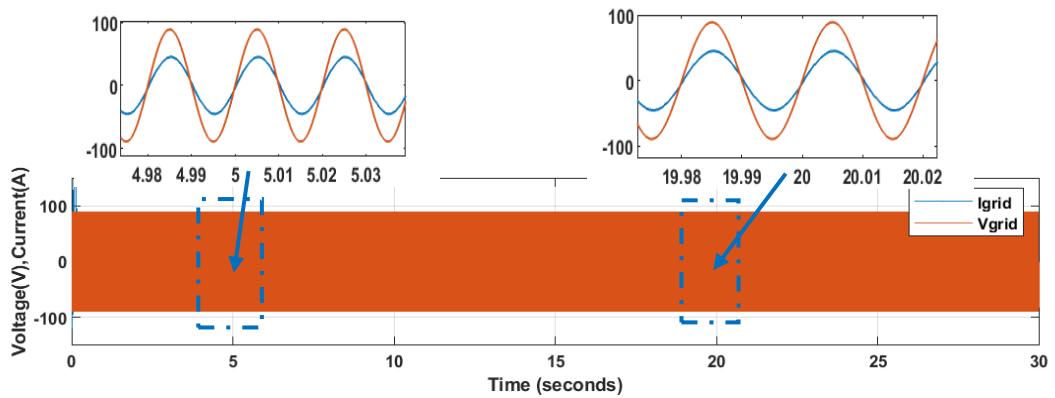
Figure 5. 6 Simulation results Using Euler Method with switching frequency 5 kHz: (a) Grid current, (b) Inverter current and its reference, (c) Grid voltage and Grid current (scale $I * 20$).



(a)



(b)



(c)

Figure 5. 7 Simulation results Using 4oRK Method with switching frequency 10 kHz: (a) Grid current, (b) Inverter current and its reference, (c) Grid voltage and Grid current (scale $I * 20$)

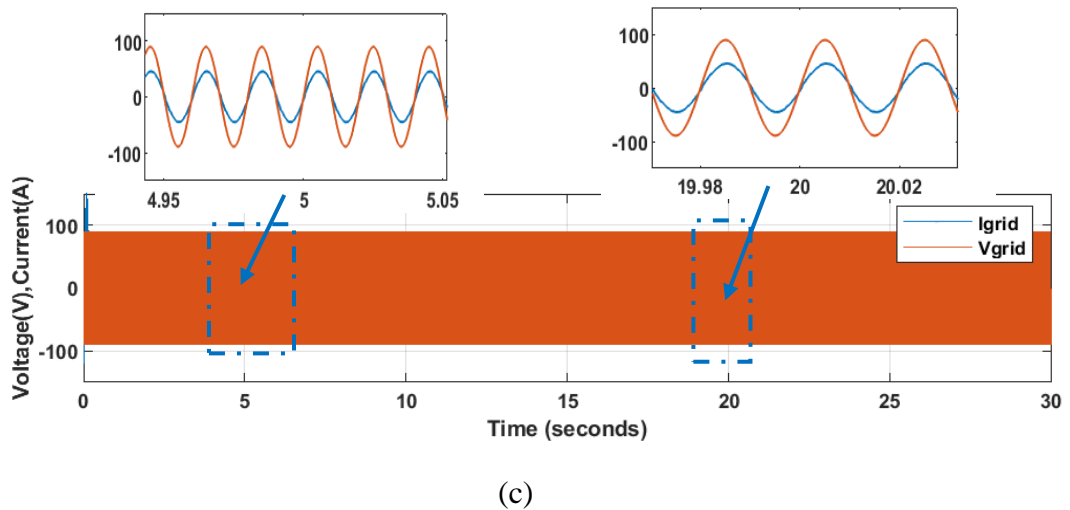
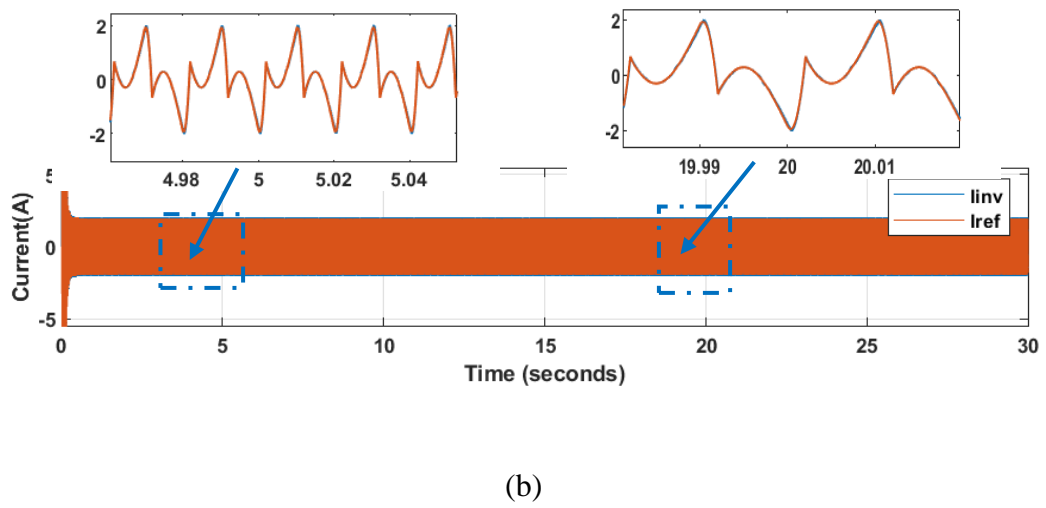
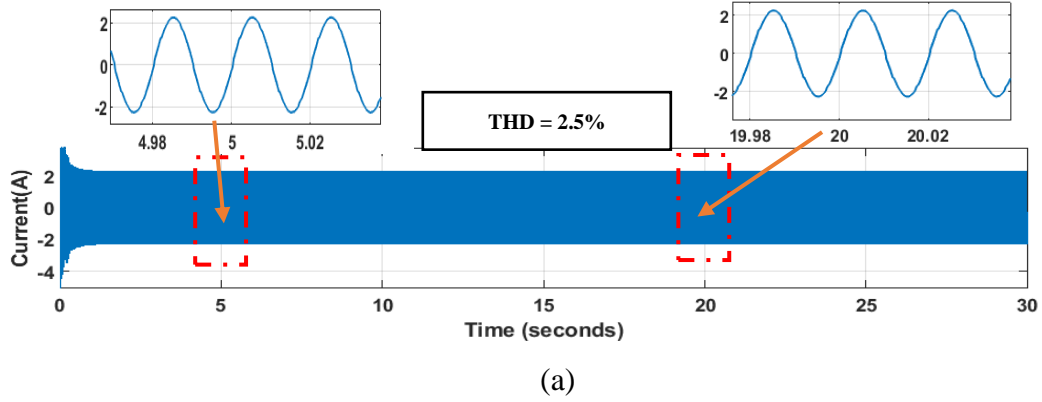
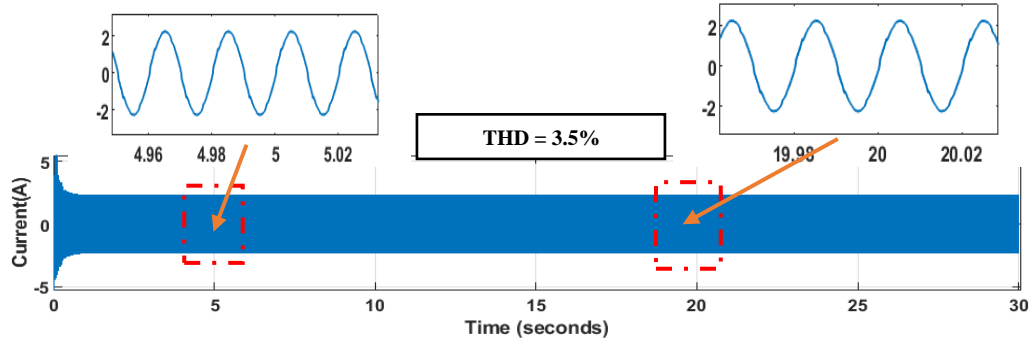
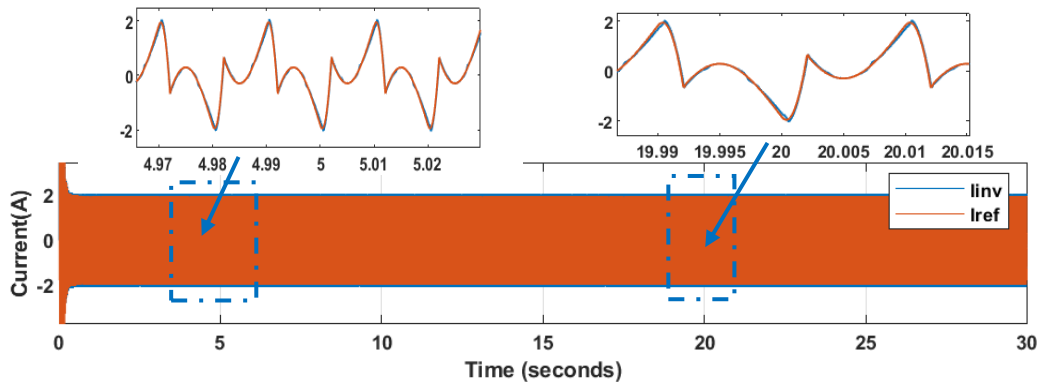


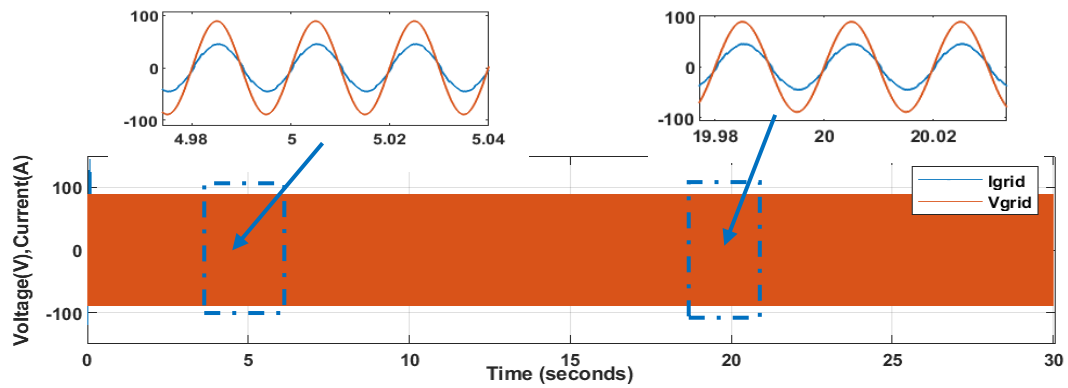
Figure 5. 8 Simulation results Using 4oRK Method with switching frequency 5 kHz: (a) Grid current, (b) Inverter current and its reference, (c) Grid voltage and Grid current (scale $I * 20$)



(a)



(b)



(c)

Figure 5. 9 Simulation results Using 4oRK Method with switching frequency 3 kHz: (a) Grid current, (b) Inverter current and its reference, (c) Grid voltage and Grid current (scale $I * 20$)

Table 5. 2 THD comparison of the simulation results.

Switching frequency \ MPC Method	10 kHz	5 kHz	3 kHz
Euler Method	5.95%	10.31%	-
4oRK Method	1.4%	2.5%	3.5%

5.5 Experimental results

Six 600V, 12A, IGBT active switches of type G4PC30UD were used to construct a laboratory prototype for the proposed multifunction solar active filter. Utilizing a Real-time CU-SLRT Standard (DS1104 Equivalent interface+ features), two distinct designed controllers are implemented: MPC Control Design Using Euler Method and Using 4oRK Method. With a 6-core 2.6GHz CPU, FPGA-based I/Os, 16 analog inputs, 8 analog outputs, 16 digital I/O ports, and 16 PWM outputs, the Real-time CU-SLRT board has the same characteristics as the DS1104 but superior calculation capabilities and more integrated functionalities. It also features two encoders and RS232 and Ethernet connections for communication interfaces. Figure 5.10 displays the prototype for the experiment. The Real-time CU-SLRT generates pulses to the FPGA card to integrate a 3 μ s dead time allowing to avoid a short circuit in the PUC7. Finally, the signals are received by the gate drive card to control the six IGBTs of the PUC7 inverter. The same system parameters are employed in simulations as they are in practical testing which are shown in Table 5.1. Both techniques were used in the experiment to allow for comparison and highlight the effectiveness of each strategy.

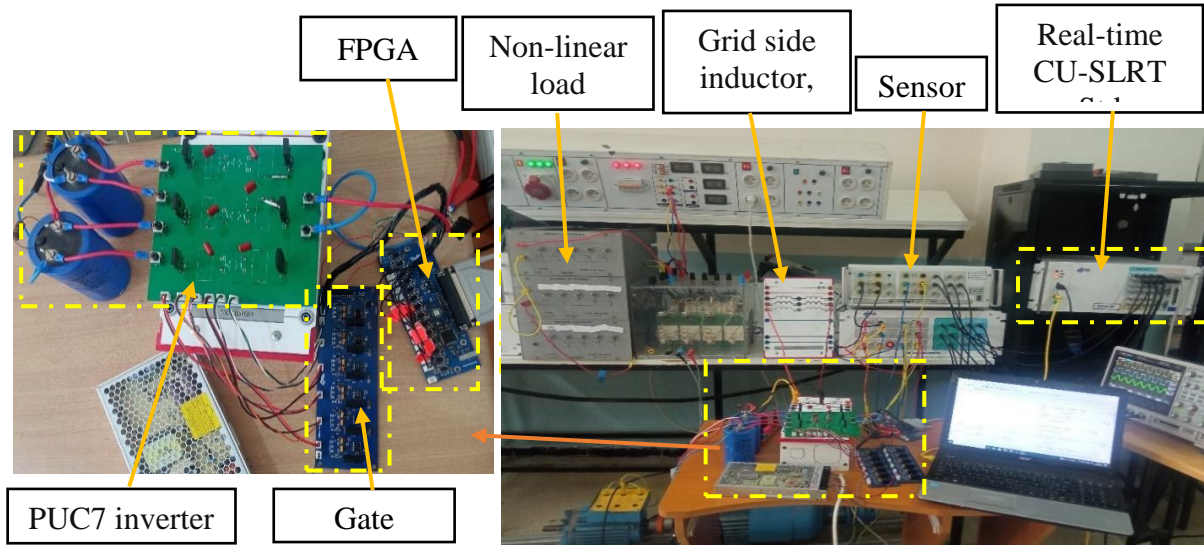


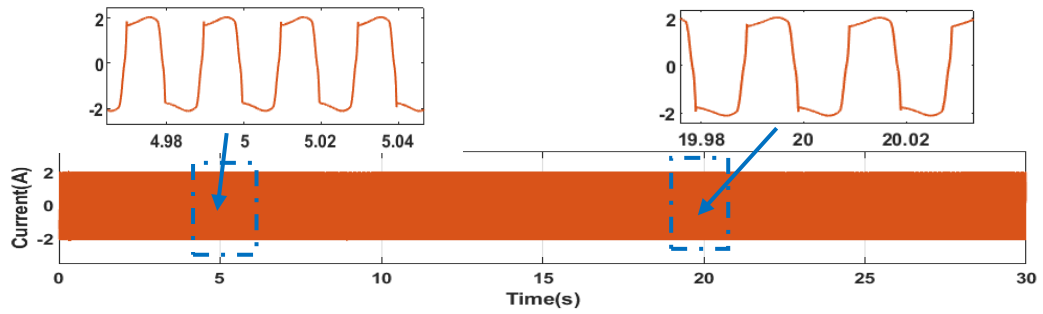
Figure 5. 10 The built prototype for the experiment.

Figure 5.11 displays the experimental results obtained from the Euler Method at a switching frequency of 10 kHz. The results include: (a) load current; (b) grid current; (c) inverter current and its reference; (d) grid voltage and grid current; (e) power factor; (f) DC-link capacitor voltages; and (g) inverter output voltage. As a result, the grid current becomes sinusoidal while the nonlinear load continues to consume a distorted current, as seen in Figs. 5.11 (b) and 5.11 (a), respectively.

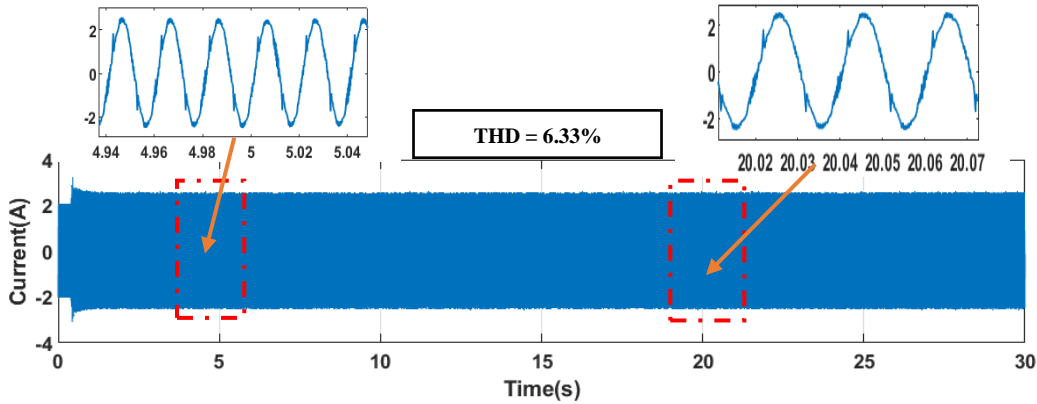
Figure 5.12 displays the experimental findings obtained using the Euler Method at a 5 kHz switching frequency. It seems that the Total Harmonic Distortion (THD) is more than what we have found while using 10 kHz switching frequencies. This implies that when applied to low frequencies, the Euler technique performs worse.

Figure 5.13 displays the experimental findings utilizing the 4oRK Method at a switching frequency of 10 kHz. A noteworthy result of this method's superior performance over the Euler approach is its Total Harmonic Distortion (THD), which is 4.39%. Furthermore, we found that when we lower the switching frequency, the THD is still superior to that produced by the Euler approach, as seen in Figs. 5.14 (at 5 kHz) and 5.15 (at 3 kHz) with a THD = 3.7%. Regarding the THD outcome, the grid current becomes sinusoidal and, in accordance with IEEE 519-2022[74], the THD stays below 5% without causing any changes to the non-

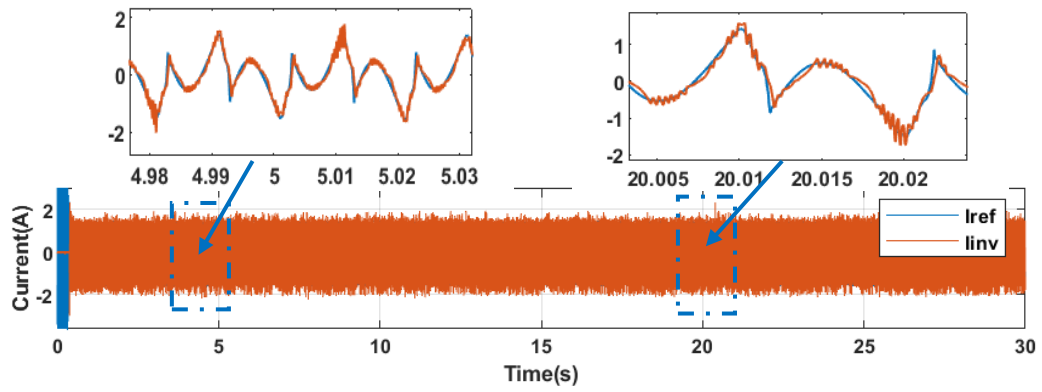
linear load that keeps absorbing a distorted current. It is therefore safe to say that the 4oRK Method performs particularly effectively at low switching frequencies. A comparison of the experimental results for Total Harmonic Distortion (THD) is shown in Table 5.4. We conclude that the Runge-Kutta method outperforms the Euler technique, especially at low switching frequencies.



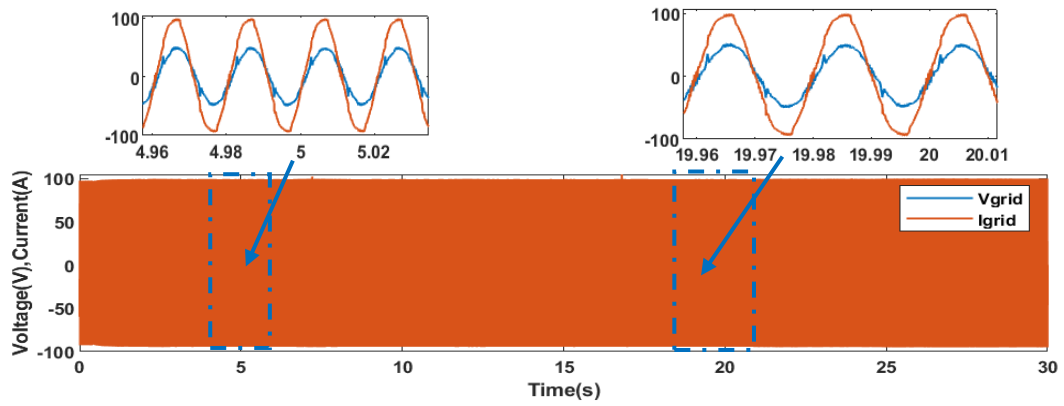
(a)



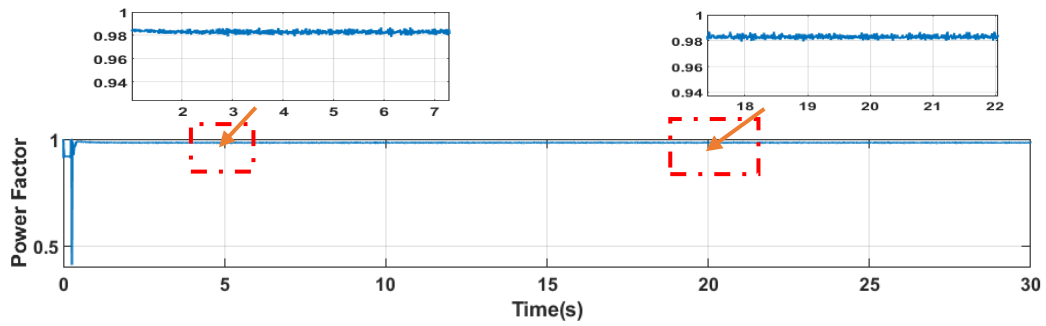
(b)



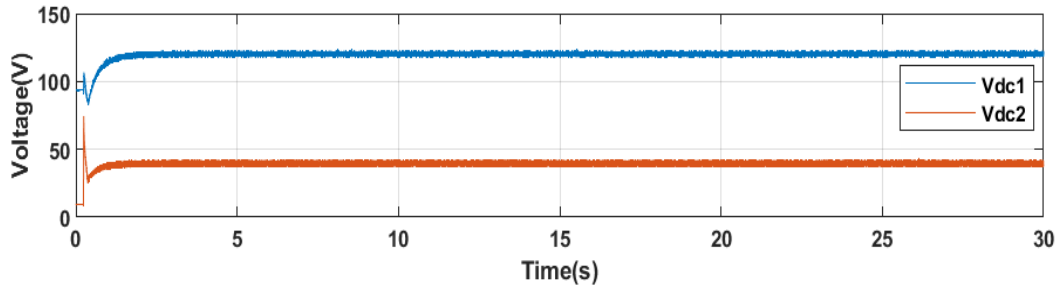
(c)



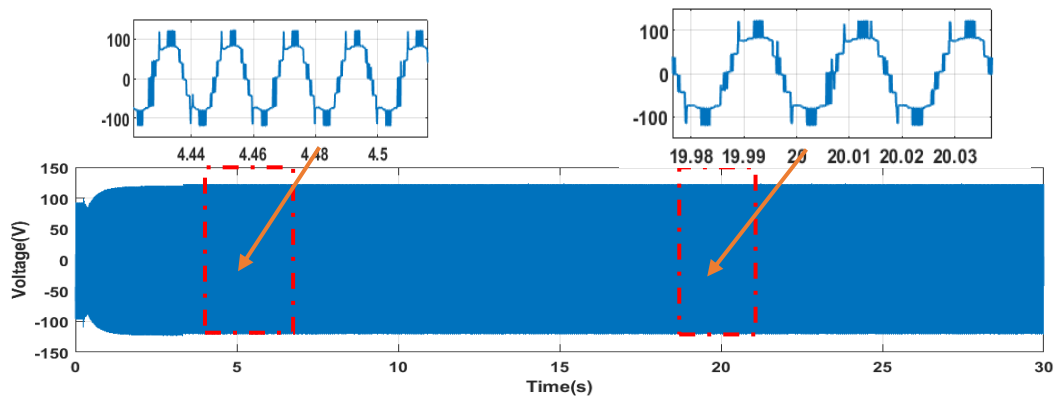
(d)



(e)

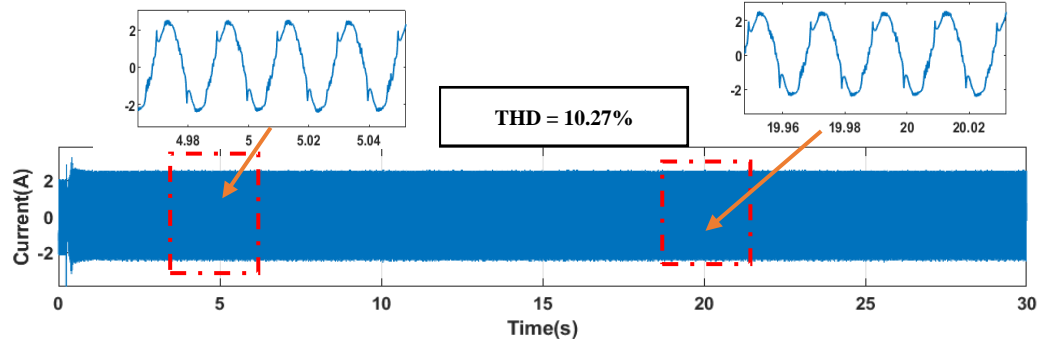


(f)

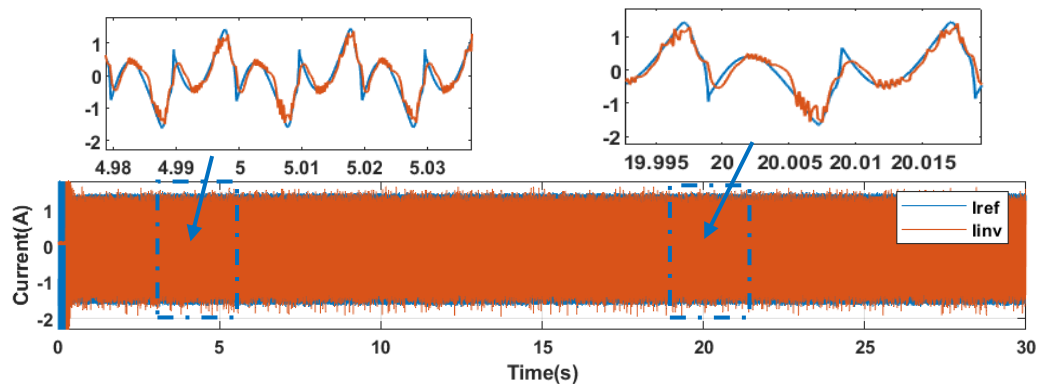


(g)

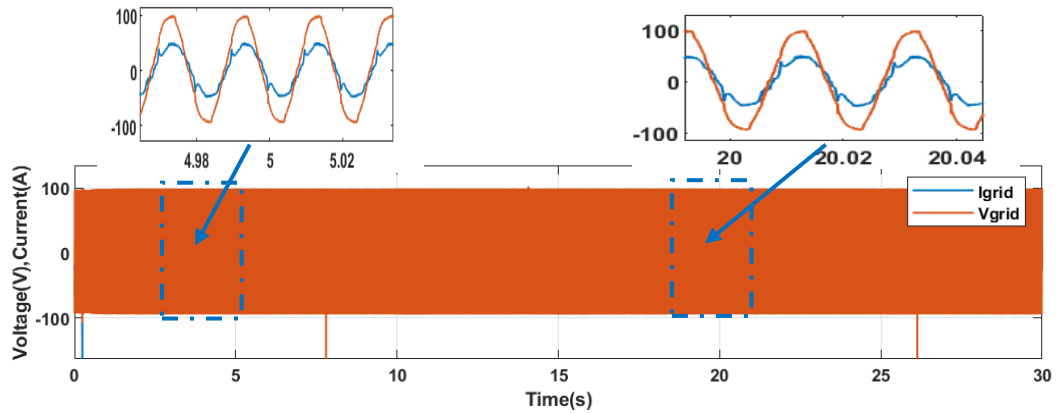
Figure 5. 11 The experimental results Using Euler Method with switching frequency 10 kHz:: (a) load current; (b) grid current; (c) inverter current and its reference; (d) Grid voltage and Grid current (scale $I * 20$); (e) power factor; (f) DC-link capacitor voltages; and (g) inverter output voltage.



(a)

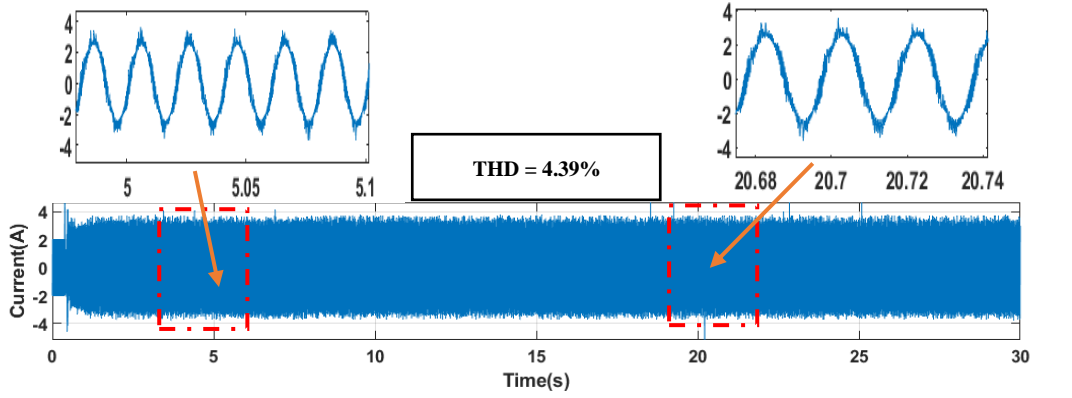


(b)

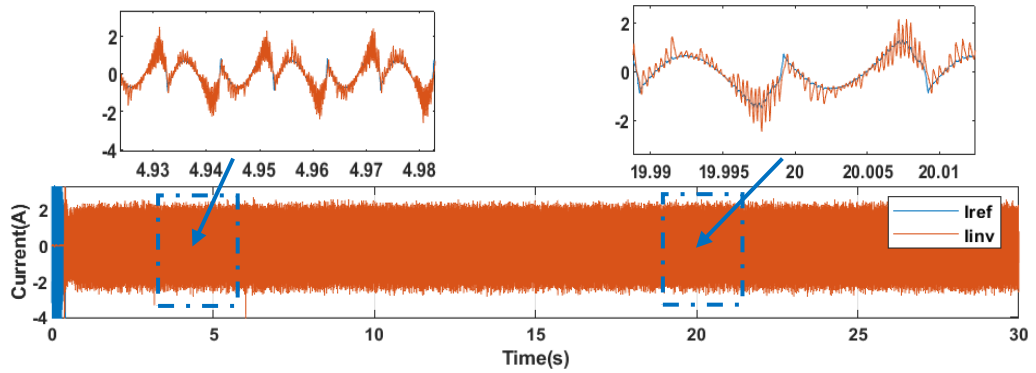


(c)

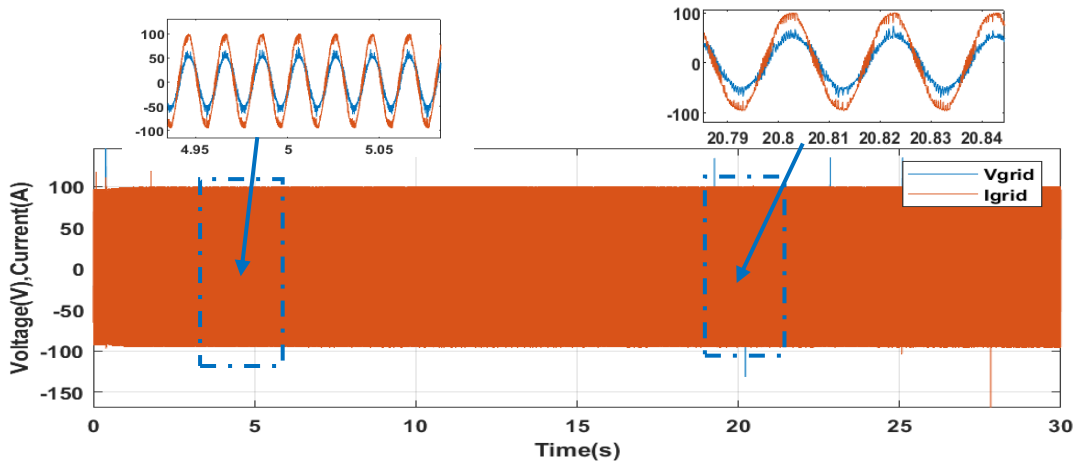
Figure 5. 12 Experimental results Using Euler Method with switching frequency 5 kHz: (a) Grid current, (b) Inverter current and its reference, (c) Grid voltage and Grid current (scale $I * 20$).



(a)



(b)

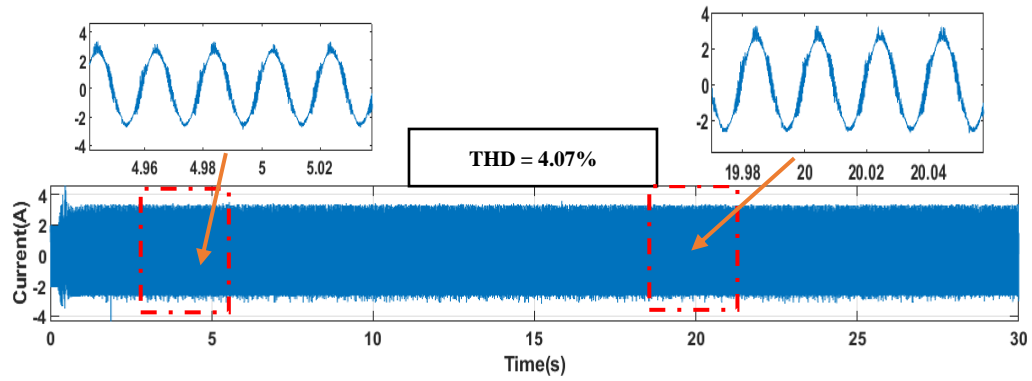


(c)

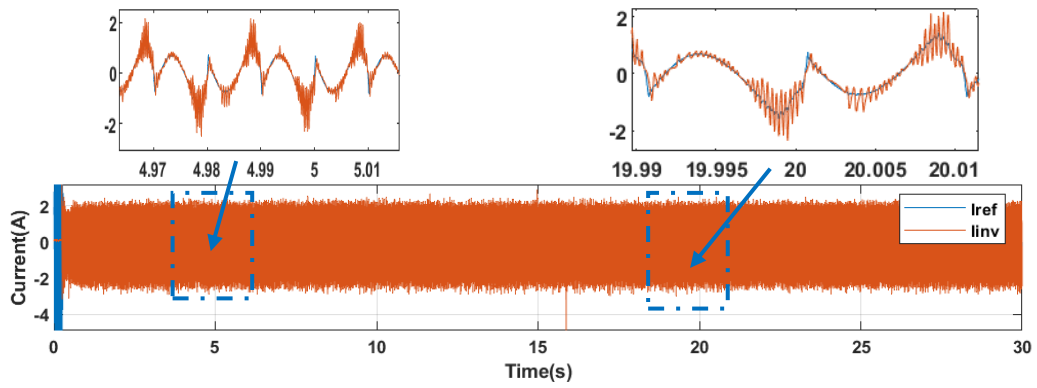
Figure 5. 13 Experimental results Using 4oRK Method with switching frequency 10 kHz:

(a) Grid current, (b) Inverter current and its reference, (c) Grid voltage and Grid current

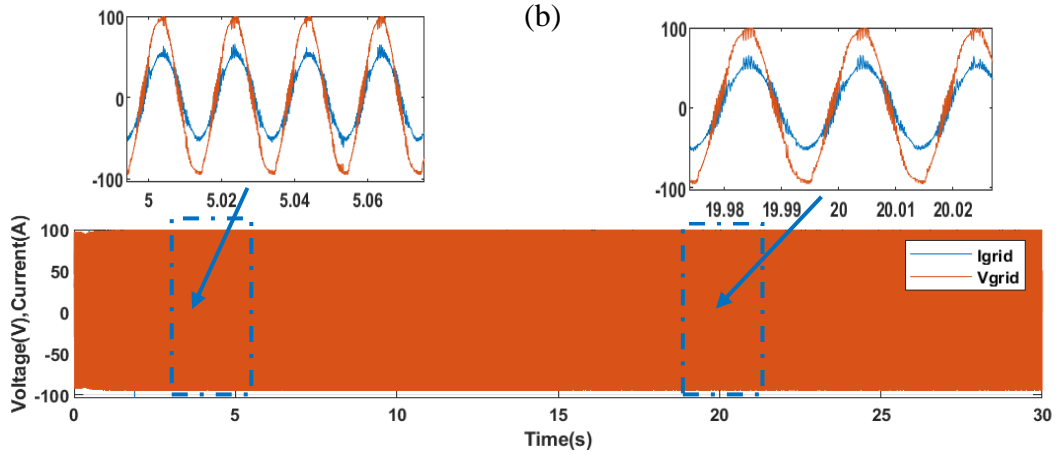
(scale I *20)



(a)



(b)



(c)

Figure 5. 14 Experimental results Using 4oRK Method with switching frequency 5 kHz: (a) Grid current, (b) Inverter current and its reference, (c) Grid voltage and Grid current (scale $I * 20$)

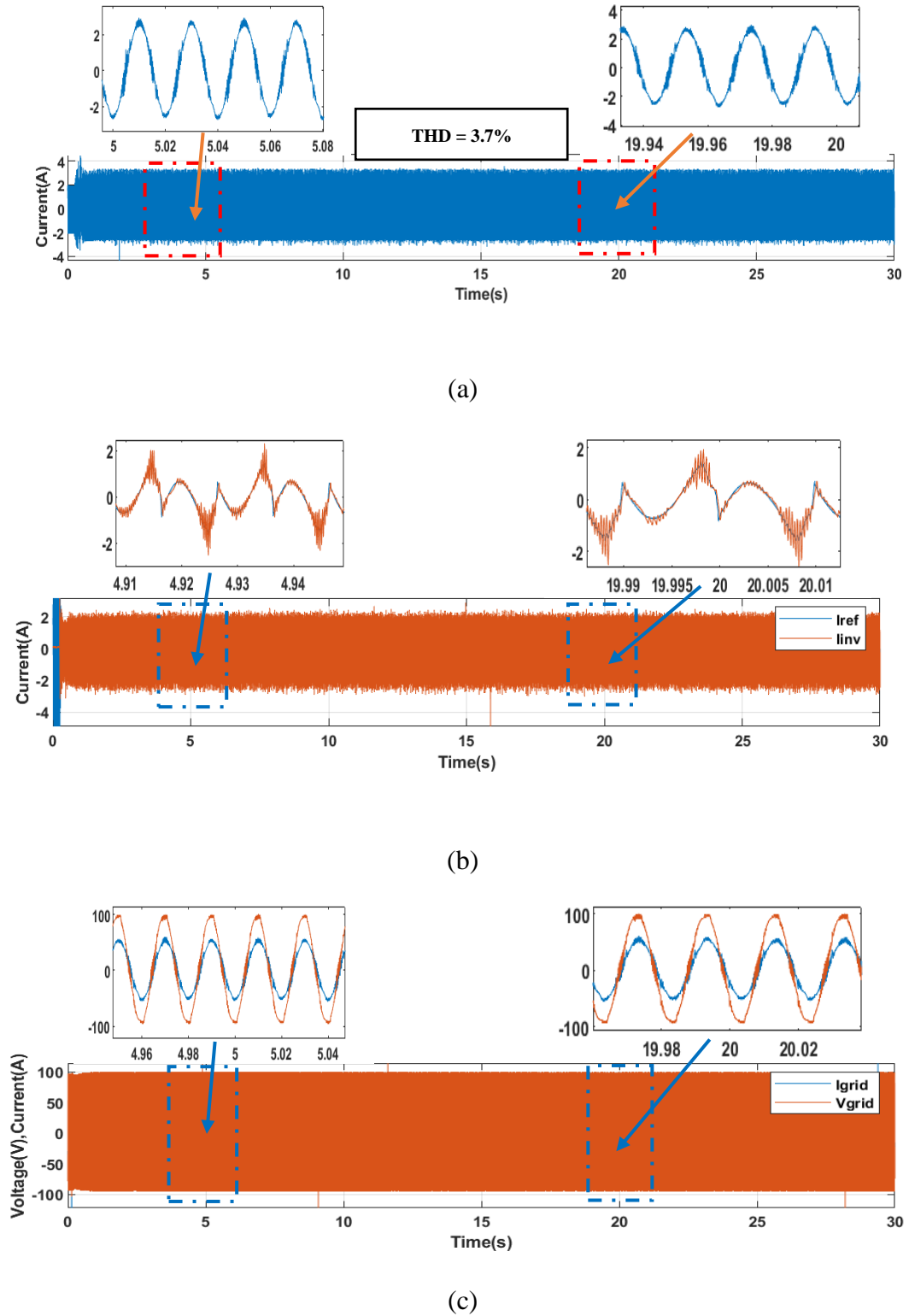


Figure 5. 15 Experimental results Using 4oRK Method with switching frequency 3 kHz: (a) Grid current, (b) Inverter current and its reference, (c) Grid voltage and Grid current (scale $I * 20$)

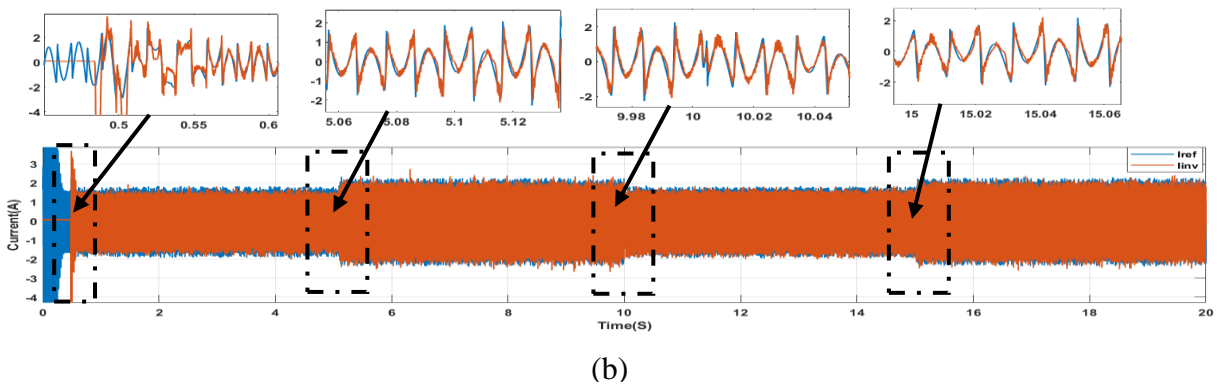
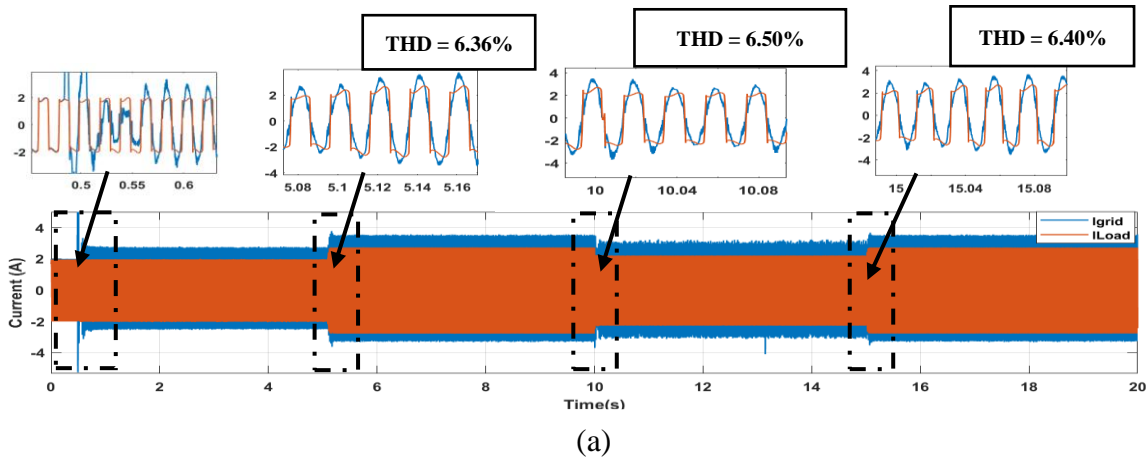
Table 5. 3 THD comparison of the experimental results.

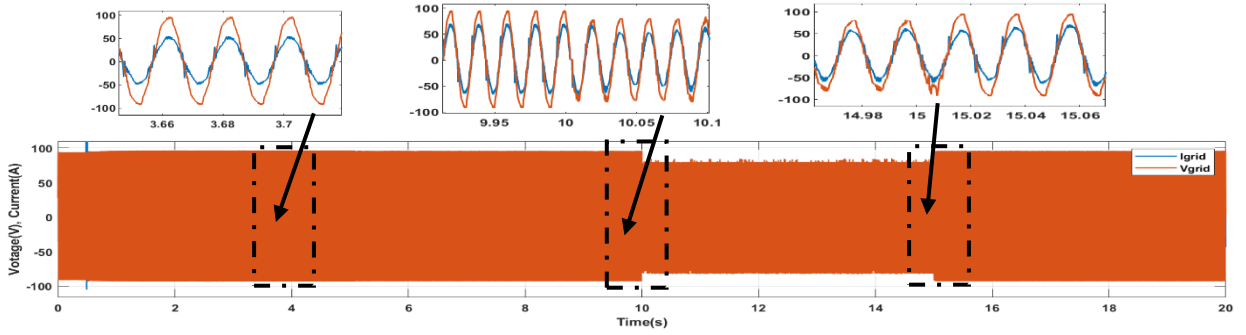
Switching frequency \ MPC Method	10 kHz	5 kHz	3 kHz
Euler Method	6.33%	10.27%	-
4oRK Method	4.39 %	4.07%	3.7%

In Table 5.3, a comprehensive comparison of various approaches highlights distinct attributes for each configuration, particularly focusing on Total Harmonic Distortion (THD), Active Power Filter (APF) implementation, and switching frequency. The comparison is based on factors such as inverter type, validation method, THD value, and control algorithm for reducing switching frequency. Our Proposed method demonstrates several advantages: it produces minimal harmonic distortion current, exhibits superior current tracking capability at low switching frequencies, and effectively reduces switching losses through real experimental validation. Notably, with a THD of 3.7% in the grid current. Our proposed configuration outperforms classical inverters and even the MPUC5 inverter. Its viability for real-world applications is evident, making it a standout choice.

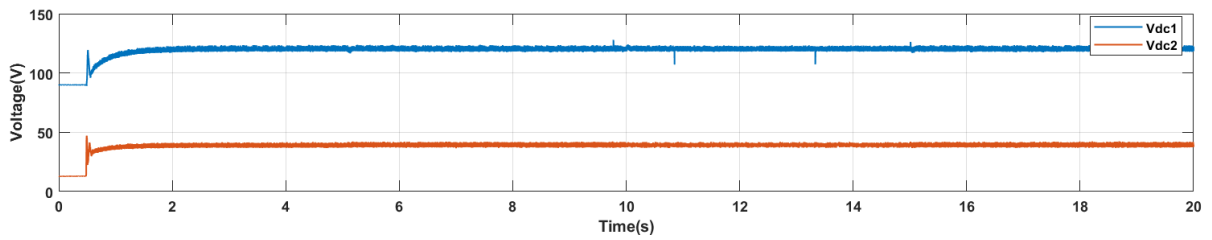
To assess the robustness and adaptability of the proposed method, a series of experiments were conducted under diverse operating conditions. The experimental setup involved varying load profiles and introducing voltage sag disturbances. Figures 5.16–5.19 illustrate the findings using the Euler method and the fourth-order Runge-Kutta (4oRK) method, providing a comparative analysis of their performance. The results for the Euler method under different scenarios are depicted in Figure 5.16: (a) Grid current and load current (b) Inverter current and its reference (c) Grid voltage and grid current (scaled by $I \times 20$) (d) DC-link capacitor voltages. The findings show that while the nonlinear load continues to draw a distorted current, the grid current becomes sinusoidal, as illustrated in Figure 5.16 (a). However, the total harmonic distortion (THD) of the grid current remains above 5%, indicating limitations in harmonic suppression. Figure 5.17 presents the corresponding results when the 4oRK method is applied under identical conditions: (a) Grid current and load current (b) Inverter current and its reference (c) Grid voltage and grid current (scaled by $I \times 20$) (d) DC-link capacitor voltages. The 4oRK method demonstrates superior performance, with the grid current becoming sinusoidal while the nonlinear load maintains its distorted profile, as

observed in Figure 5.17 (a). Importantly, the THD of the grid current is reduced to below 5% across all scenarios, highlighting the effectiveness of the 4oRK method in mitigating harmonic distortion. These results validate the robustness and flexibility of the 4oRK approach. Figure 5.18 illustrates the grid's power characteristics, revealing that the 4oRK method significantly reduces power losses compared to the Euler method. This improvement emphasizes the enhanced efficiency of the 4oRK method in managing power dynamics within the grid-connected system. Figure 5.19 compares the computational efficiency of the two methods by analyzing task execution times: (a) Euler Method (b) 4oRK Method. The analysis shows that the task execution time for both methods is nearly identical, indicating that the 4oRK method does not introduce additional computational complexity despite its superior performance in harmonic mitigation and power loss reduction.



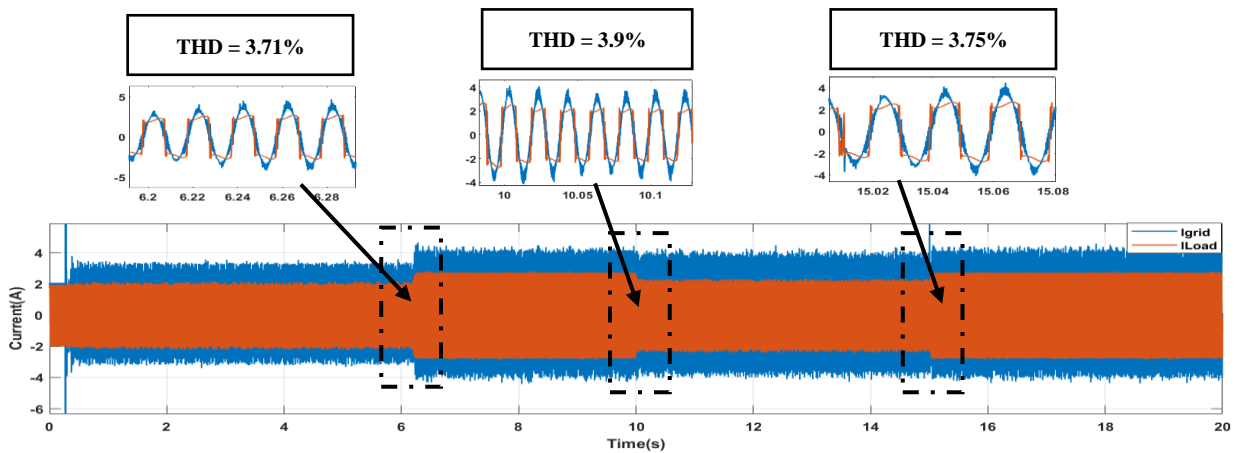


(c)

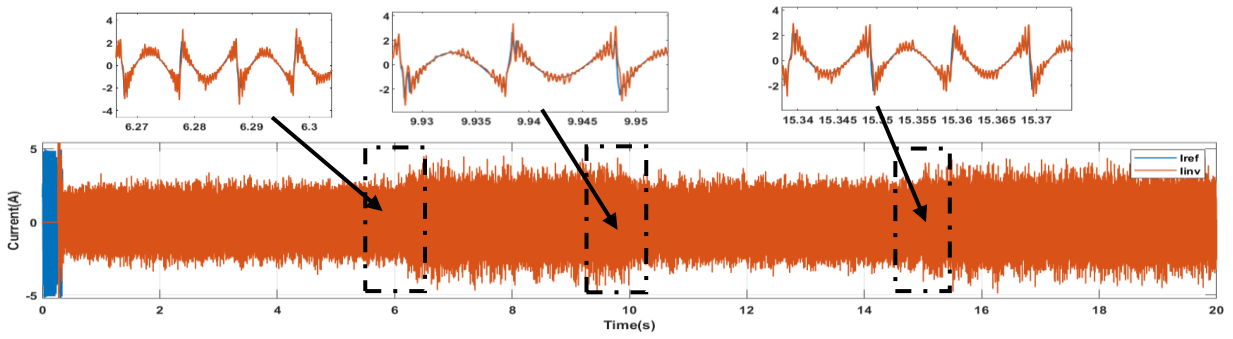


(d)

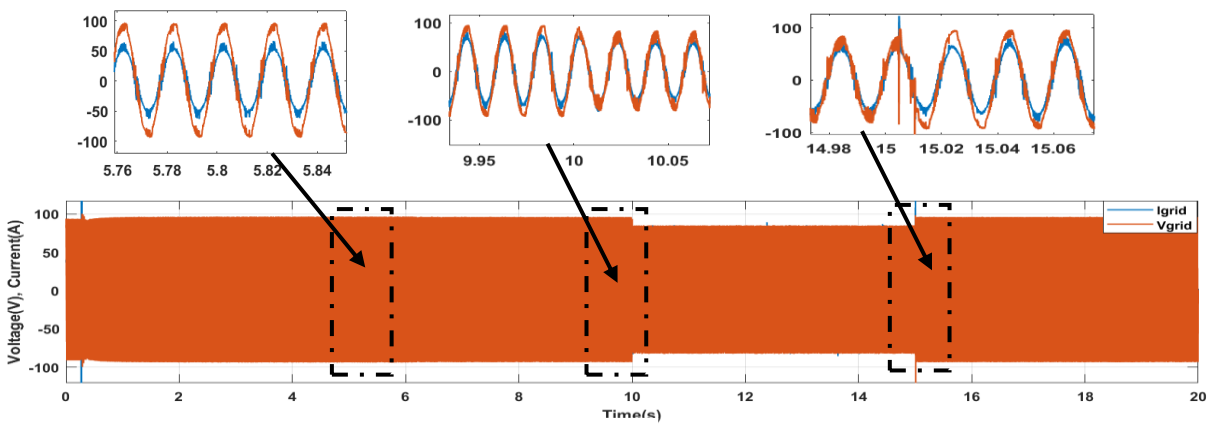
Figure 5. 16 Experimental Results Utilizing the Euler Method Across Various Scenarios with 10 KHz: (a) Grid current, Load current (b) Inverter current and its reference, (c) Grid voltage and Grid current (scale $I * 20$), (d) DC-link capacitor voltages.



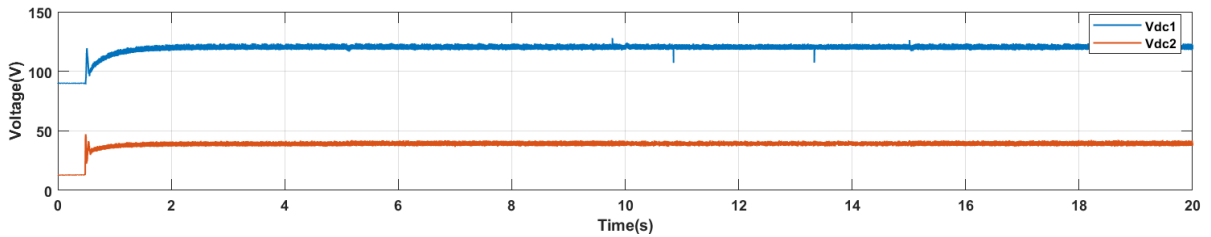
(a)



(b)



(c)



(d)

Figure 5. 17 Experimental Results Utilizing the 4oRK Method Across Various Scenarios with 3 KHz : (a) Grid current, Load current (b) Inverter current and its reference, (c) Grid voltage and Grid current (scale I *20), (d) DC-link capacitor voltages.

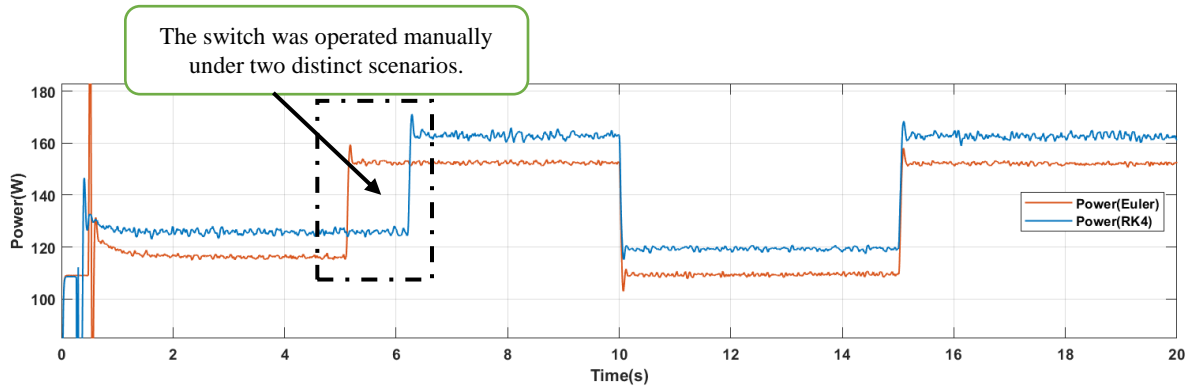


Figure 5. 18 Power of the grid

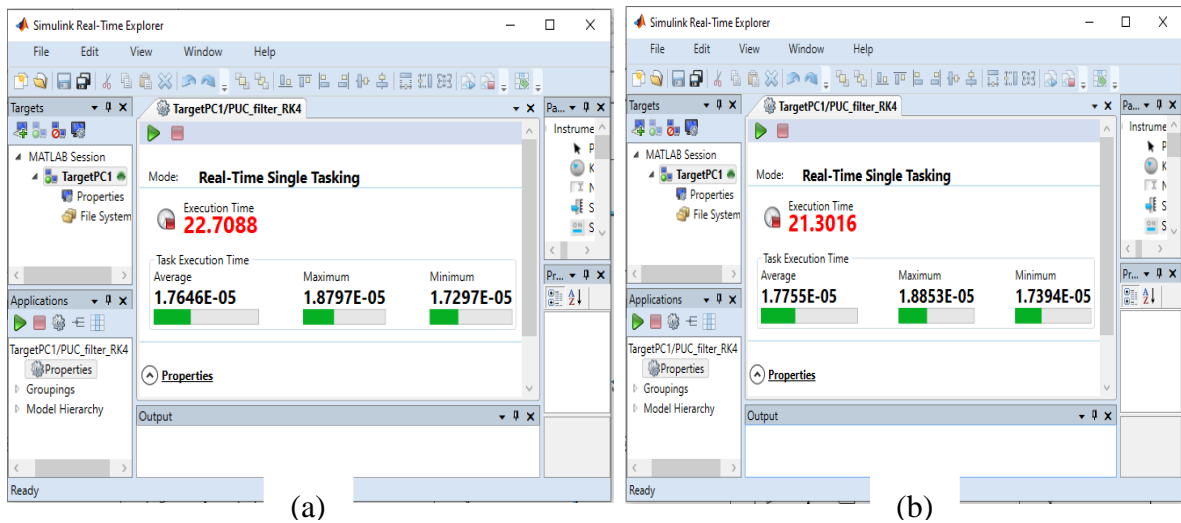


Figure 5. 19 Task Execution Time: (a) Euler Method, (b) 4oRK Method.

5.6 Conclusion

This article [75] proposes a novel MPC approach for active power filters based on the Runge–Kutta integration method. Specifically, the 4th-order Runge-Kutta (4oRK) integration method is introduced, along with the computing process of the control variables trajectory. We evaluated the performance of the proposed Model Predictive Control (MPC) method using a single-phase PUC7 shunt active power filter. A comprehensive analysis of both simulation and experimental data confirmed the practicality and effectiveness of the

approach, with the system demonstrating excellent performance across various switching frequencies. In addition, a detailed comparison between the proposed 4oRK-based MPC and the traditional Euler method-based MPC highlights significant improvements. The experimental results revealed that while the Euler method struggled to achieve Total Harmonic Distortion (THD) levels below 5% under nonlinear load and voltage sag conditions, the 4oRK-based MPC consistently maintained THD below this threshold across all scenarios. Furthermore, the 4oRK method significantly reduced power losses, as illustrated by the power grid characteristics, and maintained comparable task execution times to the Euler method, demonstrating no additional computational complexity. The proposed MPC method offers distinct advantages: it generates lower harmonic distortion currents, achieves better current tracking accuracy at low switching frequencies, and reduces switching losses by minimizing the switching frequency. These findings validate the robustness, flexibility, and superior performance of the 4oRK-based MPC, making it a promising approach for power electronic systems requiring precise control and high efficiency.

Looking forward, future research will focus on addressing these challenges by developing more robust control strategies that incorporate these non-idealities. The approach will be extended to three-phase systems, with adaptations to control strategies tailored for multi-phase operations. Moreover, the integration of renewable energy sources, such as solar and wind, into grid-tied inverters will be explored to further enhance system sustainability and resilience. Adaptive control algorithms will also be investigated to optimize the performance of the system under varying operational conditions. These advancements will allow the 4oRK-based MPC to better adapt to practical, real-world scenarios and provide more efficient solutions for power conversion systems.

GENERAL CONCLUSION

In this study [76], a double-stage, single-phase PUC7 inverter with an MPC control was demonstrated. The inverter is designed to serve multiple purposes, including power injection from the PV array into the grid, reactive power compensation, and filtering the grid current harmonics. Various experimental and simulation results were conducted and analyzed, which are considered highly relevant and validate the proposed strategies. The system demonstrated good performance across three different scenarios. The proposed I-V tracer of the PV array allows to effectively check the validity of the MPPT operation. In other words, the identified P-V curve allows, at the moment of the experiment, to identify the maximum power point as well as the optimum PV voltage. During the experiment, the extracted maximum power is compared to the identified one to check the performance of the MPPT algorithm. Therefore, conducting outdoor experiments that required the use of sensors is now possible without the need for these sensors.

Furthermore, a novel MPC approach based on the 4th-order Runge-Kutta (4oRK) integration method was introduced, offering a significant advancement in control precision and efficiency for the active power filter. By leveraging the 4oRK integration, the control variables' trajectory was computed more accurately, ensuring improved current tracking and harmonic distortion reduction. Comparative results demonstrated that, unlike the traditional Euler-based MPC, the 4oRK-based MPC consistently maintained THD levels below 5%, even under challenging conditions such as nonlinear loads and voltage sags. This method also reduced power losses without adding computational complexity.

Besides, the proposed MPC strategy guarantees stable voltage profiles, even during variable load conditions. This stability is evidenced by the sustained voltage across capacitors with the required proportionality. A comparative analysis with existing research highlights the distinction of the proposed approach. Specifically, the operation of multifunctional active power filters under real-life outdoor conditions while THD is minimized and the power factor is unity. Additionally, the P&O algorithm demonstrated its efficiency in tracking and delivering the maximum PV power. As a result, the proposed topology exhibits remarkable

flexibility in adapting to load variations, including power factor adjustment, reactive power compensation, and active power injection.

The matching observed between our experimental and simulated results serves as compelling evidence for the precision and effectiveness of our control system and identification process, making the proposed solar active filter configuration a new contribution to the advancement of renewable energy utilization and grid power quality. As further work, the present study can be extended to verify the MPPT tracking during the variation of sunlight or irradiance. This can be achieved by finding an automatic way to alter the power output of the PV array. Afterward, the variation of the PV output can be checked within the same experiment, and consequently, one may check the MPPT tracking not only under uniform irradiance but also under non-uniform irradiance conditions. Additionally, exploring the robustness of the 4oRK-based MPC under reduced sampling frequency scenarios could further demonstrate its potential for applications demanding high efficiency and reliability.

While the presented solutions demonstrate significant advantages, further research is necessary to enhance their robustness and practical applicability. For the PUC7-based multifunction SAF, real-time testing under diverse grid conditions and integration with adaptive control algorithms can further improve its harmonic compensation capabilities. Additionally, expanding its implementation in three-phase systems would validate its scalability. Regarding the 4ORk-based MPC of active filters, optimizing computational efficiency and implementing hardware-in-the-loop (HIL) testing would strengthen its real-time feasibility. Further comparative studies against state-of-the-art methods in industrial environments will solidify the superiority of these approaches.

BIBLIOGRAPHY

1. Sarita, K., Saket, R.K., Khan, B.: Reliability, availability, and condition monitoring of inverters of grid-connected solar photovoltaic systems. *IET Renewable Power Gener.* 17(7), 1635–1653 (2023)
2. Jogunuri, S., FT, J., Stonier, A.A., Peter, G., Jayaraj, J., Ganji, V.: Random forest machine learning algorithm based seasonal multi-step ahead short term solar photovoltaic power output forecasting. *IET Renewable Power Gener.* 1–16 (2024)
3. Menesy, A.S., Almomin, S., Sultan, H.M., Habiballah, I.O., Gulzar, M.M., Alqahtani, M., Khalid, M.: Techno-economic optimization framework of renewable hybrid photovoltaic/wind turbine/fuel cell energy system using artificial rabbits' algorithm. *IET Renewable Power Gener.* 1–18 (2024)
4. Eiva, U.R., Fahim, T.M., Islam, S.S., Ullah, M.A.: Design, performance, and techno-economic analysis of a rooftop gridtied PV system for a remotely located building. *IET Renewable Power Gener.* 1–17 (2023)
5. Khosravi, N., et al.: A novel control approach to improve the stability of hybrid AC/DC microgrids. *Appl. Energy* 344, 121261 (2023)
6. Kheldoun, A., Refoufi, L., Khodja, D.E.: Analysis of the self-excited induction generator steady state performance using a new efficient algorithm. *Electr. Power Syst. Res.* 86, 61–67 (2012)
7. Bradai, R., Boukenoui, R., Kheldoun, A., Salhi, H., Ghanes, M., Barbot, J.P., Mellit, A.: Experimental assessment of new fast MPPT algorithm for PV systems under non-uniform irradiance conditions. *Appl. Energy* 199, 416–429 (2017)
8. Belkhier, Y., et al.: Experimental analysis of passivity-based control theory for permanent magnet synchronous motor drive fed by grid power. *IET Control Theory Appl.* 18(4), 495–510 (2024)
9. Chakraborty, S., Mukhopadhyay, S., Biswas, S.K.: A hybrid compensator for unbalanced ac distribution system with renewable power. *IEEE Trans. Ind. Appl.* 59(1), 544–553 (2022)
10. Hasan, K., et al.: Shunt active power filter based on Savitzky-Golay filter: Pragmatic modelling and performance validation. *IEEE Trans. Power Electron.* 38, 8838–8850 (2023)
11. Wu, T.-F., et al.: PV power injection and active power filtering with amplitude-clamping and amplitude-scaling algorithms. *IEEE Trans. Ind. Appl.* 43(3), 731–741 (2007)
12. Pradhan, S., et al.: Performance investigation of multifunctional on-grid hybrid wind–PV system with OAScandMAF-based control. *IEEE Trans. Power Electron.* 34(11), 10808–10822 (2019)
13. Kheldoun, A.B.R.B., Bradai, R., Boukenoui, R., Mellit, A.: A new golden section method-based maximum power point tracking algorithm for photovoltaic systems. *Energy Convers. Manage.* 111, 125–136 (2016)

14. Khosravi, N., et al.: A new approach to enhance the operation of M-UPQC proportional-integral multiresonant controller based on the optimization methods for a stand-alone AC microgrid. *IEEE Trans. Power Electron.* 38(3), 3765–3774 (2022)
15. Defaÿ, F., Llor, A.-M., Fadel, M.: A predictive control with flying capacitor balancing of a multicell active power filter. *IEEE Trans. Ind. Electron.* 55(9), 3212–3220 (2008)
16. Junaid, K.M., et al.: Combined T-type and NPC seven-level boost active neutral point clamped inverter for medium voltage applications. *Iran. J. Sci. Technol.* 48(1), 201–212 (2023)
17. Tanguturi, J., Keerthipati, S.: Power balancing strategy for cascaded H-bridge inverter in a grid-connected photovoltaic system under asymmetrical operating conditions. *IEEE Trans. Ind. Electron.* 71(6), 5853–5862 (2023)
18. Vahedi, H., et al.: Modified seven-level pack U-cell inverter for photovoltaic applications. *IEEE J. Emerging Sel. Top. Power Electron.* 6(3), 1508–1516 (2018)
19. Khawaja, R., Sebaaly, F., Kanaan, H.Y.: Design of a 7-level single stage/phase PUC grid-connected PV inverter with FS-MPC control. In: 2020 IEEE International Conference on Industrial Technology (ICIT). Buenos Aires, Argentina (2020)
20. Chebbah, M.T., Vahedi, H., Al-Haddad, K.: Real-time simulation of 7-level Packed U-Cell shunt active power filter. In: 2015 IEEE 24th International Symposium on Industrial Electronics (ISIE). Buzios, Brazil (2015)
21. Vahedi, H., Al-Haddad, K.: Real-time implementation of a seven level packed U-cell inverter with a low-switching-frequency voltage regulator. *IEEE Trans. Power Electron.* 31(8), 5967–5973 (2015)
22. Vahedi, H., Labbé, P.-A., Al-Haddad, K.: Sensor-less five-level packed U cell (PUC5) inverter operating in stand-alone and grid-connected modes. *IEEE Trans. Ind. Inf.* 12(1), 361–370 (2015)
23. Metri, J.I., et al.: Real-time implementation of model-predictive control on seven-level packed U-cell inverter. *IEEE Trans. Ind. Electron.* 63(7), 4180–4186 (2016)
24. Dekka, A., et al.: Model predictive control of high-power modular multilevel converters—An overview. *IEEE J. Emerging Sel. Top. Power Electron.* 7(1), 168–183 (2018)
25. Pourmirasghariyan, M., et al.: A maximum power point tracking scheme for PV systems using model predictive control in grid-connected packed U-cell inverters. In: 2022 12th Smart Grid Conference (SGC). Kerman, Iran, Islamic Republic of (2022)
26. Rodriguez, J., Cortes, P.: *Predictive Control of Power Converters and Electrical Drives*. John Wiley & Sons, Hoboken, NJ (2012)
27. Maldonado, J.L., et al.: Optimal planning of collective photovoltaic arrays in energy communities through a multi-cut benders' decomposition strategy. *Sustainable Cities Soc.* 104, 105307 (2024)
28. Sun, Y., et al.: Artificial neural network for control and grid integration of residential solar photovoltaic systems. *IEEE Trans. Sustainable Energy* 8(4), 1484–1495 (2017)
29. Arab, N., et al.: A multifunctional single-phase grid-integrated residential solar PV systems based on LQR control. *IEEE Trans. Ind. Appl.* 55(2), 2099–2109 (2018)

30. Sahli, A., et al.: Energy management and power quality enhancement in grid-tied single-phase PV system using modified PUC converter. *IET Renewable Power Gener.* 13(14), 2512–2521 (2019)
31. International Energy Outlook 2019 with projections to 2050, pp.1– 169. U.S. Energy Information Administration and U.S. Department of Energy, Washington, DC 20585 ,2019
32. Renewable Energy Policy Network for 21st Century (REN21). *Renewable 2018 Global Status Report*, (2018)
33. Yacine Ayachi Amor, Farid Hamoudi, Aissa Kheldoun, “Three-phase Three level Inverter Grid-tied PV System with Fuzzy Logic Control based MPPT”, *ALGERIAN JOURNAL OF SIGNALS AND SYSTEMS (AJSS)*, p.101, September 2018
34. Yacine Ayachi Amor, Farid Hamoudi, Aissa Kheldoun, Gaëtan Didier, Zakaria Rabiai, “Fuzzy logic enhanced control for a single-stage grid-tied photovoltaic system with shunt active filtering capability”, p.3, 21 June 2021
35. IEEE Std 141-1993 IEEE Recommended Practice for Electric Power Distribution for Industrial Plants. The Institute of Electrical and Electronics Engineers, New York, 1993.
36. G. W. Chang and T. C. Shee, “A novel reference compensation current strategy for shunt active power filter control”, *IEEE Transactions on Power Delivery*, vol. 19, no. 4, pp. 1751–1758, 2004. References
37. H. Akagi, “Control strategy and site selection of a shunt active filter for damping of harmonic propagation in power distribution systems”, *IEEE Transactions on Power Delivery*, vol.12, no. 1, pp. 354–362, 1997.
38. A. Cavallini and G. C. Montanari, “Compensation strategies for shunt active filter control”, *IEEE Transactions on Power Electronics*, vol. 9, no. 6, pp. 587–593, 1994.
39. H. Akagi, H. Fujita, and K. Wada, “A shunt active filter based on voltage detection for harmonic termination of a radial power distribution line”, *IEEE Transactions on Industry Applications*, vol. 35, no. 3, pp. 638–645, 1999.
40. H. Fujita and H. Akagi, “A practical approach to harmonic compensation in power systems—series connection of passive and active filters”, *IEEE Transactions on Industry Applications*, vol. 27, no. 6, pp. 1020–1025, 1991.
41. F. Z. Peng, H. Akagi, and A. Nabae, “A new approach to harmonic compensation in power systems—a combined system of shunt passive and series active filters”, *IEEE Transactions on Industry Applications*, vol. 26, no. 6, pp. 983–990, 1990.
42. D. Basic, V. S. Ramsden, and P. K. Muttik, “Hybrid filter control system with adaptive filters for selective elimination of harmonics and inter harmonics”, *IEE Proceedings: Electric Power Applications*, vol. 147, no. 4, pp. 295–303, 2000.
43. S. Senini and P. J. Wolfs, “Hybrid active filter for harmonically unbalanced three phase three wire railway traction loads”, *IEEE Transactions on Power Electronics*, vol. 15, no. 4, pp. 702–710, 2000.
44. P. Salmeron, J. C. Montano, J. R. Vázquez, J. Prieto, and A. Pérez, “Compensation in non-sinusoidal, unbalanced three-phase four-wire systems with active power-line conditioner”, *IEEE Transactions on Power Delivery*, vol. 19, no. 4, pp. 1968–1974, 2004.

45. H. Akagi, "New trends in active filters for power conditioning", *IEEE Transactions on Industry Applications*, vol. 32, no. 6, pp.1312–1322, 1996
46. H. L. Jou, J. C. Wu, and K. D. Wu, "Parallel operation of passive power filter and hybrid power filter for harmonic suppression", *IEEE Proceedings: Generation, Transmission and Distribution*, vol.148, no. 1, pp. 8–14, 2001.
47. X. Zha and Y. Chen, "The iterative learning control strategy for hybrid active filter to dampen harmonic resonance in industrial power system", in *Proceedings of the IEEE International Symposium on Industrial Electronics*, vol. 2, pp. 848–853, 2003.
48. Nabae, A.; Takahashi, I.; Akagi, H. A New Neutral-Point-Clamped PWM Inverter. *IEEE Trans. Ind. Appl.* 1981, IA-17, 518–523.
49. Abd Halim, W.; Ganeson, S.; Azri, M.; Azam, T.T. Review of multilevel inverter topologies and its applications. *J. Telecommun. Electron. Comput. Eng. (JTEC)* 2016, 8, 51–56.
50. Rathore, S.; Kirar, M.K.; Bhardwaj, S. Simulation of cascaded H-bridge multilevel inverter using PD, POD, APOD techniques. *Electr. Comput. Eng. Int. J. (ECIJ)* 2015, 4, 27–41.
51. Rodriguez, J.; Jih-Sheng, L.; Fang Zheng, P. Multilevel inverters: A survey of topologies, controls, and applications. *IEEE Trans. Ind. Electron.* 2002, 49, 724–738.
52. Srinivasan, G.K.; Rivera, M.; Loganathan, V.; Ravikumar, D.; Mohan, B. Trends and Challenges in Multi-Level Inverter with Reduced Switches. *Electronics* 2021, 10, 368.
53. Krishna, R.A.; Suresh, L.P. A Brief Review on Multi Level Inverter Topologies. In *Proceedings of the International Conference on Circuit, Power and Computing Technologies (ICCPCT)*, Nagercoil, India, 18–19 March 2016; pp. 1–6.
54. Jih-Sheng, L.; Fang Zheng, P. Multilevel converters-a new breed of power converters. *IEEE Trans. Ind. Appl.* 1996, 32, 509–517.
55. Shanono, I.H.; Abdullah, N.R.H.; Muhammad, A. A survey of multilevel voltage source inverter topologies, controls, and applications. *Int. J. Power Electron. Drive Syst.* 2018, 9, 1186.
56. Abu-Rub, H.; Malinowski, M.; Al-Haddad, K. *Power Electronics for Renewable Energy Systems, Transportation and Industrial Applications*; John Wiley & Sons: West Sussex, UK, 2014.
57. Meynard, T.A.; Foch, H. Multi-Level Conversion: High Voltage Choppers and Voltage-Source Inverters. In *Proceedings of the PESC '92 Record, 23rd Annual IEEE Power Electronics Specialists Conference, Toledo, Spain, 29 June–3 July 1992; Volume1*, pp. 397–403.
58. Lavieville, J.-P.; Carrere, P.; Meynard, T. Electronic Circuit for Converting Electrical Energy, and A Power Supply Installation Making Use Thereof. U.S. Patent 5,668,711, 16 September 1997.
59. Dokić, B.L.; Blanuša, B. Introduction to Multilevel Converters. In *Power Electronics*; Springer: Berlin/Heidelberg, Germany, 2015; pp. 559–592.

60. Subarnan, J.G. Multilevel Inverters: An Enabling Technology. In Hybrid-Renewable Energy Systems in Microgrids; Elsevier: Amsterdam, The Netherlands, 2018; pp. 61–80.
61. Baker, R.H.; Bannister, L.H. Electric Power Converter. U.S. Patent 3,867,643, 18 February 1975.
62. Marchesoni, M. High-performance current control techniques for application to multilevel high-power voltage source inverters. *IEEE Trans. Power Electron.* 1992, 7, 189–204.
63. Prabakaran, N.; Palanisamy, K. A comprehensive review on reduced switch multilevel inverter topologies, modulation techniques and applications. *Renew. Sustain. Energy Rev.* 2017, 76, 1248–1282.
64. Ounejjar, Y., K. Al-Haddad, and L.-A.J.I.T.o.I.E. Gregoire, *Packed U cells multilevel converter topology: theoretical study and experimental validation*. *IEEE Transactions on Industrial Electronics*, 2010. **58**(4): p. 1294-1306
65. Belmadani, H., et al., A twofold hunting trip African vultures algorithm for the optimal extraction of photovoltaic generator model parameters. *Energy Sources, Part A: Recovery, Utilization, Environmental Effects*, 2022. 44(3): p. 7001-7030.
66. Mohapatra, A., et al., *A review on MPPT techniques of PV system under partial shading condition*. *Renewable Sustainable Energy Reviews*, 2017. **80**: p. 854-867.
67. Bollipo, R.B., et al., *Hybrid, optimal, intelligent and classical PV MPPT techniques: A review*. *CSEE Journal of Power Energy Systems*, 2020. **7**(1): p. 9-33.
68. Akagi, H., Y. Kanazawa, and A.J.I.T.o.i.a. Nabae, Instantaneous reactive power compensators comprising switching devices without energy storage components. *IEEE Transactions on industry applications*, 1984(3): p. 625-630.
69. Khadkikar, V., A. Chandra, and B.N.J.I.P.E. Singh, Generalised single-phase pq theory for active power filtering: simulation and DSP-based experimental investigation. *IET Power Electronics*, 2009. 2(1): p. 67-78.
70. Sun, Y., et al., *Artificial neural network for control and grid integration of residential solar photovoltaic systems*. *IEEE transactions on sustainable energy*, 2017. 8(4): p. 1484-1495.
71. Wu, T.-F., et al., *A single-phase inverter system for PV power injection and active power filtering with nonlinear inductor consideration*. *IEEE Transactions on Industry Applications*, 2005. 41(4): p. 1075-1083
72. Arab, N., et al., *A multifunctional single-phase grid-integrated residential solar PV systems based on LQR control*. *IEEE Transactions on Industry Applications*, 2018. 55(2): p. 2099-2109.
73. Sahli, A., et al., *Energy management and power quality enhancement in grid-tied single-phase PV system using modified PUC converter*. *IET Renewable Power Generation*, 2019. 13(14): p. 2512-2521
74. IEEE standard, *IEEE Standard for Harmonic Control in Electric Power Systems*. Transmission and Distribution Committee, 2022. DOI.10.1109/IEEESTD.2022.9848440.

75. Khettab, S., Kheldoun, A., Bradai, R.: A novel Runge-Kutta-based model predictive controller for PUC7-based single-phase shunt active power filter. *Computers and Electrical Engineering* Volume 123, Part A, April 2025, 110051

76. Khettab, S., Kheldoun, A., Bradai, R., Oubelaid, A., Kumar, S., Khosravi, N.: Performance evaluation of PUC7-based multifunction single-phase solar active filter in real outdoor environments: Experimental insights. *IET Renew. Power Gener.* 1–18 (2024).